Industrial-based Masters Thesis

André Fargette

Department of Mechanical Engineering

Thermal-hydraulic modeling of the high pressure pre-heater (nuclear power plant Neckarwestheim I)

Strathclyde supervisor: Mr. R. C. McLean

AREVA NP supervisors: Mr. Markus Delzeit and Mr. Thomas Schwarz

List of figures and Tables

Abstract

In advanced steam-turbine power plants, pre-heating is an essential means by which the thermodynamic efficiency of the Rankine cycle can be improved. The high-pressure pre-heater is one of the last steps of pre-heating before the feedwater is fed into the steam-generator.

This paper presents an analysis of GKN I's HP pre-heater. Steam bled from the high-pressure turbine and condensate from the re-heater flow on the shell-side of the component and account for a 35°C temperature rise of the feedwater.

A thermal model predicting the tube and shell outlet temperatures on the basis of all the boundary conditions and the geometrical characteristics of the component is presented. Head losses and static pressure variations inside the heat-exchanger are also calculated.

The velocity distributions inside the shell and the tube-bundle were estimated on the basis of a thermally-driven flow of the steam through the component. The results of this analysis were then used later on to determine if the heat-exchanger was prone to damage caused by fluid-elastic instabilities or vortex shedding in the condensation zone or in the subcooling enclosure (Kühlkasten).

Finally, a simplified Rankine cycle with one stage of pre-heating was simulated in order to understand the impact of heat-exchange area variations inside the pre-heater on the performance of the plant. The entropy generation and exergy destruction of the various components of the cycle were studied and general guidelines for the design of the HP pre-heater were deduced.

Foreword

This report covers all the work carried out from May 2007 to August 2007 with AREVA NP / NEEG-G in Erlangen, Germany. The official title of this work is "Thermal hydraulic modeling of the high pressure preheater for the turbine island in nuclear power plants". The overall objective of this work is to provide a tool to the R&D group in charge of the maintenance and replacement of the HP pre-heater.

My work includes a thermal analysis of the component, velocity, head loss and pressure drop calculations. A thermodynamic analysis of the impact of pre-heating is also presented, which helps understanding how the component could be optimized.
A second-law based analysis of the performance of steam-generators and a model accounting for the impact of non-uniform velocity and temperature distributions in a heat-exchanger are presented in appendices A and B. Both of these problems are independent of my work on the pre-heater but were assigned to me given their similarity with the analysis of the pre-heater.
It is further to be noted that I was asked to base my work on analytical models and empirical correlations and not on CFD calculations since my tutors were interested in obtaining instant answers where all physical assumptions could be checked easily. Given the complexity of the geometry, CFD calculations are indeed very time and resource consuming.

All the sections of my work are therefore coupled with excel spreadsheets which enable the user to get instant answers simply by modifying the desired parameter (the calculations are either carried out automatically or by means of a macro when iterations are required). Even though these spreadsheets are not presented here (they require special excel add-ins developed by AREVA with the thermodynamic properties of steam), they represent a considerable effort and a practical tool with which my models can be used by fellow engineers. These excel-sheets might eventually be adapted and turned into visual basic programs in the forthcoming months.

I would finally like to thank my supervisors Mr. Delzeit and Mr. Schwarz for helping me with all the administrative and scientific aspects of my work and making sure I felt at ease in my working environment. Last but not least, special thanks to Mr. Bruce for his enlightened tips during editing!

Erlangen, September 2007

André Fargette

AREVA NP / NEEG-G

1 Introduction

1.1 The GKN power plant

GKN (Gemeinschaftskernkraftwerk Neckar) is a German nuclear power plant situated in Baden-Württemberg, near Heilbronn. This power plant is composed of two blocks (I and II) which started operating in 1976 and 1988 respectively. These two blocks are independent and although they are both pressurized water reactors, their design is different. In this paper, the pre-heater studied belongs to block I.
GKN I's cycle is hybrid since the steam generators feed steam into two loops, one powering a railway line (160 MW electric) and the second one producing electricity (710 MW) for grid purposes. These two loops are partly independent (separate HP and LP turbines, separate condensers, separate train of LP pre-heaters) but they share the same HP pre-heater.

1.2 The Rankine cycle and the HP pre-heater

The Rankine cycle is the logical evolution of Carnot's cycle applied to power generation. Instead of compressing a steam-liquid mixture (which is a difficult process), the steam from the turbine is entirely condensed and a simple pump feeds it into the boiler. Even though the thermal efficiency of Rankine's cycle is less than that of Carnot's cycle, its work ratio is greater (little work necessary to compress pure liquid) and so is its specific steam consumption.

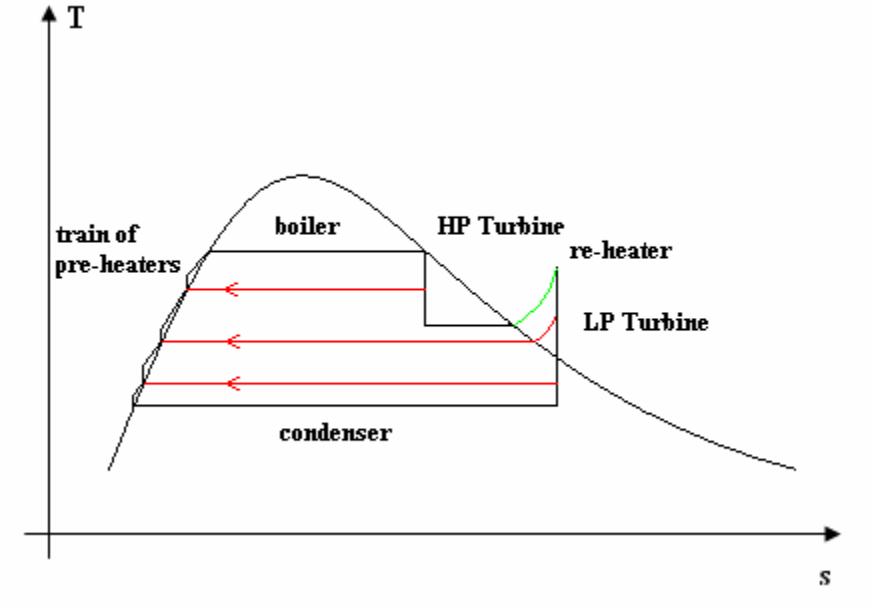

Figure 1: Rankine cycle with re-heating and pre-heating

This basic Rankine cycle is usually modified in order to improve its thermal efficiency. In the GKN I plant, these modifications include reheating and preheating (see Figure 1: Rankine cycle with re-heating and pre-heating).

- There are two turbines (the high pressure turbine and the low-pressure turbine) in the cycle (in reality there are 4: 2 for the train power plant and 2 for the grid power plant). A combined water-separator / re-heater is placed between these two turbines. This component is essential because the water-steam mix coming out of the HP turbine cannot be further expanded (the proportion of water in the flow would increase dramatically, thus leading to erosion problems and a low turbine efficiency). The water-separator channels away most of the water and the remaining saturated steam is superheated in the reheater and then fed into the LP turbine

- Pre-heating is the process by which the feedwater is heated before it is fed into the steam generator. This is done by bleeding steam from the LP and HP turbines (or by using the warm condensate flowing out of the water-separator) and thus gradually heating the feedwater in a series of heat-exchangers: one of these is the HP pre-heater. The improvement brought about by such a measure might not seem obvious at first sight. However its impact will be studied at length in the chapter devoted to the thermodynamic optimization of the component. We can rather loosely say that it “improves the thermal efficiency of the cycle”.

The components of the cycle surrounding the HP pre-heater have been represented in Figure 2. The feedwater flows from the feedwater tank (also called deaerator) into the pre-heater (on the tube-side of the component). After exiting from the HP pre-heater, it is then pre-heated one last time in the condensate cooler before it is fed into the steam generator.
On the shell-side, steam bled from the HP turbine and condensate from the water separator are fed into the HP pre-heater. The subcooled condensate obtained at the outlet is then cascaded into the feedwater tank.

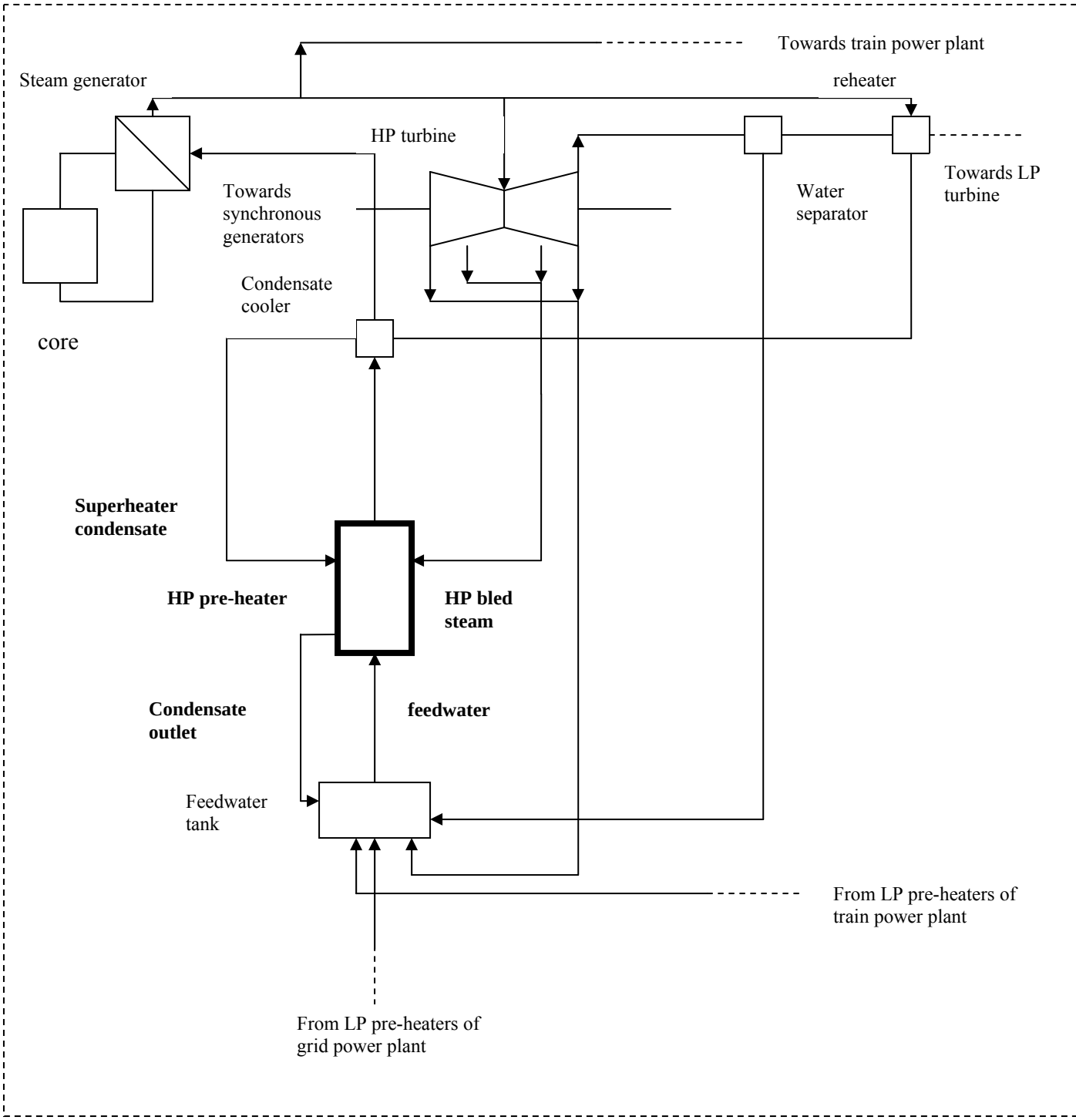

Figure 2: The HP pre-heater and its immediate neighbours in the GKN I plant

1.3 Presentation of the component and the flow pattern

GKN1's high-pressure pre-heater consists of a condensation zone (in which the steam bled from the turbine condenses) and a subcooling zone in which the condensate (i.e. the condensated steam and the condensate coming from the reheater) further preheats the feedwater. This subooling zone will thereafter be referred to as the Kühlkasten.
The HP steam enters at the top of the component and condenses along the cold tubes in which flows the feedwater. Further down, the condensate from the re-heater pours into the component and flows straight down to the water surface. The condensed steam also flows downwards along the tubes and finally reaches the water surface at which stage it mixes with the condensate from the re-heater.
The condensate then enters the Kühlkasten (upward flow), exchanges heat with the tubes inside the Kühlkasten and finally exits near the top of the component.

On the tube-side, the feedwater enters on the right-hand side of Figure 3 and Figure 4 and flows downwards towards the bottom of the heat-exchanger. It then makes a U-turn and flows upwards towards the top of the component and exits at the top left-hand side of the HP pre-heater.

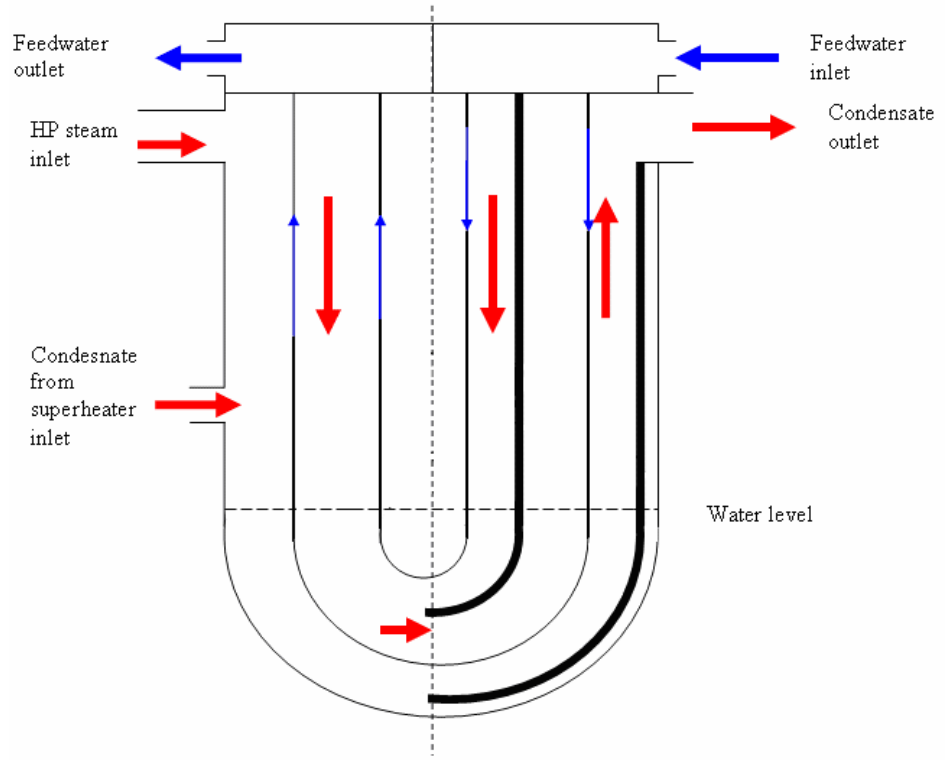

Figure 3: Side view of the HP pre-heater

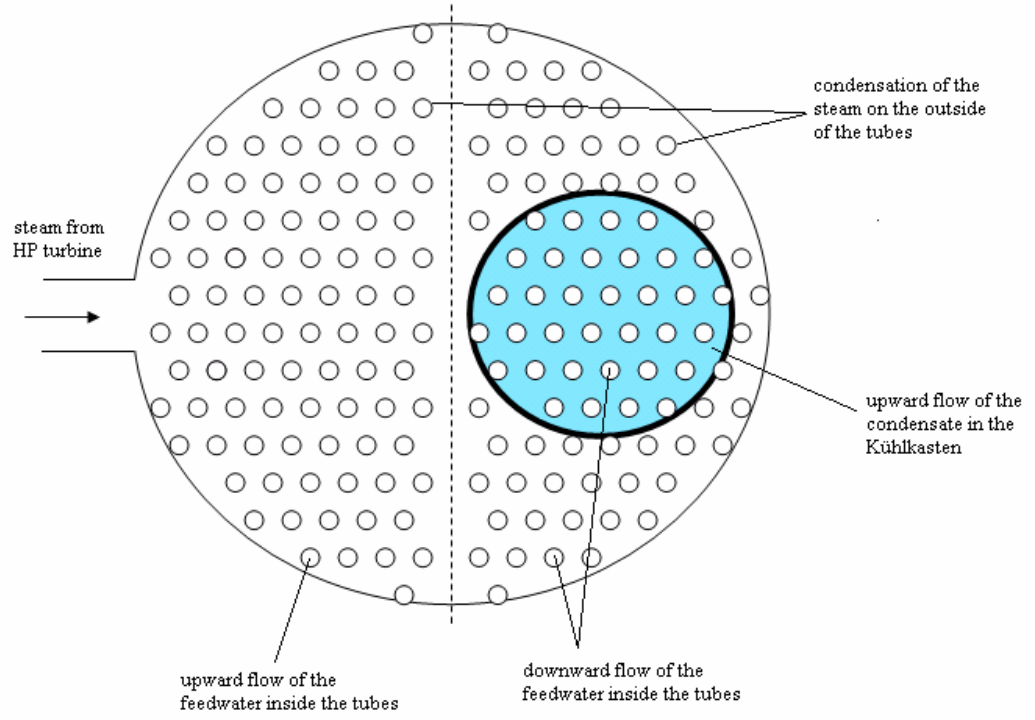

Figure 4: View from above of the HP pre-heater

Note: see Appendix C: 3D view of the HP pre-heater for further details on the geometry of the component

1.4 Exergy, entropy and second-law efficiencies: a review of thermodynamics

Power plant analysis (and even engineering studies) usually suffer from what could be called a "first-law bias" i.e. that most calculations are concerned with energy balances and energy transfer rates. With this approach, the layout of a real power plant with its superheaters, reheaters and numerous pre-heaters is quite incomprehensible and the performance of all these components is difficult to appreciate.
In reality, power plant design and analysis is all about the transfer of exergy rather than energy.

Therefore, most of the thermodynamic optimization and performance assessment of the systems will rely on exergy-based calculations and the associated second law efficiencies and entropy balances. These very important tools and concepts are treated in many standard textbooks. However, a short review of a few essential results will be presented here to help the reader understand the calculations carried out in sections 4 and 7and the general "philosophy" of these sections.

1.4.1 The exergy concept

Exergy can be defined as the maximal mechanical power that can be extracted from a substance. The exergy of a substance is defined with respect to a "dead" state, which refers to the properties of this substance when it is at equilibrium with the environment. Once this dead state has been reached, it is impossible for the substance to undergo any more changes (nor is it possible to extract any more work from it). This dead state is defined by means of the temperature, the pressure and the chemical potential of the substances in the environment. There is usually a further distinction between the restricted dead state (same temperature and pressure as the environment) and the unrestricted dead state (same temperature, pressure and chemical composition as the environment).
The exergy of a substance i flowing in a system is then defined as:

$$ex_i = \left[(h_i - h_0) - T_0(s_i - s_0)\right] + \left[x_i(\mu_{i0} - \mu_i^{\,0})\right] \qquad \text{Equation 1}$$

Where the subscript 0 refers to the conditions in the restricted dead state, x_i is the mole fraction of substance i, μ_{i0} is the chemical potential of the substance i at the restricted dead state and μ_i^0 is the chemical potential of the substance i in the environment (unrestricted dead state). The first term in brackets is the thermomechanical flow exergy of the substance (living state – restricted dead state) and the second term is the chemical flow exergy (restricted dead state – unrestricted dead state). Although the chemical flow exergy can be of great importance when studying systems involving chemical reactions (combustion of fuel etc…), it will be irrelevant in our work in which no chemical reaction take place. The exergy we are going to refer to will therefore always be the thermomechanical exergy:

$$ex_i = (ex_i)_{thermomechanical} = \left[(h_i - h_0) - T_0(s_i - s_0)\right] \qquad \text{Equation 2}$$

Furthermore, the forthcoming work will only be concerned with water and steam. The restricted dead state will therefore refer to saturated vapor at T_0, the temperature of the environment (note that saturated water at T_0 could also be chosen since saturated water and steam both have the same free enthalpy).

When energy is transferred between two systems a and b, exergy is also transferred. The first law of thermodynamics states that the amount of energy received by b must be equal to the amount delivered by a. This is not the case with exergy: the amount of exergy received by b is always smaller than the amount delivered by a. These two amounts are only equal in the ideal case of a reversible process.
The thermodynamic perfection of a component such as a heat exchanger can therefore be assessed by calculating its second-law efficiency, i.e. the ratio of the exergy received by the cold side of the exchanger and the exergy delivered by the hot side:

$$\eta_{II} = \frac{\Delta ex_{cold}}{\Delta ex_{hot}} \qquad \text{Equation 3}$$

The closer this ratio to 1, the greater the efficiency of the component. Note that the common first law efficiency is of little use here since it is always equal to 1 (if we neglect heat leaks). Second-law efficiencies are extremely important criterions in systems such as power cycles since the goal of the plant is to transfer the greatest possible fraction of exergy (rather than energy) from the primary loop to the turbine. For example, we will see that the advantage of pre-heating cannot be understood from an energetic point of view (the energy produced in the core can be transferred between primary and secondary loops without the help of pre-heaters) but can be understood from an exergetic or entropic point of view.

1.4.2 Entropy balances

An entropy balance is an indispensable tool when it comes to estimating the irreversibility of a component. This can indeed be done by calculating the entropy generation rate in the component. For a flow system, an entropy balance reads:

$$\sum_{in} s_i \dot{m}_i + \dot{S}_g + \frac{\dot{Q}}{T} = \frac{\partial S}{\partial t} + \sum_{out} s_i \dot{m}_i \qquad \text{Equation 4}$$

where $\dot{S}_g$ is the rate of entropy generation, $\frac{\dot{Q}}{T}$ is the entropy flux associated with the heat flux entering the system at temperature T, S is the entropy of the entire system and s_i is the entropy per unit mass of a substances flowing in (or out) of the system with a mass flow rate of $\dot{m}_i$. For a steady-state, adiabatic flow system, we obtain:

$$\dot{S}_g = \sum_{out} s_i \dot{m}_i - \sum_{in} s_i \dot{m}_i \qquad \text{Equation 5}$$

In the previous paragraph we hinted that there was a link between entropy generation and exergy: there is indeed no exergy destruction in a system if this system operates reversibly i.e. if there is no entropy generation. The gap between these two notions is bridged by the Guoy-Stodola theorem which states that the rate of exergy destruction is proportional to the rate of entropy creation and that the proportionality constant is the temperature of the environment:

$$\dot{E}x_{destroyed} = T_0 \dot{S}_g \qquad \text{Equation 6}$$

2 Thermal model of the HP Pre-heater

2.1 Breakdown of the component

As explained previously, the purpose of the HP Pre-heater is to heat the feedwater before it is fed into the steam-generator by bleeding hot steam from the high-pressure turbine. In addition to the steam from the turbine, high-pressure condensate coming from reheater is also cascaded into the component. These two streams of high temperature steam and water (shell-side) will exchange heat with the colder feedwater (tube-side), thus increasing its temperature.
The HP Pre-heater is composed of various zones.
-Most of the heat-exchange takes place by direct condensation of the steam along the tube bundle. The condensate then flows down along the tubes (film condensation) until it reaches the surface of the water.
- A small fraction of the heat is then exchanged underwater by the immersed tubes
-Finally, the condensate flows upwards in the "Kühlkasten" (subcooling zone enclosure) which is simply another shell and tube heat exchanger equipped with baffles to enhance the heat exchange. The condensate is therefore subcooled when it leaves the HP Pre-heater.

This description of the HP-Preheater suggests that it might be useful to break down the model into three separate parts, each governed by different heat transfer equations since the conditions are different:
-condensation of saturated steam in the upper part of the HP Pre-heater (zones 1,2,3)
-a flooded zone under the water surface (heat-exchange conditions to be defined, zone 5)
-a counter-flow water/water heat exchange zone in the Kühlkasten (zone 4)

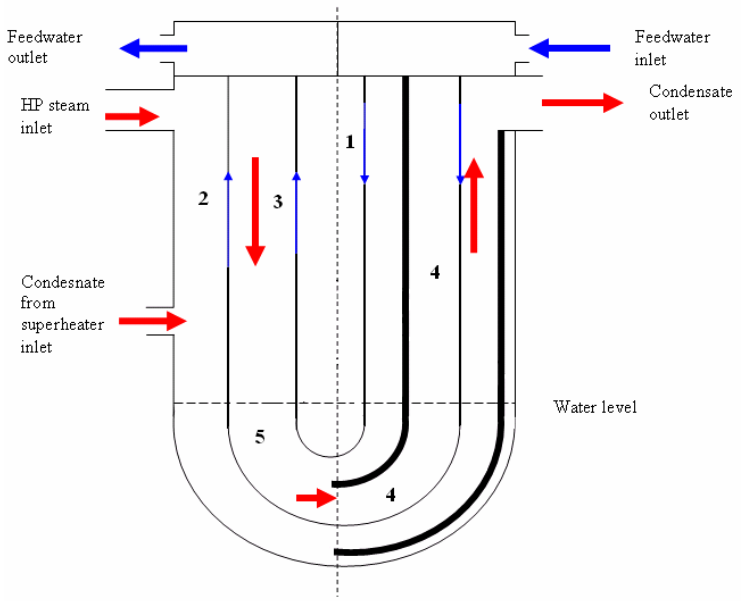

Figure 5: HP pre-heater

2.2 Mathematical model and assumption for the different parts of the heat-exchanger

2.2.1 Steam condensation zone

Since the steam is condensing along the tubes, the shell-side temperature is constant and equal to the saturation temperature of the HP steam (216,61°C) (we do indeed neglect pressure losses in the thermal analysis).
Regarding the tubes in the condensation zone, it is important to differentiate two categories:
-those in which the feedwater is flowing downwards (part of the right-hand half or the heat-exchanger) (zone 1)
-those in which the feedwater is flowing upwards (left-hand half of the heat-exchanger) In this second category, we can further differentiate the tubes coming out of the Kühlkasten (zone 2) and those which were outside the Kühlkasten (zone 3).

Consequently, there will be three tube-side temperature profiles in the condensation zone (strictly speaking, each tube has its own temperature profile since the tube length and heat exchange surface is a function of the tube's distance from the center of the pre-heater. However, this aspect will be neglected and average lengths and heat-exchange surfaces will be derived).
In all cases, the tube-side temperature will increase as the feedwater flows along the tube since heat is transferred from the hot condensing steam.

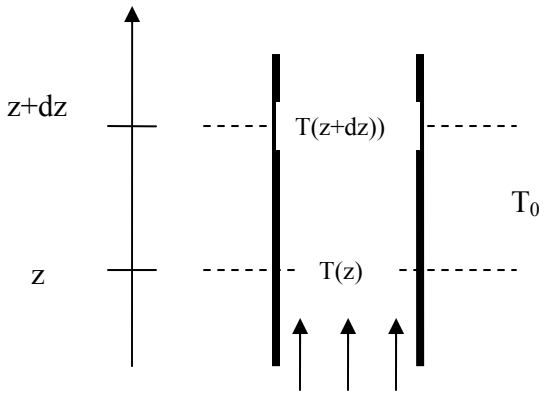

Figure 6: Microbalance in the condensation zone

We are going to set up an energy microbalance on the feedwater flowing in the tubes in order to derive the temperature profile.
In the following thermal analysis, the following assumptions will be made:

-constant c_p for water

$$-\left(\frac{\partial h}{\partial p}\right)_{T,water} = 0$$

-constant overall heat transfer coefficient along the tube
-steady-state conditions
An energy balance between z and z+dz yields:

$$\dot{m}c_p T(z) + UPdz(T_0 - T(z)) = \dot{m}c_p T(z+dz) \qquad \text{Equation 7}$$

$$\frac{dT}{T - T_0} = -\frac{UP}{\dot{m}c_p}dz \qquad \text{Equation 8}$$

Where P is the outside perimeter of the tube and U is the overall heat transfer coefficient defined with respect to the outside tube surface.
Integrating between T_{in} and T and 0 and z respectively, we obtain:

$$\ln\left(\frac{T - T_0}{T_{in} - T_0}\right) = -\frac{UP}{\dot{m}c_p}z \qquad \text{Equation 9} \qquad T(z) = (T_{in} - T_0)e^{\frac{-UPz}{\dot{m}c_p}} + T_0 \qquad \text{Equation 10}$$

Where T_{in} is the inlet temperature of the feedwater flowing in the tube.
NB: this result is mathematically equivalent to that which would have been obtained by applying the LMTD method to the tube.
If we are given the inlet temperature of the feedwater, we are therefore able to predict the temperature for any given z (and therefore the outlet temperature).
The previous model can be applied to zones 1,2,3.

Another important feature of the condensing zone is the condensate inlet from the superheater. The pressure of this condensate is much higher than that of the steam from the HP turbine. The condensate therefore expands in a valve and reaches the saturation pressure of the steam from the HP turbine (isenthalpic expansion).
Two scenarios are possible:

-if the enthalpy of the condensate is greater than that of the saturated liquid (at the saturation temperature dictated by the steam from the HP turbine), then the condensate will partially evaporate and the steam thus released will eventually condense on the tubes of zones 1,2,3. The fraction of condensate turning into steam can easily be calculated from an enthalpy balance between the inlet and outlet of the valve:

$$h_{condenste} = x_s h_{steam,sat} + (1 - x_s)h_{water,sat}$$

$$x_s = \frac{h_{condensate} - h_{water,sat}}{h_{steam,sat} - h_{water,sat}} \qquad \text{Equation 11}$$

Therefore, the mass flow rate of steam coming from the superheater condensate inlet is:

$$\dot{m}_{steam} = \dot{m}_{condensate} x_s \qquad \text{Equation 12}$$

-if the enthalpy of the condensate is greater than that of the saturated liquid, then the condensate will not evaporate. Its pressure will of course drop to that of the saturated water/steam mix from the HP turbine and its temperature T will vary in order to satisfy:

$$h(T_{condesnate}, P_{condensate}) = h(T, P_{sat}) \qquad \text{Equation 13}$$

In practice, $T \approx T_{condensate}$ since the enthalpy of a liquid is nearly independent of pressure. We will therefore have a jet of pure and colder water (relatively speaking, $T<T_{sat}$) entering the pre-heater. The saturated steam will therefore condense directly on the water-jet (at the expenses of the tubes). The model's assumption, i.e "condensation of the steam on the tubes" is no longer valid, which invalidates the results of the model. Besides, since $h_{condensate}<h_{water,sat}$, the mass flow obtained via equation 12 is negative, which leads to aberrant calculations in the model.

2.2.2 Flooded zone (zone 5)

2.2.2.1 Thermal model

Since the condensate's velocity in this part of the heat-exchanger is low, the shell-side heat resistance is high and the heat transfer rate low. This part of the pre-heater is therefore often neglected in thermal calculations. However, we will attempt to calculate an order of magnitude of the heat transfer rate in this zone.
If we have a closer look at the geometry, the flow pattern in the flooded zone is probably fairly complex and cannot be considered as purely counter- or parallel-flow. A direct attempt to calculate the heat transfer is analytically impossible and would require advanced computer modeling. A simple way of avoiding such complexities is by assuming that the temperature of the condensate is roughly constant in the entire flooded zone. This assumption is acceptable as long as:
-the power exchanged in this zone is low (which means that the temperature drop of the condensate between inlet and outlet is small)
-the water is sufficiently mixed (homogenous temperature)

If this assumption holds, we need not worry about the flow pattern: the heat exchanged can be directly derived from an equation similar to that of the condensation zone (since the main assumption, that is to say constant shell-side temperature, is also valid):

$$T(z) = (T_{in} - T_{condensate}) e^{\frac{-Upz}{\dot{m}c_p}} + T_{condensate} \qquad \text{Equation 14}$$

The main difficulty is to select a proper condensate temperature in the flooded zone. This problem will be addressed later on in the section (see paragraph 2.3.2).
NB: this part of the heat exchanger will thereafter be referred to as zone 5

2.2.2.2 Heat exchange surface

The heat exchange surfaces to consider in the flooded zone cannot be determined directly since, depending on the tube row considered, the fraction of the tube that is underwater varies.

Each tube coming out of the Kühlkasten describes a quarter of a circle in the flooded zone. The curvature of the tubes vary in the Kühlkasten, but the average curvature of a tube <R> is equal to that of the middle tube row (see Figure 7).

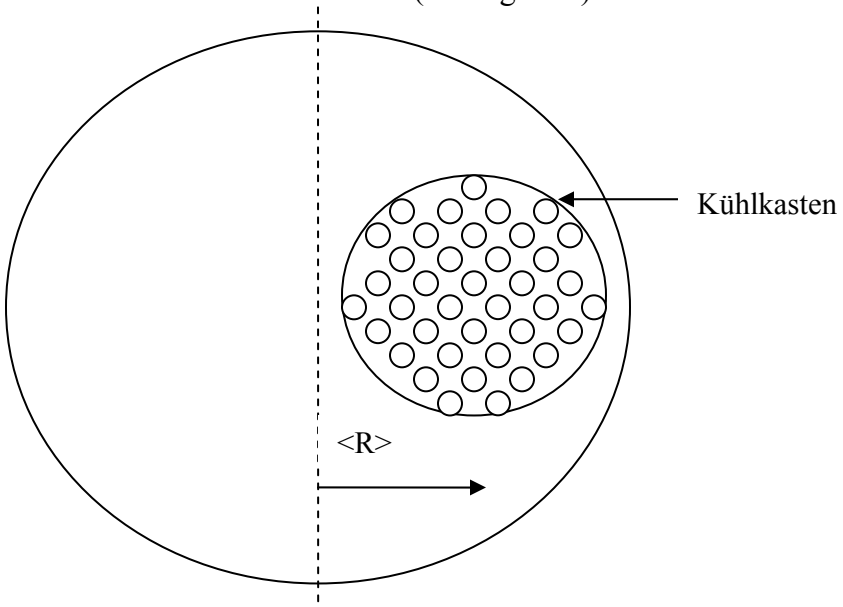

Figure 7: Cross-section of the pre-heater

The heat-exchange surface to consider is therefore:

$$S_1 = 2\pi r_{out} n \frac{2\pi < R >}{4} = < R > r_{out} \pi^2 n \qquad \text{Equation 15}$$

Where r_{out} is the outer radius of a tube and n is the total number of tubes in the Kühlkasten.

The calculation is more complicated for the rest of the tubes, given that the geometry considered is a semicircle minus the Kühlkasten.
In this second case, each tube outside the Kühlkasten describes an entire semicircle underwater. The exact surface could be calculated by a summation of the surface of each tube:

$$S_2 = \sum_i (2\pi r_{out}) \pi R_i \qquad \text{Equation 16}$$

If we consider the tube distribution as homogenous, then S_2 can be approximated by:

$$S_2 = \int_{\theta=0}^{\pi} \int_{R=0}^{R} \alpha(2\pi r_{0ut})\pi R R d\theta dR - 2S_1 \qquad \text{Equation 17}$$

α is the tube density per unit surface ($\alpha = \frac{n_{tot}}{\pi R^2/2}$),$2\pi r_{out}\pi R$ is the surface contribution of one tube and RdθdR is an elementary surface in polar coordinates. We must substract $2S_1$ from the previous integral since these tubes belong to the Kühlkasten.

$$S_2 = n_{tot}(2\pi r_{out})\pi\frac{2R}{3} - 2 < R > r_{out}\pi^2 n \qquad \text{Equation 18}$$

2.2.3 Kühlkasten counter-flow heat exchange zone

This part of the pre-heater can be modeled as a simple shell-and-tube heat exchanger. The condensate flows upwards around the baffles and the feedwater flows straightly downwards in the tubes. In order to avoid an iterative calculation process, we will resort to the NTU method of heat-transfer calculation. The heat transfer coefficient is this zone is calculated in such a way that the flow has to be considered as "counterflow": the counterflow NTU correlation will therefore be used.
The number of transfer units (NTU) is defined as:

$$NTU = UA/C_{min} \qquad \text{Equation 19}$$

Where C_{min} is the minimum $\dot{m}c_p$ (heat capacity rate), on the shell-side in our case.
We have two independent equations (the integrated form of Newton's law provided by the NTU equation and the energy balance) and two unknowns, namely the shell and tube outlet temperatures:

$$\begin{cases} \varepsilon = \dfrac{T_{s,in} - T_{s,out}}{T_{s,in} - T_{t,out}} = \dfrac{1 - e^{-NTU(1-C_r)}}{1 - C_r e^{-NTU(1-C_r)}} \\ \dot{m}_s c_{p,s}(T_{s,in} - T_{s,out}) = \dot{m}_t c_{p,t}(T_{t,out} - T_{t,in}) \end{cases} \qquad \text{Equation 20}$$

where Cr is the following ratio:

$$Cr = \frac{C_{\min}}{C_{\max}} = \frac{m_s c_{p,s}}{m_t c_{p,t}} \qquad \text{Equation 21}$$

Once the inlet and outlet temperatures calculated (by solving equation system 20), it is possible to calculate the temperature of any given point in this heat exchange zone. This can simply be done by applying the NTU method between the shell-side inlet and any z-coordinate:

$$\begin{cases} \varepsilon = \dfrac{T_{s,in} - T_s(z)}{T_{s,in} - T_t(z)} = \dfrac{1 - e^{-NTU(z)(1-C_r)}}{1 - C_r e^{-NTU(z)(1-C_r)}} \\ \dot{m}_s c_{p,s}(T_{s,in} - T_s(z)) = \dot{m}_t c_{p,t}(T_{t,out} - T_t(z)) \end{cases} \qquad \text{Equation 22}$$

Where NTU(z) is defined as previously but with the surface A(z) (surface between ordinates 0 and z) instead of the total surface A.
The two unknowns $T_s(z)$ and $T_t(z)$ can be obtained by solving the system. Note that it is not possible to solve this system before having applied the NTU method to the entire component since $T_{t,out}$ would not be known. We can therefore solve equation system 22 only *after* equation system 20.
NB: this part of the heat exchanger will thereafter be referred to as zone 4

2.3 Assembly of the different parts of the model

2.3.1 Degrees of freedom in zones 1,2,3

One might point out that if the outlet temperature of, say, zones 1 and 3 are determined via equation 10, the outlet temperature of zone 2 can be calculated directly via an energy balance on the condensing zone (Newton's law need not be used for zone 2).

$$\dot{m}_{steam}\Delta h_{l,v} = \dot{m}_1 c_{p,1}(T_{out,1} - T_{in,1}) + \dot{m}_2 c_{p,2}(T_{out,2} - T_{in,2}) + \dot{m}_3 c_{p,3}(T_{out,3} - T_{in,3}) \qquad \text{Equation 23}$$

If we do use the equation derived from Newton's law in order to calculate the outlet temperature of zone 3, then the energy balance may be violated.
In other words, this is an indication that the problem is overdetermined (there are more equations than unknowns). Consequently, the system requires another degree of freedom. At first it was assumed that the water-level would adjust itself so that the surface over which the condensation takes place would be the required degree of freedom (the water-surface would move up and down in order to make both sides of the energy equation match). However, after discussing this problem with engineers from the system department, it turns out that the water-level is controlled via a throttling device on the outlet condensate. By acting on this throttle, the control system makes sure that the water level does not vary in the pre-heater.

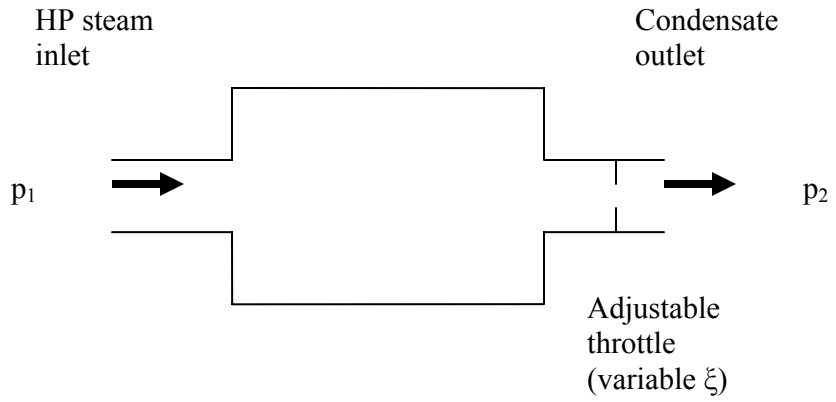

Figure 8: Water level control principle

Pressures p_1 and p_2 upstream and downstream of the pre-heater are fixed. Therefore, $\Delta p=p_1-p_2$ is also fixed. Neglecting the head losses in the component itself, this pressure drop must be equal to that created by the throttle:

$$\Delta P_{throttle} = \xi \rho \frac{V^2}{2} \qquad \text{Equation 24}$$

For a given value of ξ (given opening of the throttle), equation 24 therefore determines the velocity and thus the mass flow rate of steam traveling through the pre-heater.
If ξ increases (reduction of the flowing gap in the throttle), V (and therefore the mass flow) must decrease in order to maintain the fixed ΔP. Conversely, if ξ decreases (opening of the throttle), V (and therefore the mass flow) must increase.
Now let us suppose that the water-level in the pre-heater is too low. If we reduce the opening in the throttle, less steam will be sucked through the component. This means that the heat-exchange surface required to condense this steam (zones 1,2,3) will decrease. In other words, the water-level will rise. Conversely, if the water-level is too high, opening the throttle will lower the water-level.
It is thus possible to maintain a set water-level in the pre-heater. Consequently, the degree of freedom that we require is no longer the water-level but the mass flow rate of steam from the HP-preheater (via the throttling control system).
The mass flow of HP steam from the turbine is therefore no longer an input of the model but an output: for each set of operating conditions, the model will have to be iterated for different mass flows rates of steam until the energy balance in zones 1,2 and 3 matches.

2.3.2 Possible solving path

The different pieces of the model must now be combined in order to predict the outlet temperatures of the entire heat-exchanger.
For most of the zones we defined previously, it is not possible to calculate the outlet temperatures and temperature profiles directly since the inlet temperatures of the zone in question depends on the outlet temperature of other zones: the problem must be solved step by step.
A possible path goes as follows:

- Step 1: Assume a mass-flow rate of steam from the HP pre-heater

- Step 2: Determine the tube-side outlet temperature of zone 1: this is possible since we know the tube side inlet temperature and the shell-side temperature (saturation temperatures of the HP steam).

- Step 3: Assume a homogenous shell-side water temperature for zone 5 (flooded zone)

- Step 4: Deduce the Kühlkasten's shell-side and tube-side outlet temperature. This is possible since the shell-side and tube-side inlet temperatures are known (via the assumption of step 3 and via the feedwater inlet temperature respectively). Besides, the mass-flow rate of condensate is also known since we assumed a mass-flow rate of steam from the HP pre-heater in step 1.

- Step 5: Determine the tube-side outlet temperatures of zone 5 (flooded zone). Note that two outlet temperatures must be calculated here, one for the tubes previously in the Kühlkasten (zone 4) and another for the tubes previously in zone 1. This calculation is now possible since the outlet temperatures from zones 4 and 1 are known and the shell-side temperature is assumed constant (and equal to our assumed temperature, step 3).

- Step 6: Set up an energy balance over zone 5 (flooded zone): this is possible since we know the inlet and outlet tube-side temperatures and the inlet and outlet shell-side temperatures (HP steam saturation temperature and assumed homogenous temperature respectively). If the two sides of the energy balance don't match, go back to step 2 and reiterate the calculations with a different homogenous temperature for zone 5. If the two sides of the energy balance match, move on to step 7.

- Step 7: Determine the outlet temperatures of zones 2 and 3. Both can be obtained by using equation 10. Check the energy balance on the condensing zone and if it does not match go back to step 1 and reiterate for a different mass flow rate of steam from the HP-turbine.

2.4 Calculation of the heat transfer coefficients

The overall heat resistance takes into account three local resistances:

-a film transfer resistance between the tube and the outer fluid: h_{out}
-a conductive resistance due to the tube itself
-a film transfer resistance between the tube and the inner fluid: h_{in}

Mathematically, the overall resistance is given for a cylindrically-shaped tube by the following equation:

$$U = \frac{1}{\frac{A_0}{A_{out}h_{out}} + \frac{A_0}{A_{in}h_{in}} + \frac{A_0 \ln(\frac{r_{out}}{r_{in}})}{2\pi L\lambda}} \qquad \text{Equation 25}$$

where A_{out} and A_{in} represent the outer and inner surfaces of the tube respectively, L represents the total length of the tube, A_0 is the surface considered when writing Newton's law, λ is the thermal conductivity and r_{out} and r_{in} represent the outer and inner radii of the tube.

2.4.1 Tube-side heat transfer coefficient

According to [1], the average h_{out} coefficient can be calculated via the following Nusselt number correlation:

$$Nu_{m,T} = \frac{(\xi/8)\,\mathrm{Re}\,\mathrm{Pr}}{1+12{,}7\sqrt{\xi/8}(\mathrm{Pr}^{2/3}-1)}(1+(\frac{d_i}{l})^{2/3}) \qquad \text{Equation 26}$$

$$\xi = (1{,}8\log_{10}(\mathrm{Re}) - 1{,}5)^{-2} \qquad \text{Equation 27}$$

l is the tube length and d_i is the hydraulic diameter:

$$d_i = \frac{4A}{U} \qquad \text{Equation 28}$$

where A is the cross-sectional area of the flow and U is the related contact length (d_i is equal to the tube's inner diameter in the case of flow inside pipes).
Re and Pr numbers were calculated for the average mean pressure and temperature.
This correlation is valid for $2300<Re<10^6$ and $d_i/l<1$ (these conditions were indeed fulfilled in our case).

The influence of the wall's temperature was then taken into account by multiplying the previous Nu number by $\left(\frac{\mathrm{Pr}}{\mathrm{Pr}_w}\right)^{0,11}$:

$$Nu = Nu_m\left(\frac{\mathrm{Pr}}{\mathrm{Pr}_W}\right)^{0,11} \qquad \text{Equation 29}$$

where Pr_w is the fluid's Prandt number at the wall's temperature.

2.4.2 Shell-side heat transfer coefficient in zone 5 (flooded zone)

The shell-side heat transfer coefficient in this zone was also obtained with the previous Nusselt correlation. The velocity used in the Reynolds number was that of the condensate as it flows downwards towards the inlet of the Kühlkasten:

$$v = \frac{\dot{m}}{\rho A} \qquad \text{Equation 30}$$

Where A is the available flow surface, that is to say the surface of the cross-section of the pre-heater minus the surface occupied by the tubes and the Kühlkasten.
Strictly speaking, the length l (length along which the shell-side water flows) varies with the tube considered, which means that a different Nu number should be calculated for each tube. This problem was simplified by considering the average flow length in the flooded zone. If we approximate the discrete tube layout by a continuous layout, the average tube distance from the centre of the preheater is:

$$\langle r \rangle = \frac{\int_{\theta=0}^{\theta=2\pi}\int_{r=0}^{r=R} r^2 dr d\theta}{\pi R^2} = \frac{2R}{3} \qquad \text{Equation 31}$$

If we consider that the shell-side water flows along one fourth of the underwater tube-circle between inlet and outlet of the flooded zone, the length to consider in the Nu correlation can be approximated by:

$$l \approx \frac{2\pi\langle r \rangle}{4} = \frac{\pi R}{3} \qquad \text{Equation 32}$$

2.4.3 Shell-side heat transfer coefficient in zones 1,2,3 (condensation zones)

All calculations were carried out according to [2].

In the following calculations, given the moderate steam velocity, the shear stress of the flowing steam was neglected.
The average Nu number is obtained as follows:

$$Nu = ((f_{well} Nu_l)^n + Nu_t{}^n)^{1/n} \qquad \text{Equation 33}$$

$$\text{where } f_{well} = \mathrm{Re}_F{}^{0,04} \text{ Equation 34} \quad \text{and } \mathrm{Re}_F = \frac{\dot{m}_F}{n\pi d\eta} \quad \text{Equation 35}$$

where $\dot{m}_F$ is the mass flow rate of condensed steam flowing around the tube at the end of condensing zone and n the number of tubes upon which the steam condenses.
The turbulent and laminar Nusselt numbers are calculated as follows:

$$Nu_l = 0{,}943 \left(\frac{1 - \rho_D / \rho}{\frac{PhGa^{1/3}}{\mathrm{Pr}}} \right)^{1/3} \qquad \text{Equation 36}$$

$$\text{and } Nu_t = a \left(\frac{PhGa^{1/3}}{\mathrm{Pr}} \right)^b \mathrm{Pr}^c \qquad \text{Equation 37}$$

(in our case, a=2,137E-4 , b=0,6181 and n=1,67)

$$\text{Where } Ga^{1/3} = \frac{L}{\ell} \qquad \text{Equation 38} \qquad \ell = \left(\frac{\nu^2}{g} \right)^{1/3} \qquad \text{Equation 39}$$

and L is the tube length in the condensing zone

$$Ph = \frac{c_p (\vartheta_D - \vartheta_W)}{\Delta h_v} \qquad \text{Equation 40}$$

where D refers to the steam (Dampf in German) and W to the wall.
The Nusselt number itself is defined in this case as:

$$Nu = \frac{h\ell}{\lambda} \qquad \text{Equation 41}$$

In order to estimate the wall temperatures, an order of magnitude of the inner and outer transfer coefficients had to be assumed. The outer wall temperature was then obtained by solving the following equation:

$$h_{out} (T_{out} - T_{out,wall}) = h_{overall} (T_{out} - T_{in}) \qquad \text{Equation 42}$$

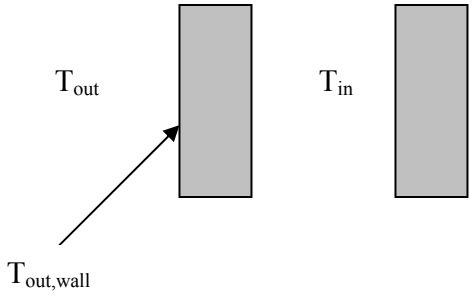

Figure 9: Inner, outer and wall temperatures

2.4.4 Shell-side heat transfer coefficient in the Kühlkasten (zone 4)

On the shell-side of the Kühlkasten, the flow of the condensate is partly cross-flow and partly counter-flow since the baffles constrain the flow.
However, the flow can be considered 100% counter-flow if the heat transfer coefficient is calculated accordingly. According to [3], the Nusselt number in this case is given by:

$$Nu_{0,AW}=f_W\, Nu_{0,\,Bündel} \qquad \text{Equation 43}$$

Where $Nu_{0,\,Bündel}$ is the Nusselt number calculated for a bundle in cross-flow conditions and f_W is a correction factor taking into account the various differences between the ideal cross-flow situation and the actual situation on the shell-side of the heat exchanger.

$$Nu_{0,\,Bündel} = f_A Nu_{l,0} \qquad \text{Equation 44}$$

where f_A is a parameter taking into account the tube pattern in the bundle

$$Nu_{l,0} = 0{,}3 + \sqrt{Nu_{l,lam}{}^2 + Nu_{l,turb}{}^2} \qquad \text{Equation 45}$$

$$\text{Where } Nu_{l,lam} = 0{,}664\sqrt{\mathrm{Re}_{\psi,l}}\,\mathrm{Pr}^{1/3} \qquad \text{Equation 46}$$

$$Nu_{l,turb} = \frac{0{,}037\,\mathrm{Re}_{\psi,l}{}^{0,8}\,\mathrm{Pr}}{1 + 2{,}443\,\mathrm{Re}_{\psi,l}(\mathrm{Pr}^{2/3} - 1)} \qquad \text{Equation 47}$$

where $\mathrm{Re}_{\psi,l} = \frac{wl}{\psi\nu}$ Equation 48, $\psi = 1 - \frac{\pi}{4ab}$ Equation 49

$$l = \frac{\pi}{2} d_a \qquad \text{Equation 50}$$

(d_a is the tube outer diameter) and a and b are the ratio of the tube pitch (in the x and y directions respectively) and the tube diameter.
For a staggered layout, f_A is given by:

$$f_{A,stag} = 1 + \frac{2}{3} b \qquad \text{Equation 51}$$

The correction factor f_w is the product of three separate factors f_G,f_L and f_B accounting for the non-pure counter-flow, the leakage flow in-between tubes and baffle bores and the bypass-flow respectively.

$$f_G = 1 - R_G + 0{,}524 R_G^{\,0{,}32} \qquad R_G = n_F/n \qquad \text{Equation 52}$$

where n is the total number of tubes and n_F is the number of tubes in the top and bottom windows (a window is defined as the space not blocked by a baffle).

$$f_L = 0{,}4 + \frac{A_{SRU}}{A_{SG}} + (1 - 0{,}4 \frac{A_{SRU}}{A_{SG}}) e^{-1{,}5 R_L} \qquad \text{Equation 53}$$

$$A_{SRU} = (n - \frac{n_F}{2}) \frac{\pi (d_B^{\,2} - d_a^{\,2})}{4} \qquad \text{Equation 54}$$

$$A_{SMU} = \frac{\pi}{4} (D_i^{\,2} - D_l^{\,2}) \frac{360 - \gamma}{360} \qquad \text{Equation 55}$$

where d_b is the diameter of a baffle-bore, d_a the outer diameter of a tube, D_i the inner shell diameter and D_l the diameter of a baffle and γ is the angle defined by the two ends of the straight edge of the baffle and the centre of the baffle.

$$R_L = \frac{A_{SG}}{A_E} \qquad \text{Equation 56} \qquad \text{where} \qquad A_{SG} = A_{SRU} + A_{SMU} \qquad \text{Equation 57}$$

$$\text{and } A_E = SL_E \qquad \text{Equation 58}$$

where L_E is the shortest free path between tubes from one end of the baffle to the other (measured along a diameter) and S is the pitch between baffles.

In our case:

$$f_B = e^{-\beta R_B (1-(\frac{2n_s}{n_w})^{1/3})} \qquad \text{Equation 59}$$

Where β=1,35 , the number of "anti-bypass" plates n_s=0 and

$$R_B = \frac{A_B}{A_E} \qquad \text{Equation 60} \qquad \text{where} \qquad A_B=S(D_i-D_B-e) \qquad \text{Equation 61}$$

D_B is the diameter of the circle that encompasses the outer tube row, S is the distance between two consecutive baffles and e is the distance between two adjacent tubes along a diameter.

2.4.5 Fouling thermal resistance

The early versions of the model do not take into account any fouling on the tubes. However, it turns out that the tubes are prone to fouling, especially on the shell-side (the feedwater is very pure indeed and tube-side deposits are therefore unlikely).
Version 3 (and all later versions) of the model enable the user to specify the thickness and the thermal conductivity of the deposit.
In order to keep the reference surfaces valid in all the previous calculations, the heat transfer coefficients still refer to the surface of the tubes *without any deposit*, that is to say the outer surface of the metallic tubes.
The heat exchanged by a tube of length L can be written (per unit time):

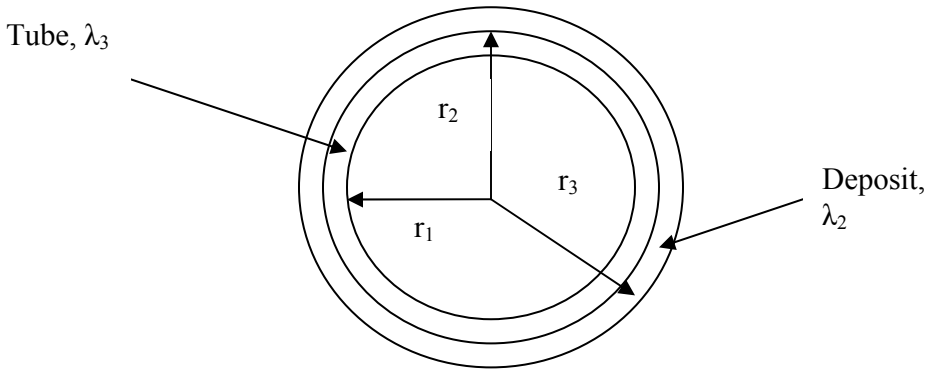

Figure 10: tube with fouling deposit

$$\Phi = \frac{T_{out} - T_{in}}{\frac{1}{h_{in} L 2\pi r_1} + \frac{\ln(r_2 / r_1)}{2\pi\lambda_1 L} + \frac{\ln(r_3 / r_2)}{2\pi\lambda_2 L} + \frac{1}{h_{out} L 2\pi r_3}} \qquad \text{Equation 62}$$

If we choose $L2\pi r_2$ (outer metallic surface) as the reference surface, then we obtain:

$$\Phi = L2\pi r_2 U (T_{out} - T_{in}) = L2\pi r_2 \frac{1}{\frac{r_2}{h_{in} r_1} + \frac{\ln(r_2 / r_1) r_2}{\lambda_1} + \frac{\ln(r_3 / r_2) r_2}{\lambda_2} + \frac{r_2}{h_{out} r_3}} (T_{out} - T_{in})$$

Equation 63

Equation 63 defines the overall heat transfer coefficient U that has to be considered in the calculations.

2.5 Implementation of the model on excel and model limitations

2.5.1 Excel version of the model

The coefficients required by the model (especially the heat transfer coefficients) and the iterative solving-process make the model extremely time-consuming to implement by hand. Therefore, all the correlations and equations were entered in an excel spread-sheet. The inlet conditions and the geometrical parameters defining the system were all gathered on one page of the spread-sheet. Overall results such as heat fluxes and outlet temperatures for each zone and for the entire component were gathered on another page. Finally, details for each zone on the heat-transfer calculations were displayed on specific pages.

The time-consuming iterative process can be accelerated by using the iterative function of excel. The mass flow rate of steam from the HP-turbine can first be iterated until the "zone 3" energy balance matches. The "zone 5 condensate temperature" can thereafter be iterated until the "zone 5" energy balance matches. The modifications involved by this second iteration will make it necessary to reiterate the mass flow rate (and, in turn, the zone 5 condensate temperature). However, the model converges quickly and after two or three steps, the values obtained are stable.

2.5.2 Limitations of the model

Inlet parameters and geometrical features can be varied around the usual operating conditions in order to test the response of the pre-heater. However, these variations should remain small for a number of reasons:

-the properties of water underpinning the calculations of the heat transfer coefficients (such as the density, the specific heat or the thermal conductivity) may not remain valid if the operating conditions change dramatically. The user will therefore have to modify the "estimated temperatures" the properties refer to.

-the correlation used in the heat transfer coefficients are only valid for a given range of Prandtl and Reynold numbers. Exceeding the boundary values for the correlations will lead to inaccurate results

-If the temperature of the inlet steam from the HP turbine is too high, the condensate coming from the superheater will not evaporate at all (and the steam from the HP turbine will condense directly on the water jet). The assumption "condensation of the steam on the tubes" is violated. Besides, we obtain a negative mass flow of steam from equation 12 which leads to aberrant results in the model.

2.6 Results

In the following paragraphs, the results of the model are presented. The white cells correspond to inputs of the model, the grey cells to results.
NB: all the geometric characteristics of the system (which make up most of the inputs) are not presented here

2.6.1 Operating conditions

Inlet parameters		mass flow rate (kg/s)	Temperature (°C)	Pressure (bar)	steam fraction (-)
tube-side		705,1	178,8	80	-
shell-side	bled steam (and water)	54,7814	216,61	21,72632043	0,9107
	condensate from superheater	37,24	218,3	56,17	-

Table 1: Non-geometrical model inlet parameters

Note that the mass flow rate of bled steam is not an input of the model but an output since it was calculated in order to make the energy balance in zones 1,2 and 3 match (hence the grey cell). The pressure of the bled steam is also determined by the model since the steam is saturated and we know its temperature.

2.6.2 General results

	Temperatures	°C	°C	Heat flux (MW)
entire pre-heater		inlet	outlet	
	shell-side	216.61	179.84	108.90
	tube-side	178.8	213.53	108.79
zone 1		inlet	outlet	
	shell-side	216.61	216.61	
	tube-side	178.8	207.45	61.21
zone 2		inlet	outlet	
	shell-side	216.61	216.61	
	tube-side	193.19	210.96	17.68
zone 3		inlet	outlet	
	shell-side	216.61	216.61	
	tube-side	207.90	214.71	14.82
zone 4		inlet	outlet	
	shell-side	212.28	179.84	13.36
	tube-side	178.8	192.35	13.26
zone 5		inlet	outlet	
	shell-side	216.61	212.28	1.82
	tube-side, tubes from zone 1	207.45	207.90	0.99
	tube-side, tubes from zone 4	192.35	193.19	0.82

Table 2: Model results

The mass flow rate of bled steam is: 54,78 kg/s

Note: the shell-side and tube-side energy balances do not match exactly because of the constant c_p assumption necessary for the model and the imperfect iteration.

As expected, most of the energy (approximately 85%) is exchanged in zones 1,2 and 3 where the steam condenses. The contribution of the flooded zone is small (approximately 1.5%), which is why it was neglected in all the previous reports.

2.6.3 Comparison with design conditions

The design conditions were retrieved from [4]. They have been recapped in Table 3.

Inlet parameters		mass flow rate (kg/s)	Temperature (°C)	Pressure (bar)	steam fraction (-)
tube-side		705,1	178,8	80	-
shell-side	bled steam (and water)	55,86	216,61	21,72632043	0,9107
	condensate from superheater	37,24	218,3	56,17	-

	Temperatures	°C	°C	Heat flux (MW)
entire pre-heater		inlet	outlet	
	shell-side	216,61	186,50	108,1
	tube-side	178,8	213,30	108,1

Table 3: Design parameters

Now if we compare the design conditions with the model's output we notice that the feedwater outlet temperature and the heat flux match quite well (213,3°C and 213,53°C; 108,1MW and 108,9MW respectively).
The amount of steam drawn by the component from the turbine is slightly smaller in the model (54,78 kg/s in the model and 55,86 kg/s in the design data) which means that the actual heat transfer rate in the condensation zone is not quite as high as expected.
The main discrepancy between the model and the design parameters is the outlet temperature of the condensate: 179,84°C according to the model and 186,5°C according to the design data. We are going to check that this difference is not aberrant with a back-of-the-envelope calculation.

The extra subcooling of the condensate in the model's calculation must offset:
-the slightly greater heat flux: 108,9-108,1=0,8 MW
-the smaller amount of heat transferred via condensation (due to the smaller mass flow rate of HP steam): $(55,86\text{-}54,78)*\Delta h_{w,s} = 2,02$ MW
The power difference is therefore 2,02+0,8=2,82 MW. The order of magnitude of expected temperature difference is therefore:

$$\Delta T = \frac{W}{\dot{m}c_p} = \frac{2,82*10^6}{(54,78+37,24)*4420} \approx 6,9°C$$ which is consistent with the actual 186,5-179,84=6,66°C temperature difference between model and design data.

Physically speaking, this greater subcooling is partly achieved because we did not neglect zone 5 (flooded zone) in our calculations (it creates roughly an extra 4,3°C temperature drop in the condensate). This zone was indeed neglected in all design calculations.

The second main reason is that, as was pointed out in report [5], the in-built heat exchange surface in the Kühlkasten is much larger than the required surface.

2.6.4 Effect of fouling on the pre-heater

Simulations have been run with shell-side fouling on various zones of the pre-heater. The results have been summarised in the following table.

		outlet (°C)	MW	m of HP steam (kg/s)
Design data	shell-side	186,50	108,10	55,860
	tube-side	213,30	108,10	
Model with no deposit	shell-side	179,69	108,91	54,758
	tube-side	213,53	108,81	
Model with $\lambda_{deposit}$=4 $W.m^{-1}.K^{-1}$ and...				
1,5mm deposit **only on zones 4 and 5** R_f=3,75E-4 $m.W^{-1}.K^{-1}$	shell-side	186,14	108,34	55,867
	tube-side	213,34	108,20	
1,5 mm of deposit on zones 1,2,3,4,5 R_f=3,75E-4 $m.W^{-1}.K^{-1}$	shell-side	183,67	81,66	40,921
	tube-side	204,95	81,56	
1 mm of deposit on zones 1,2,3,4,5 R_f=2,5E-4 $m.W^{-1}.K^{-1}$	shell-side	182,60	89,43	44,906
	tube-side	207,41	89,33	
0,5 mm deposit on zones 1,2,3,4,5 R_f=1,25E-4 $mW^{-1}.K^{-1}$	shell-side	181,26	98,70	49,619
	tube-side	210,32	98,59	
0,1mm deposit on zones 1,2,3,4,5 R_f=2,5E-5$m.W^{-1}.K^{-1}$	shell-side	180,01	106,88	53,740
	tube-side	212,89	106,78	

Table 4: Effect of fouling on the pre-heater's performance

The first result of these simulations is that fouling has a much more detrimental effect on the condensation zone (zones 1,2 and 3) than elsewhere. This can be seen by comparing the simulation with no deposit and the simulation with deposits on zones 4,5 and zones 1,2,3,4,5. Fouling in zones 4,5 reduces the heat flux by approximately 0,57MW whereas fouling on zones 1,2,3,4 and 5 reduces the heat flux by 27,25MW! This is simply because most of the heat exchange (85%) takes place in zones 1,2 and 3: an additional thermal resistance has therefore a greater effect.

The second result is that unlike fouling in zones 4 and 5, fouling in the condensation zone *reduces* the amount of HP steam drawn from the turbine. This can be simply accounted for: fouling in the condensation zone decreases the heat transfer rate which in turn decreases the amount of required steam.

A third interesting result is that fouling in zones 4 and 5 *increases* the amount of HP steam bled from the turbine! This surprising result can be explained as follows. Fowling in zone 4 and 5 will significantly reduce the temperature of the feedwater which is to enter zone 2. Since the tube-side temperature is lower in zone 2, the heat exchange is enhanced and the amount of steam required is thus increased.

With a homogenous fouling on all zones, it is not possible for the pre-heater to reach the design conditions: reaching the design outlet temperatures automatically modifies the amount of bled steam which no longer matches that of the design conditions.
However, if we only impose fouling on zones 4 and 5 (which has a weaker impact on the mass flow rate of bled steam), conditions close to that of the design sheet can be reached. This is visible in the table with a 1,5mm deposit on zones 4 and 5. The equivalent thermal resistance is then:

$$R_f \approx \frac{e}{\lambda} = \frac{1{,}510^{-3}}{4} = 3{,}7510^{-4}\, m.W^{-1}.K^{-1} \qquad \text{Equation 64}$$

3 Velocity profiles in the condensation-zone of the pre-heater

3.1 Flow pattern in the pre-heater

In the thermal analysis of the pre-heater, we pointed out that the amount of high-pressure steam which is bled from the turbine depends on the heat-exchange surface in the condensation zone and on the temperature of the tubes in this zone. Given these conditions (surface and temperature), the pre-heater will draw enough steam from the turbine to provide the required amount of heat to the tubes.
On a more local scale inside the condensation-zone of the pre-heater (zones 1,2,3), the amount of steam reaching a given tube is also determined by its temperature. The steam mass-flow rate (and thus the velocities) inside the bundle is therefore driven by the temperature distribution.
In order to reach a given surface and condense there, the steam could theoretically flow along any "path". However, a resistance is associated to each path: the greater the resistance of the path, the smaller the mass-flow rate flowing along this path. This means that the bulk of the steam will flow along the path of lowest resistance.
If we apply these considerations to the pre-heater, most of the steam is likely to flow as follows to reach a given point in the bundle:

-downwards or upwards flow around the bundle in the space between the bundle and the shell

-once the required vertical ordinate has been reached, penetration of the bundle and horizontal flow to the desired tube

This path will indeed present a much smaller resistance than a direct penetration of the bundle and then a vertical flow inside the bundle to the desired vertical ordinate.

These facts suggest that it would be interesting to calculate two separate velocity profiles:

-the vertical velocity of the upward/downward flow between the bundles and the shell

-the horizontal velocity of the stream penetrating the bundle (for a given vertical ordinate). Calculating this "cross-flow" velocity is especially important since it might lead to flow-induced vibrations in the bundle (see section 6).

Near the HP steam inlet, a protection plate deflects the high-velocity steam in order to avoid erosion and vibration problems. This special configuration (which leads to higher average horizontal velocities since part of the flow surface is blocked) is considered in 3.3.2.

3.2 Vertical velocity profile between the bundle and the shell

3.2.1 Model

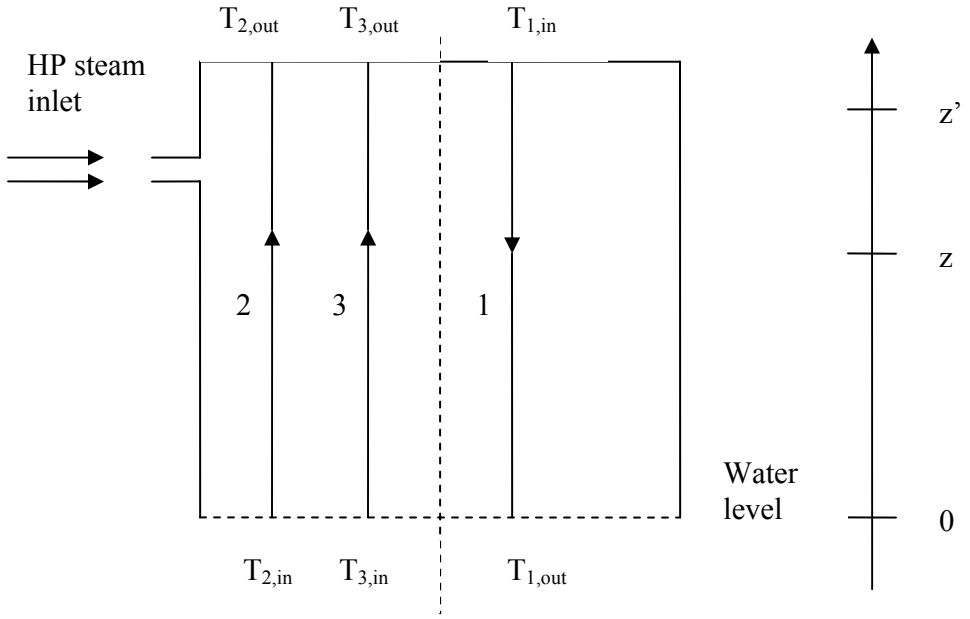

Figure 11: Velocity profile model

As explained in 3.1, the steam mass-flow rate and the velocity profiles are governed by the heat-exchange equations which determine the amount of steam required. By setting up an energy balance, we can calculate this amount for any given ordinate.
If the vertical ordinate we consider is above the HP steam inlet, the steam flows upwards and an energy balance yields:

$$\dot{m}(z')\Delta h_{s,w} = \dot{m}_1 c_p (T_1(z') - T_{1,in}) + \dot{m}_2 c_p (T_{2,out} - T_2(z')) + \dot{m}_3 c_p (T_{3,out} - T_3(z')) \quad \text{Equation 65}$$

The velocity is therefore:

$$v(z') = \frac{\dot{m}_1 c_p (T_1(z') - T_{1,in}) + \dot{m}_2 c_p (T_{2,out} - T_2(z')) + \dot{m}_3 c_p (T_{3,out} - T_3(z'))}{\Delta h_{s,w} \rho A} \quad \text{Equation 66}$$

Where A is the area available for steam-flow between the shell and the bundle. This available area is represented in Figure 12.

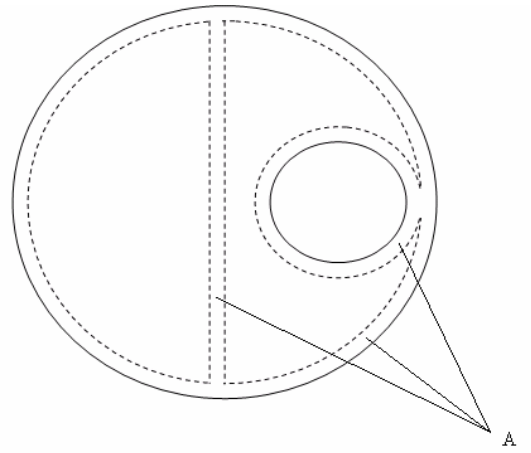

Figure 12: Available flow surface

If the vertical ordinate we consider is below the HP steam inlet, the steam flows downwards and an energy balance between 0 and z reads:

$$\dot{m}(z)\Delta h_{s,w} = \dot{m}_1 c_p (T_{1,out} - T_1(z)) + \dot{m}_2 c_p (T_2(z) - T_{2,in}) + \dot{m}_3 c_p (T_3(z) - T_{3,in}) \quad \text{Equation 67}$$

The velocity is therefore:

$$v(z) = \frac{\dot{m}_1 c_p (T_{1,out} - T_1(z)) + \dot{m}_2 c_p (T_2(z) - T_{2,in}) + \dot{m}_3 c_p (T_3(z) - T_{3,in}}{\Delta h_{s,w} \rho A}) \quad \text{Equation 68}$$

3.2.2 Results

The flow area A is roughly 0,75m^2. This leads to the following results.

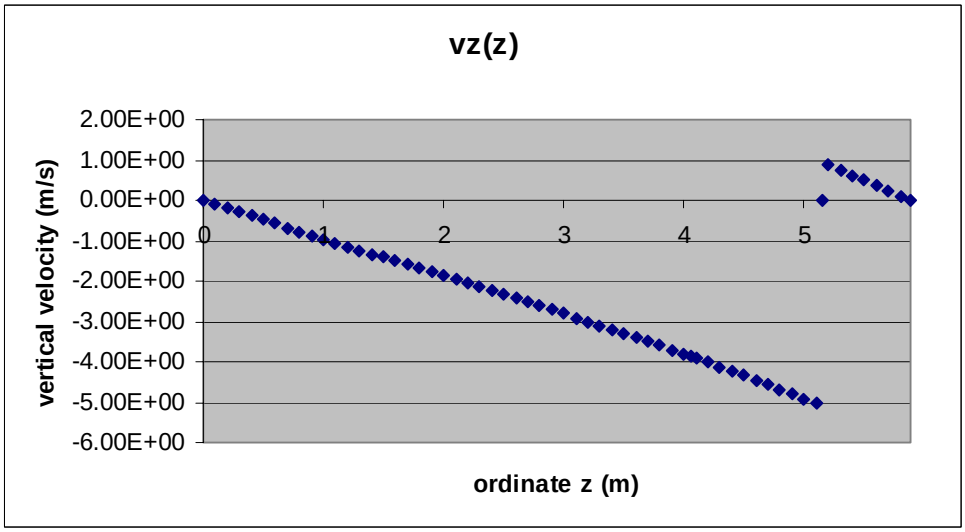

Figure 13: Axial velocity for different ordinates

As the steam enters the shell (z=5.155m) it splits into two separate streams which flow either upwards or downwards. However, most of the steam flows downwards since most of the condensing surface is situated below the HP-steam inlet (hence the greater downwards velocity on the graph). As the steam moves away from the inlet, it condenses. This explains why $|v(z)|$ decreases when we move away from z = 5.155m
Eventually, at the top of the bundle and at the water surface, the velocity drops to 0 since there is no steam left.

3.3 Horizontal velocity profile

3.3.1 Flow far from the HP steam inlet

3.3.1.1 Model

For each vertical ordinate, the amount of steam required by tube zones 1, 2 and 3 are known (via the energy balance). If we know which surface (per unit length) is available for this flow, we can determine the average velocity of the steam entering the bundle.

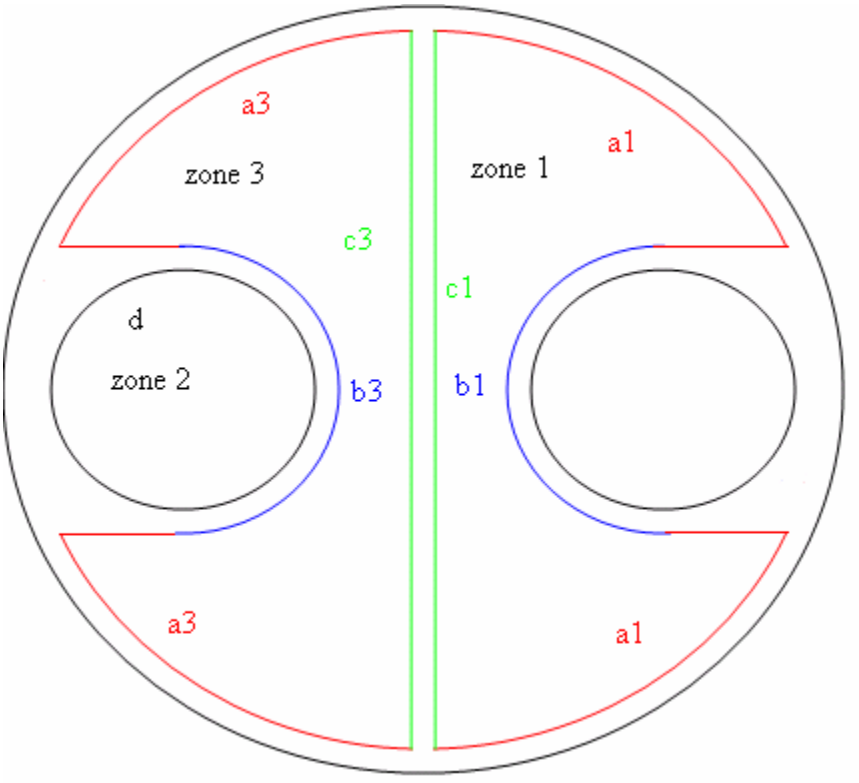

Figure 14: Possible flow surfaces

Unfortunately, it is not entirely clear whether the steam can take advantage of the total surface when entering a tube zone (the support grid may screen off part of the theoretically available surface). The available surface was therefore split into a sum of smaller surfaces which were taken into account or neglected according to the scenario considered.
For example in tube zone 1, it is certain that the steam will flow through a_1 but the flow through b_1 and c_1 is more hypothetical. Therefore, various scenarios taking into account a_1 alone, a_1 and b_1, a_1 and c_1 or a_1, b_1 and c_1 were considered.

For any vertical ordinate z, we can write:

$$\dot{m}_i'(z)\Delta h_{s,w} = US(T_{out} - T_i(z)) \qquad \text{Equation 69}$$

Where $i \in \{1,2,3\}$ and refers to the tube zone considered, $\dot{m}_i'(z)$ is the mass flow rate per unit length that enters zone i, T_{out} is the saturation temperature of the HP steam, U is the overall heat transfer coefficient and S is the tube surface per unit length (heat-exchange surface per unit length).
Once $\dot{m}_i'(z)$ determined via equation 69, the steam velocity at the inlet of the tube bundle $v_i(z)$ can be calculated via:

$$v_i(z) = \frac{\dot{m}_i'(z)}{\alpha\rho S^*} = \frac{US(T_{out} - T_i(z))}{\alpha\rho S^* \Delta h_{s,l}} \qquad \text{Equation 70}$$

Where S* is the surface (per unit length) considered in the scenario for tube zone i and α is the available volume fraction in the bundle. The steam entering the bundle can indeed only flow through the gaps in-between tubes. The calculation of α is presented at the end of 3.3.2.2.

3.3.1.2 Results

The velocity profiles presented in this section have been obtained with the following flow lengths:

reference	a1	a1 and b1	a1 and c1	a1 and b1 and c1	d/2	d
length (m)	3,16	4,54	5,31	6,69	1,20	2,40

Table 5: Flow lengths

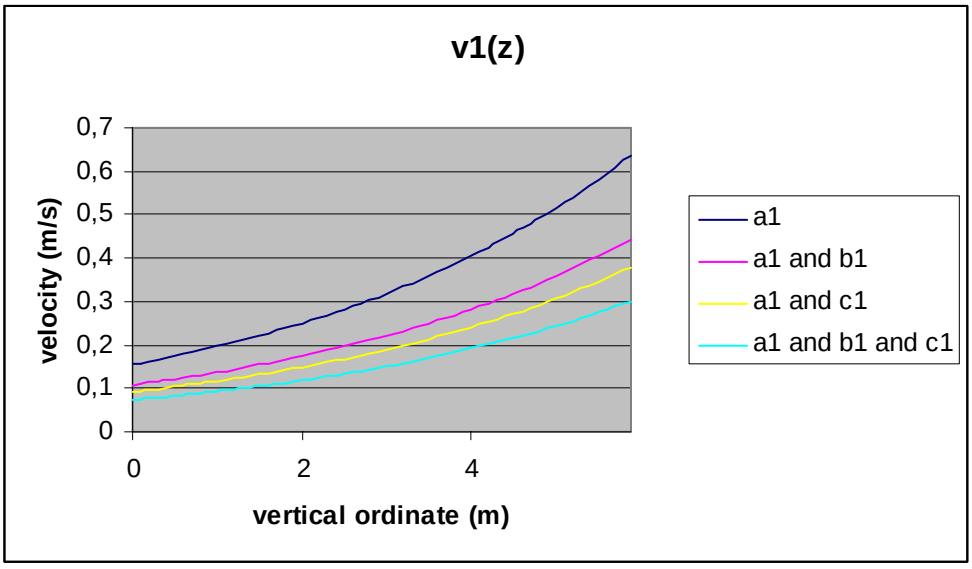

Figure 15: Bundle inlet velocity in zone 1 as a function of the ordinate

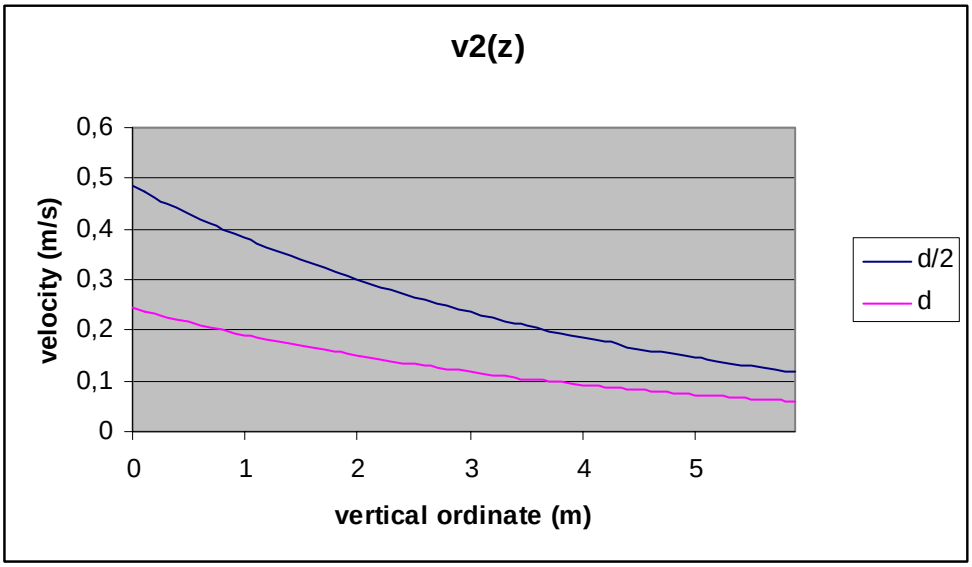

Figure 16: Bundle inlet velocity in zone 2 as a function of the ordinate

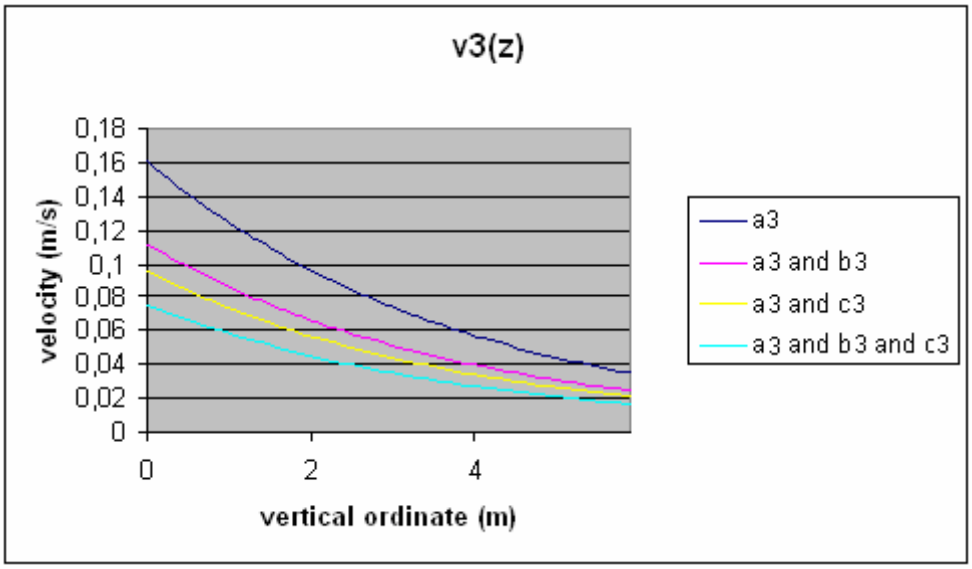

Figure 17: Bundle inlet velocity in zone 3 as a function of the ordinate

The previous velocity profiles can be understood qualitatively. In the case of tube zone 1, the (tube-side) feedwater warms up as it travels downwards which means that less and less steam condenses against the tube, thus leading to lower steam requirements and velocities. In the cases of zones 2 and 3, the tube-side feedwater warms up as it travels upwards which means that this time, the amount of steam required and the velocity of this steam decrease with z.

3.3.2 Local analysis of the high-pressure steam inlet

As explained above, at the high-pressure steam inlet, a plate is fixed to the tube bundle in order to protect the tubes from erosion (the velocity of the steam and water droplets is indeed very high, see 3.3.2.1). The purpose of this section is to present a simple model which can take into account the presence of this protection plate and assess the resulting steam velocity at the bundle inlet.
Since part of the bundle is shielded by the plate, the steam cannot enter directly into the bundle: it has to flow around or over the plate and then enter the condensation zone. If the steam takes the "over" route to reach the tubes, the resultant velocity will be axial (along the tubes), situation which is not likely to lead to flow-induced vibrations. However, if the steam flows around the plate, it will penetrate the bundle as a cross-flow stream, which might trigger off flow-induced vibrations. Strictly speaking, the flow will divide into two separate streams flowing either along the "over" or "around" route. However, in order to carry out conservative calculations, we will assume that all the steam flows around the bundle and penetrates the bundle as a cross-flow stream.

There are an infinite number of ways the steam can enter the bundle to reach the inner tubes. However, a resistance is associated to each path, and the magnitude of this resistance will determine the amount of steam that will flow along the path in question.

Little steam will flow along paths with high resistance whereas paths with low resistance will sustain a higher mass flow rate.
As can be seen in Figure 18, the steam has to flow from a given pressure P_0 outside the bundle to a pressure P_1 between zones 2 and 3. The overall mass flow rate is known since the amount of steam required can be calculated as previously with an energy balance. The question is therefore "for any given point on the outer edge of the bundle, what is the mass flow rate per unit surface (and therefore the velocity)?"

3.3.2.1 Inlet steam velocity

The purpose of this section is to calculate an order of magnitude of the HP steam velocity as it enters the pre-heater. This steam is not dry (x_s=0,9107), which means that droplets of water are carried in the flow. Strictly speaking, we have to deal with a two-phase flow problem. In order to avoid the complexities (and the highly empirical correlations) of two-phase flow and since we are only interested in an order of magnitude of the actual velocity, we are going to assume a no-slip condition between water and steam ($v_{water} = v_{steam}$).
The continuity equation reads:

$$v_s = \frac{\dot{m}_s}{\rho_s S_s} \quad and \quad v_w = \frac{\dot{m}_w}{\rho_w S_w} \quad ; \quad \dot{m} = \dot{m}_s + \dot{m}_w \qquad \text{Equation 71}$$

where S_s and S_w are the cross-sections across which the steam and the water flow, $\dot{m}_s$ is the mass flow rate of steam and $\dot{m}_w$ is the mass flow rate of water.
If we now add the no-slip condition and the cross-section constraint we obtain the following system:

$$\begin{cases} \dfrac{\dot{m}_s}{\rho_s S_s} = \dfrac{\dot{m}_w}{\rho_w S_w} \\ S = S_s + S_w \end{cases} \qquad \text{Equation 72}$$

Solving for v, we obtain:

$$v = \frac{\rho_s \dot{m}_w + \rho_w \dot{m}_s}{\rho_s \rho_w S} \qquad \text{Equation 73}$$

According to data retrieved from [4] and [6], we obtain:

V= 41,25 m/s

3.3.2.2 Mathematical model and assumptions of the flow distribution around the bundle

The pressure loss p_0-p_1 can be expressed as:

$$p_0 - p_1 = \Delta p = \xi \rho \frac{v^2}{2} \qquad \text{Equation 74}$$

Where ξ can be seen as the flow resistance of a given path. The pressure loss is due to the friction against the tubes and the numerous acceleration/deceleration processes as the steam flows in the gaps between the tube rows and the associated eddy dissipation. Note that this formula is only an approximation since the velocity of the steam will decline in the bundle as it condenses (i.e. strictly speaking $v \neq$ constant).

The first assumption of the model is that the resistance ξ is proportional to the length l of the path in the tube zone:

$$\xi = al \qquad \text{Equation 75}$$

where a is a constant
The number of tube rows that have to be flowed across is indeed proportional to the distance and so is the head loss. The length l of the path is a function of the point where the steam penetrates the bundle: it can be defined as the shortest straight line between the entry point of the steam and the free space between zones 2 and 3. This shortest line can be obtained by joining the steam's entry point and the centre of zone two and only considering the fraction of the line in zone 3 (see Figure 18).

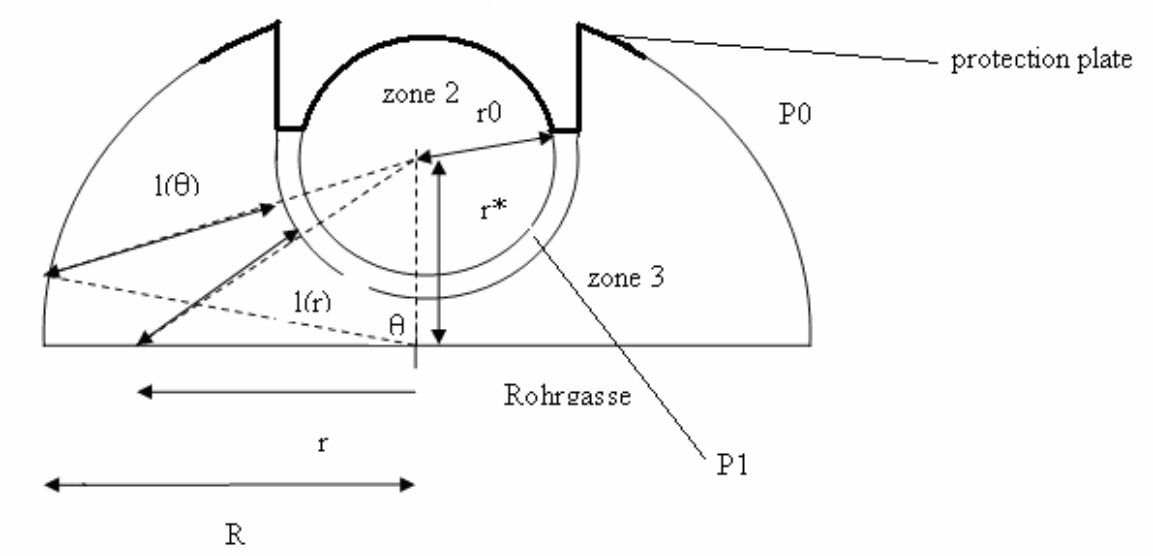

Figure 18: Protection plate and bundle near the HP steam inlet

For all inlet points on the circular part of zone 3, l is a function of θ. Basic geometric considerations lead to the following expression of l(θ):

$$l(\theta) = \sqrt{(R\cos(\theta) - r^*)^2} - r_0 \qquad \text{Equation 76}$$

For all inlet points on the straight part of zone 3 (in the so-called "Rohrgasse"), l is a function of r. Again, basic geometric considerations lead to:

$$l(r) = \sqrt{r^{*2} + r^2} - r_0 \qquad \text{Equation 77}$$

If we call $\dot{m}''(\theta)$ and $\dot{m}''(r)$ the mass flow rates per unit of *free* surface (namely once the presence of the tubes has been taken into account), we can write:

$$v(\theta) = \frac{\dot{m}''(\theta)}{\rho} \quad \text{Equation 78} \qquad \text{and } v(r) = \frac{\dot{m}''(r)}{\rho} \quad \text{Equation 79}$$

NB: note that $\dot{m}''(\theta)$ and $\dot{m}''(r)$ are expressed in $kg.s^{-1}m^{-2}$ hence the two primes.
By combining equations 74 and 75 with equations 78 and 79, we obtain a new expression of the pressure loss:

$$\Delta P = al(\theta)\frac{\dot{m}''(\theta)^2}{2\rho} \quad \text{Equation 80} \qquad \Delta P = al(r)\frac{\dot{m}''(r)^2}{2\rho} \quad \text{Equation 81}$$

We can therefore express $\dot{m}''(\theta)$ and $\dot{m}''(r)$ as follows:

$$\dot{m}''(\theta) = \sqrt{\frac{2\rho\Delta P}{al(\theta)}} \quad \text{Equation 82} \qquad \dot{m}''(r) = \sqrt{\frac{2\rho\Delta P}{al(r)}} \quad \text{Equation 83}$$

These expressions of the mass flow rate per unit surface are not directly useable since we do not know the ratio ΔP/a. However, this ratio can be obtained by solving the continuity equation. Indeed, we know the total mass flow rate of steam for any given ordinate via an energy balance:

$$\dot{m}'(z) = \frac{S_2U_2(T_{out} - T_2(z)) + S_3U_3(T_{out} - T_3(z))}{\Delta h_{steam-water}} \quad \text{Equation 84}$$

where U is the overall heat transfer coefficient, S the outer tube surface per unit length, T_{out} the condensation temperature of the high-pressure steam and $\Delta h_{steam\text{-}water}$ the enthalpy of condensation of steam. Note this time that $\dot{m}'$ is expressed in $kg.s^{-1}.m^{-1}$, hence the prime.

The continuity equation reads:

$$\dot{m}' = 2\int_{\theta_{\min}}^{\pi/2} \alpha\dot{m}''(\theta)Rd\theta + 2\int_{0}^{R} \alpha\dot{m}''(r)dr = 2\int_{\theta_{\min}}^{\pi/2} \alpha\sqrt{\frac{2\rho\Delta P}{al(\theta)}}Rd\theta + 2\int_{0}^{R} \alpha\sqrt{\frac{2\rho\Delta P}{al(r)}}dr \quad \text{Equation 85}$$

Note the introduction of α, which is defined as the available volume fraction in the bundle that is to say the fraction of space which is not occupied by the tubes. $\dot{m}''(\theta)$ and $\dot{m}''(r)$ were indeed defined as the mass flow rates per unit free surface: we must therefore not integrate over the infinitesimal length Rdθ but αRdθ (dr and αdr respectively). The calculation of α is presented in equation 90.
Also note that the lower integration limit of $\dot{m}''(\theta)$ is not 0 but θ_{min} since the protection plate prevents the steam from entering between 0 and θ_{min}.
The only unknown in the continuity equation is the ΔP/a ratio: the continuity equation can therefore be used to determine the unknown. However, we first need to calculate the following integrals:

$$\int_{\theta_{\min}}^{\pi/2} \frac{d\theta}{\sqrt{l(\theta)}} = \int_{\theta_{\min}}^{\pi/2} \frac{d\theta}{\sqrt{\sqrt{(R\cos(\theta) - r^*)^2} - r_0}}$$

$$\int_{\theta_{\min}}^{\pi/2} \frac{dr}{\sqrt{l(r)}} = \int_{\theta_{\min}}^{\pi/2} \frac{dr}{\sqrt{\sqrt{r^{*2} + r^2} - r_0}}$$

This can easily be done with a computer or a powerful pocket calculator. Once ΔP/a calculated, $\dot{m}''(\theta)$ and $\dot{m}''(r)$ can be calculated directly from equation 82 and 83 respectively and the velocities can hence be determined via equations 78 and 79.

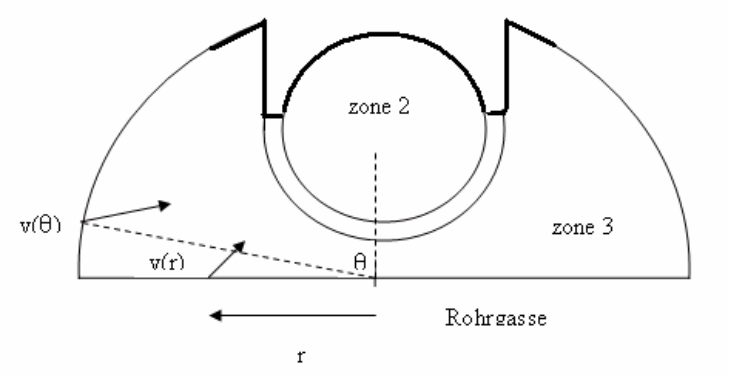

Figure 19: v(r) and v(θ) at the periphery of the bundle

The $\dot{m}'$ (mass flow rate per unit length) used in the continuity equation is valid for a given ordinate z only, that is to say it should be written $\dot{m}'(z)$: the amount of steam required is indeed a function of z since the tube temperature is a function of z. This

means that the ΔP/a ratio calculated via the continuity equation is also only valid for a given ordinate. Consequently, the bundle inlet velocity profile will vary with z:

$$v(\theta,z)=\sqrt{\frac{2\Delta P}{\rho l(\theta)a}} \qquad \text{Equation 86} \qquad\qquad v(r,z)=\sqrt{\frac{2\Delta P}{\rho l(r)a}} \qquad \text{Equation 87}$$

The greatest velocities will be obtained at the lower edge of the plate since the tube temperature is lower (which means that the amount of required steam is greater).

The case where the so-called "Rohrgasse" is not available for flow can also be considered by re-calculating the ΔP/a ratio with the following continuity equation:

$$\dot{m}'=2\int_{\theta_{\min}}^{\pi/2}\alpha\dot{m}''(\theta)Rd\theta=2\int_{\theta_{\min}}^{\pi/2}\alpha\sqrt{\frac{2\rho\Delta P}{al(\theta)}}Rd\theta \qquad \text{Equation 88}$$

This equation is similar to the previous continuity equation except that we have omitted the steam entering through the Rohrgasse. The new ΔP/a ratio is then used to obtain v(θ,z):

$$v(\theta,z)=\sqrt{\frac{2\Delta P}{\rho l(\theta)a}} \qquad \text{Equation 89}$$

- Calculation of the void fraction α

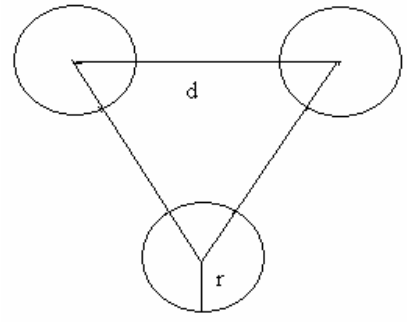

Figure 20: Tube pattern and void fraction

If d is the distance between two tube centers and r the outer radius of a tube, the void fraction is:

$$\alpha=\frac{d^2\frac{\sqrt{3}}{4}-\frac{\pi r^2}{2}}{d^2\frac{\sqrt{3}}{4}}=1-\frac{2\pi r^2}{\sqrt{3}d^2} \qquad \text{Equation 90}$$

3.3.2.3 Results

In Figure 21 and Figure 22, the Rohrgasse is supposed to be free: therefore, the steam flows in from the curved and the straight edges of the bundle. In each graph, two curves have been plotted. The first was obtained at the lower edge of the protection plate (z = 4,055 m) where the steam's velocity is higher (since the tube temperature is lower, leading to more condensation), the second at the upper edge of the plate (z = 5,555) where the velocity is lower. All velocity curves are therefore comprised between these two limits.

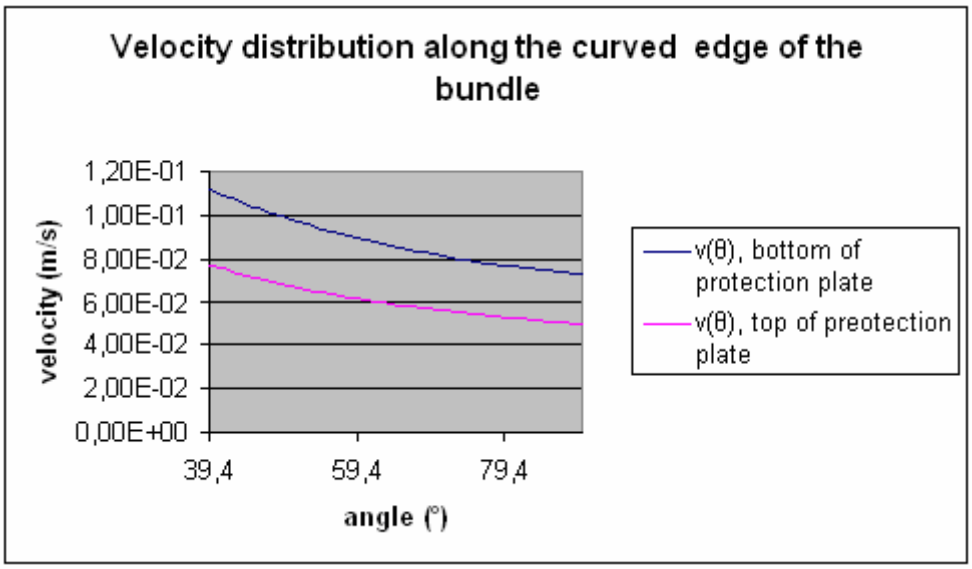

Figure 21: Velocity distribution along the curved edge of the bundle

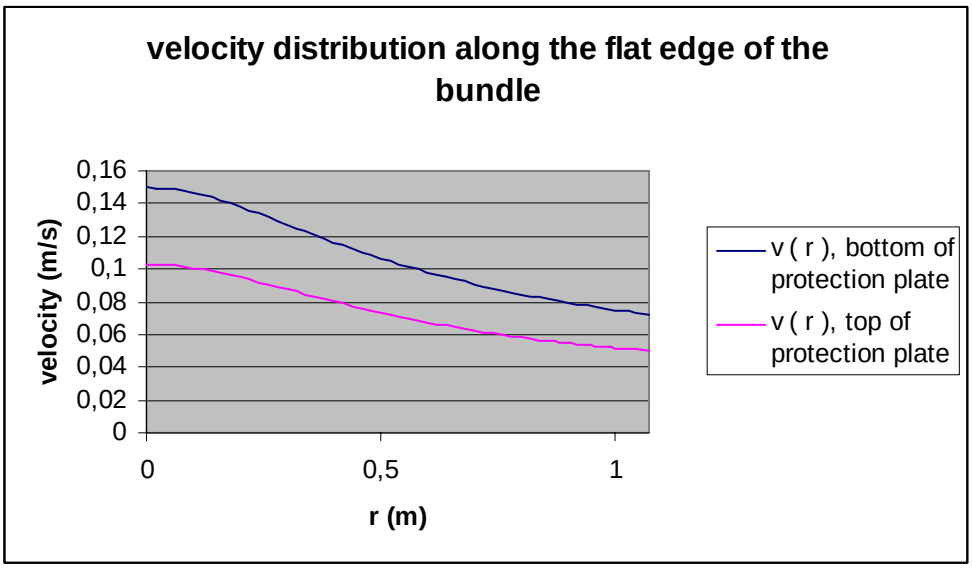

Figure 22: Velocity distribution along the flat edge of the bundle

Physically speaking, the aspect of the curves was predictable. The path-length (directly proportional to the flow resistance) increases with the angle θ, which means that the velocity decreases with θ. Similarly, the path-length increases with r which also leads to decreasing velocities. Note that the two previous graphs are consistent i.e. the velocity for $r = r_{max}$ is equal to the velocity for θ=90° (which is indeed the velocity of the same inlet point).

In Figure 23, the Rohrgasse was supposed to be unavailable which means that all the steam has to flow through the circular part of the bundle. The velocities obtained are therefore higher. Here again the velocities at the bottom and the top of the plate are displayed.

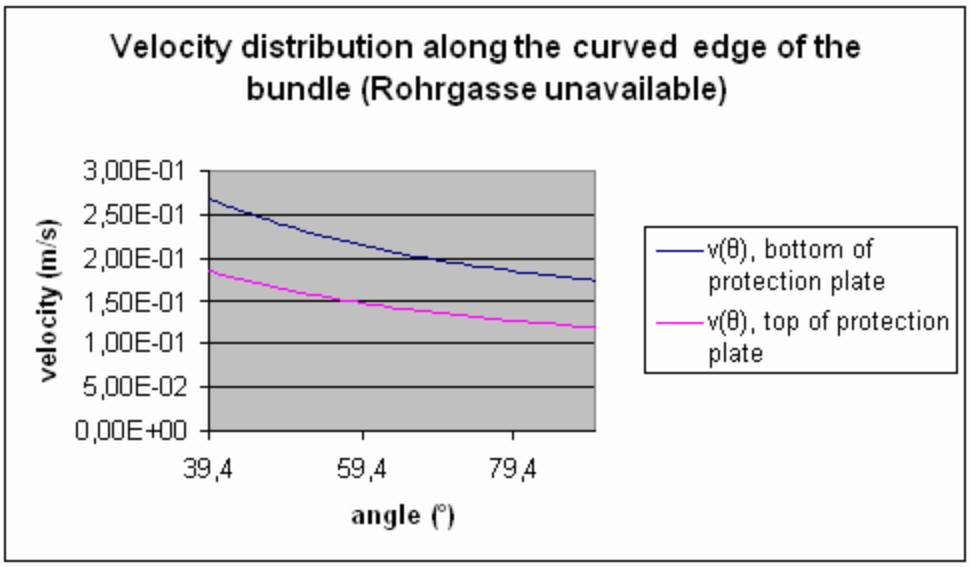

Figure 23: Velocity distribution along the curved edge of the bundle (Rohregasse unavailable)

The velocities obtained in Figure 22 / Figure 23 are of course higher than those obtained in Figure 17 (when a3 and b3 / a3 where available respectively) since the protection plate has been taken into account:

- V_{max} = 0,16 m/s (with a3 alone) or 0,1 m/s (with a3 and c3) when the protection plate is neglected
- V_{max} = 0,27 m/s or 0,15 m/s when the protection plate is taken into account

4 Thermodynamic performance of the pre-heater and impact on the entire cycle

The purpose of this chapter is to acquire a better understanding of the impact of pre-heating on the main components of a Rankine power cycle. Why does regenerative feed heating improve the overall efficiency? How does this efficiency gain increase with increasing amounts of bled steam and greater subcooling of the condensate?
The first part of this section will present a model of a simple Rankine cycle which can be used as a tool in order to assess the impact of pre-heating. In the second part of this section, the general benefits of pre-heating will be analysed (with the help of the excel model). We will then focus on the GKN1 plant itself and a complete thermodynamic analysis of the "real" pre-heater will be carried out.

4.1 Modeling of a Rankine cycle with one stage of regenerative feed heating

A recurrent problem encountered by engineers when trying to improve or optimize a component is the lack of information on the overall impact of a local modification. In other words "How can I be sure that implementing this modification will lead to a higher turbine output? And if there is an improvement, is it notable or negligible?" A power cycle is indeed based on a group of components which are bound together by complex actions and retro-actions and it is not easy to predict the influence of a sole modification.

The only satisfactory way to solve such a complex problem is to resort to a thermodynamic analysis and, more precisely, an entropy analysis. Entropy generation is indeed a yardstick against which various configurations of a plant (or a component) can be compared. Under the assumption of *thermodynamic isolation* (which can be very stringent indeed, as we will see later on) the best layout of a component is the one which produces the less entropy (see 1.4). On a more global scale, the best plant configuration is the one which produces the most electricity for a given input (in other words the configuration which produces the less entropy). The following tool enables the user to modify various parameters in a simplified cycle and to analyze the impact of these modifications on each component and on the turbine output.

4.1.1 Assumptions and parameters

In order to simplify our model, we are going to consider a Rankine cycle with one stage of regenerative feed heating, no superheating or reheating and isentropic expansions and compressions (in the turbine and the pump respectively).
The plant layout and the thermodynamic cycle are presented in Figure 24 and Figure 25 respectively.

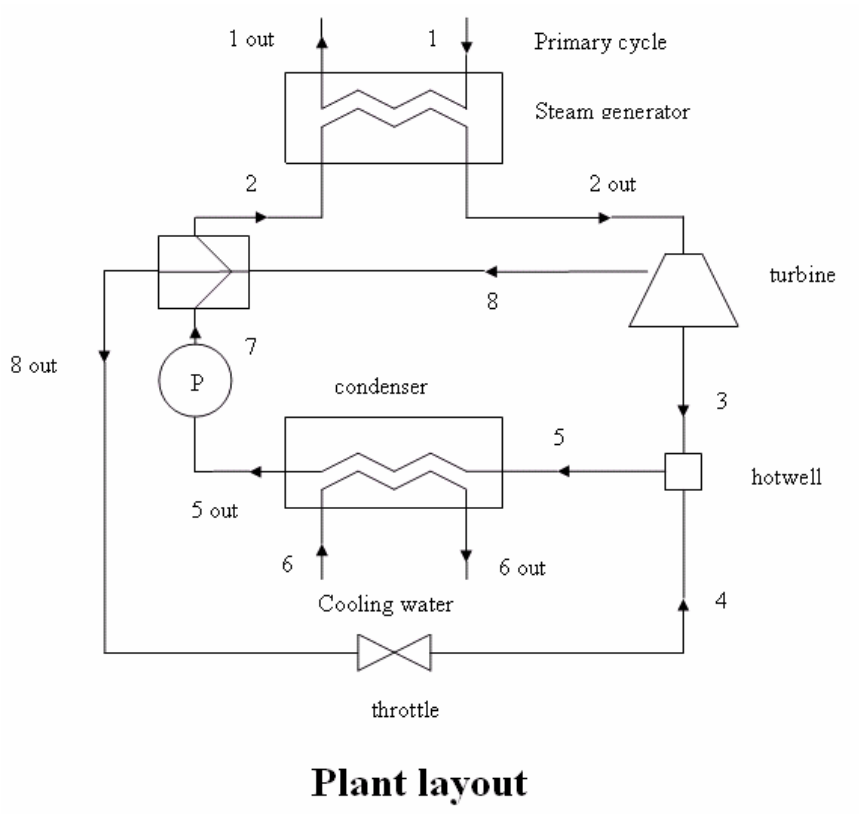

Figure 24: Plant layout

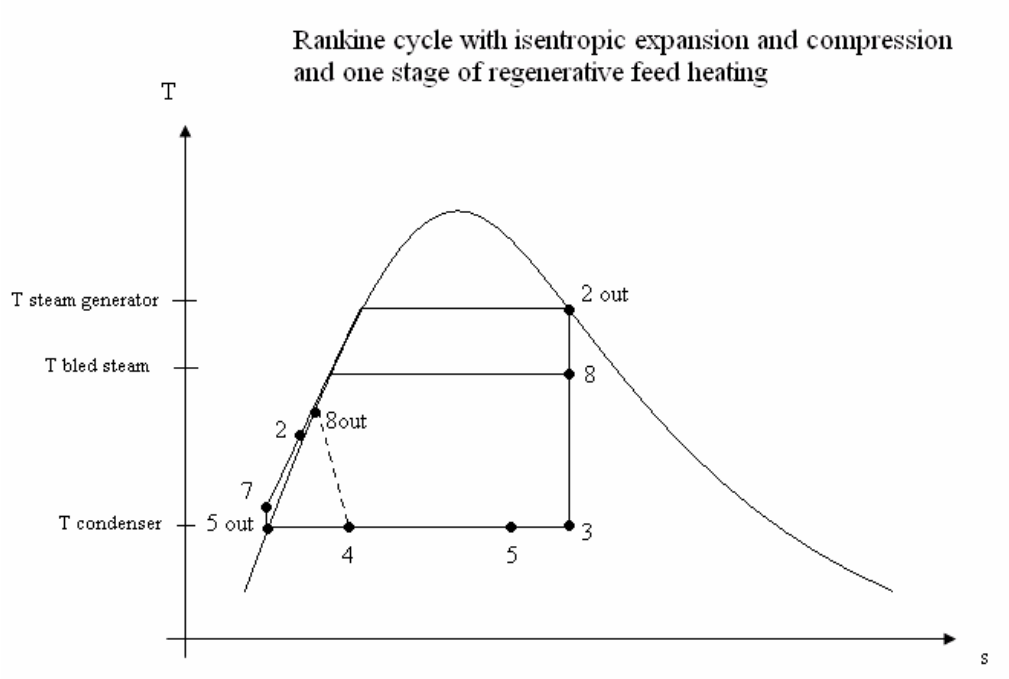

Figure 25: Thermodynamic cycle

The user has to enter a number of parameters ("n", the degrees of freedom) which will entirely determine the rest of the cycle (including its performance, entropy generation etc…). Any group of n independent parameters would do, but it is usual to select the following:

Primary cycle:

- Thermal power generation in core $\dot{Q}_c\,(MW)$
- Inlet temperature in the steam generator T_1 (°C)
- Absolute pressure of primary cycle p_{pri} (bar)
- Mass flow rate in primary cycle $\dot{m}_{pri}$ (kg/s)

Secondary cycle:

- Absolute pressure in steam generator p_{sg} (bar)
- Absolute pressure in condenser p_{con} (bar)
- **Pre-heater:**
  - Absolute pressure of bled steam p_{bled} (bar)
  - Heat transfer area in the condensation zone A_c (m^2)
  - Overall heat transfer coefficient in the condensation zone U_c (m^2)
  - Heat transfer area in the Kühlkasten (subcooling zone enclosure) A_K (m^2)
  - Overall heat transfer coefficient in the Kühlkasten U_K (m^2)

Cooling water

- Inlet temperature T_6 (°C)
- Pressure p_{cool} (bar)
- Mass flow rate of cooling water $\dot{m}_{cool}$ (kg/s)

Finally, the reference temperature for the dead state must be entered in order to complete the thermodynamic calculations (this temperature is usually equal to the inlet temperature of the cooling water).

Note that the amount of bled steam is controlled by the area and heat transfer coefficient in the condensation zone (the pre-heater draws the required amount of steam). The mass flow rate in the secondary cycle $\dot{m}_{sec}$ will also be determined by the previous parameter set.

Inside the pre-heater itself, our upcoming calculations will require the definition of point 9 which is the state of the feedwater when it leaves the Kühlkasten and when it enters the condensing zone. Note that we will assume a counterflow heat-exchange in the Kühlkasten.

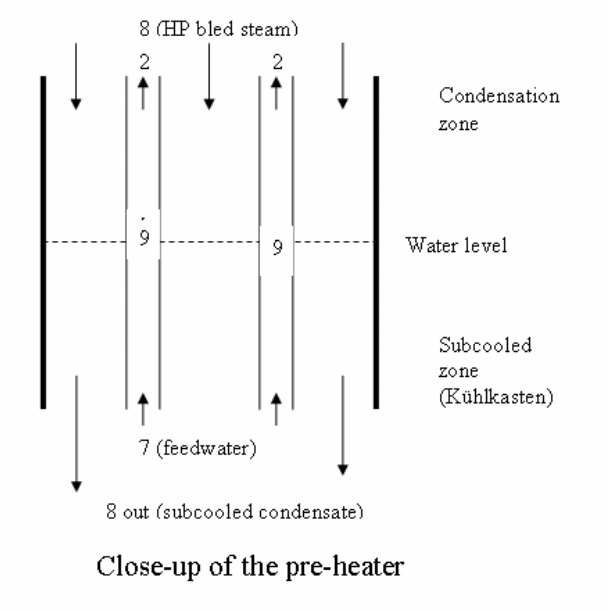

Figure 26: Close-up of the pre-heater

4.1.2 Problem solving

Once the user has entered the n = 14 independent parameters, the cycle and all its properties are fixed (there are therefore 14 degrees of freedom in the problem). Unfortunately, the problem cannot be solved linearly i.e. it is not possible to calculate the value of each unknown one after the other: an iterative process will be required.

Before presenting the calculation path, a number of points on the cycle can easily be determined.

- Point 2out: saturated steam at p = p_{sg}
- Point 8: water/steam mix at p = p_{bled} and s = s_{2out} (isentropic expansion in turbine)
- Point 3: water/steam mix at p = p_{con} and s = s_{2out} (isentropic expansion in turbine)
- Point 5out: saturated liquid at p = p_{con}
- Point 7: subcooled water at p = p_{sg} and s=s_{5out} (isentropic compression in pump)

The calculation of the previous points is straightforward. For the remaining unknowns ($\dot{m}_{sec}$, $\dot{m}_{bled}$, 2, 6out, 8out, 1out, 5, 9, 4) we must resort to an iterative solving path:

a). **Determination of point 1out:** Energy balance on the primary side of the steam generator:

$$h_{1,out} = h_1 - \frac{\dot{Q}_c}{\dot{m}_{pri}} \qquad \text{Equation 91}$$

Since h_{1out} and p_{1out}=p_{pri} are known, 1out is entirely determined.

b). **assume** $\dot{m}_{sec}$

c). **Determination of point 2:** Energy balance on the secondary side of the steam generator:

$$h_2 = h_{2,out} - \frac{\dot{Q}_c}{\dot{m}_{\text{sec}}} \qquad \text{Equation 92}$$

Since h_2 and $p_{2out} = p_{sg}$ are known, 2 is entirely determined.

d). **assume** $\dot{m}_{bled}$

e). **Determination of 8out**: subcooling effectiveness in the Kühlkasten
We must first calculate the effectiveness ε of the Kühlkasten. For a pure counterflow heat-exchanger, the effectiveness is a simple function of the number of transfer units (NTU):

$$\varepsilon = \frac{1 - e^{-NTU(1-C_r)}}{1 - C_r e^{-NTU(1-C_r)}} \qquad \text{Equation 93}$$

where

$$NTU = \frac{UA}{C_{\min}} = \frac{U_K A_K}{\dot{m}_{bled} c_p} \qquad \text{Equation 94}$$

(in this case c_p is that of saturated liquid at p_{bled})

$$C_r = \frac{(\dot{m}c_p)_{\min}}{(\dot{m}c_p)_{\max}} = \frac{(\dot{m}c_p)_{condensate}}{(\dot{m}c_p)_{feedwater}} \qquad \text{Equation 95}$$

(in this case the feedwater cp is that of point 7)

Once ε has been calculated, we can determine 8 out:

$$\varepsilon_{Kühlkasten} = \frac{h_{liq,sat}(p_{bled}) - h_{8,out}}{h_{liq,sat}(p_{bled}) - h(p_{bled}, T_7)} \qquad \text{Equation 96}$$

$$h_{8,out} = h_{liq,sat}(p_{bled}) - \varepsilon_{Kühlkasten}(h_{liq,sat}(p_{bled}) - h(p_{bled}, T_7)) \qquad \text{Equation 97}$$

Since h_{8out} and $p_8 = p_{bled}$ are known, 8out is entirely determined.

f). **Determination of 9**: energy balance on the Kühlkasten

$$h_9 = \frac{\dot{m}_{bled}}{\dot{m}_{\sec}}(h_{liq,sat}(T_8) - h_{8out}) + h_7 \qquad \text{Equation 98}$$

Since h_9 and $p_9=p_{sg}$ are known, point 9 is entirely determined.

g). **Verification of consistency of $\dot{m}_{\sec}$ (via point 2):** now that 9 and T_8 are known, we can calculate 2 via the effectiveness of the condensation zone and compare with 2 obtained in step c. If the two values are not identical, the $\dot{m}_{\sec}$ guess of step b must be reiterated for a different $\dot{m}_{\sec}$. Since steam condenses on the shell-side, the expression of the effectiveness is:

$$\varepsilon_{cond} = 1 - e^{-\frac{U_c A_c}{\dot{m}_{\sec} c_p}} \qquad \text{Equation 99}$$

Where c_p is that of subcooled water at point 9

$$\varepsilon_{cond} = \frac{h_2 - h_9}{h(p_{sg}, T_8) - h_9} \qquad \text{Equation 100}$$

$$h_2 = \varepsilon_{cond}(h(p_{sg}, T_8) - h_9) + h_9 \qquad \text{Equation 101}$$

Compare with h_2 obtained in step c and reiterate for a different $\dot{m}_{\sec}$ if necessary.

h). **Verification of the consistency of $\dot{m}_{bled}$ (via $\dot{m}_{\sec}$):** energy balance on the entire pre-heater

$$\dot{m}_{\sec} = \dot{m}_{bled}\frac{h_8 - h_{8,out}}{h_2 - h_7} \qquad \text{Equation 102}$$

Compare with $\dot{m}_{\sec}$ calculated in step b and reiterate for a different $\dot{m}_{bled}$ (step d) if necessary

i). **Determination of 4:** isenthalpic expansion in throttle
Point 4 is entirely determined since $h_4=h_{8out}$ (isenthalpic expansion) and $p_4 = p_{con}$

j). **Determination of 5:** energy balance on the hotwell

$$h_5 = \frac{\dot{m}_{bled} h_4 + (\dot{m}_{\sec} - \dot{m}_{bled})h_3}{\dot{m}_{\sec}} \qquad \text{Equation 103}$$

Since h_5 and $p_5=p_{cond}$ are known, 5 is entirely determined

k). **Determination of 6out:** energy balance on the condenser

$$h_{6out} = \frac{\dot{m}_{\text{sec}}}{\dot{m}_{cool}}(h_5 - h_{5,out}) + h_6 \qquad \text{Equation 104}$$

Point 6_{out} is entirely determined since h_{6out} and $p_{6out}=p_{cool}$ are known

4.1.3 Model outputs

Besides giving the properties of all points of the cycle (pressure, temperature, enthalpy, entropy and steam fraction when defined), $\dot{m}_{bled}$ and $\dot{m}_{\text{sec}}$, the model calculates the turbine ouput, the entropy creation of all the entropy-generating components and the related exergy destruction.

4.1.3.1 Turbine output

The gross turbine output is:

$$W_{gross} = \dot{m}_{\text{sec}}(h_{2out} - h_8) + (\dot{m}_{\text{sec}} - \dot{m}_{bled})(h_8 - h_3) \qquad \text{Equation 105}$$

Part of this is used to power the pump (we thus obtain the net output):

$$W_{net} = \dot{m}_{\text{sec}}(h_{2out} - h_8) + (\dot{m}_{\text{sec}} - \dot{m}_{bled})(h_8 - h_3) - \dot{m}_{\text{sec}}(h_7 - h_{5out}) \qquad \text{Equation 106}$$

In practice, the amount of energy used by the pump represents only around 1% of the gross output so that $W_{gross} \approx W_{net}$

4.1.3.2 Entropy generation and exergy destruction

The entropy generation of all irreversible processes in the cycle has been calculated in order to visualize how much each component drives the cycle away from its theoretical Carnot efficiency. The following entropy balance was applied to every irreversible process (see 1.4.2):

$$\dot{m}s_{in} + \dot{S}_{gen} = \dot{m}s_{out} + \dot{S}_{accu} \qquad \text{Equation 107}$$

Where $\dot{S}_{gen}$ is the rate of entropy generation and $\dot{S}_{accu}$ is the rate at which entropy accumulates in the system. Since we consider steady-state conditions, $\dot{S}_{accu} = 0$.

Once $\dot{S}_{gen}$ has been determined, the exergy destroyed by the piece of equipment in question can easily be obtained by applying the Gouy-Stodola theorem (see 1.4.2):

$$Ex_{destroyed} = T_0 S_{gen} \text{ or } \dot{E}x_{destroyed} = T_0 \dot{S}_{gen} \qquad \text{Equation 108}$$

Where T_0 is the temperature of the dead state.

- Steam generator:

$$\dot{S}_g = \dot{m}_{\text{sec}}(s_{2out} - s_2) + \dot{m}_{pri}(s_{1out} - s_1) \quad \text{Equation 109}$$

$$\dot{E}x_{destroyed} = T_0(\dot{m}_{\text{sec}}(s_{2out} - s_2) + \dot{m}_{pri}(s_{1out} - s_1)) \quad \text{Equation 110}$$

- Condenser:

$$\dot{S}_g = \dot{m}_{\text{sec}}(s_{5out} - s_5) + \dot{m}_{cool}(s_{6out} - s_6) \quad \text{Equation 111}$$

$$\dot{E}x_{destroyed} = T_0(\dot{m}_{\text{sec}}(s_{5out} - s_5) + \dot{m}_{cool}(s_{6out} - s_6)) \quad \text{Equation 112}$$

- Throttle:

$$\dot{S}_g = \dot{m}_{\text{sec}}(s_4 - s_{8out}) \quad \text{Equation 113}$$

$$\dot{E}x_{destroyed} = T_0\dot{m}_{\text{sec}}(s_4 - s_{8out}) \quad \text{Equation 114}$$

- HP pre-heater:

Kühlkasten: $\dot{S}_g = \dot{m}_{\text{sec}}(s_9 - s_7) + \dot{m}_{bled}(s_{8out} - s_{liq,satt}(T_8))$ Equation 115

Condensation zone: $\dot{S}_g = \dot{m}_{\text{sec}}(s_2 - s_9) + \dot{m}_{bled}(s_{liq,satt}(T_8) - s_8)$ Equation 116

- Hotwell: no entropy is created inside the hotwell since the pressure and temperature of the steam/water that are mixed are the same

- Cooling water: the warm cooling water which flows out of the condenser conveys a given amount of exergy since it is no longer at the dead state's temperature. Even though this exergy is not destroyed in the plant itself, it is lost (from the plant's perspective) and it will eventually be destroyed (entropy creation) as it mixes with the environment (and thus reaches the dead state).

$$\dot{E}x_{lost} = \dot{m}_{cool}((h_{6out} - h_0) - T_0(s_{6out} - s_0)) \quad \text{Equation 117}$$

$$\dot{S}_g = \frac{\dot{m}_{cool}((h_{6out} - h_0) - T_0(s_{6out} - s_0))}{T_0} \quad \text{Equation 118}$$

In the previous formulae, the subscript 0 refers to the dead state.

4.1.3.3 First and second law efficiencies

The first law efficiency of the plant is defined as the ratio of the power output of the plant (net turbine output) over the power input (thermal power generation in core).

$$\eta_I = \frac{\dot{m}_{\sec}(h_1 - h_8) + (\dot{m}_{\sec} - \dot{m}_{bled})(h_8 - h_3) - \dot{m}_{\sec}(h_7 - h_{5out})}{\dot{Q}_c} \qquad \text{Equation 119}$$

The second law efficiency of the plant is the ratio of the exergy output (net turbine power output) over the exergy input (see 1.4.1). Contrary to a first law efficiency which is limited by Carnot's efficiency, this second law efficiency can reach 1 if the cycle is endoreversible (no entropy generation inside the cycle itself) and exoreversible i.e. if the heat is exchanged reversibly between the plant and the hot and cold sources (vanishingly small temperature difference, in other words infinite heat exchange area). A second law efficiency is therefore a much more "practical" scale since the upper limit of this scale can be reached (in theory at least).

$$\eta_{II} = \frac{\dot{m}_{\sec}(h_1 - h_8) + (\dot{m}_{\sec} - \dot{m}_{bled})(h_8 - h_3) - \dot{m}_{\sec}(h_7 - h_5)}{\dot{m}_{pri}((h_1 - h_{1out}) - T_0(s_1 - s_{1out}))} \qquad \text{Equation 120}$$

4.1.4 Program warning messages

As explained in 3.1.1, the user must enter a given number of parameters before the model can be iterated. However, some combinations are physically impossible.

4.1.4.1 Steam generator heat exchange

If the characteristics of the steam generator are chosen randomly, it might be impossible to transfer the required amount of heat from the primary to the secondary cycle: the temperature of the water in the primary cycle may reach the saturation temperature of the secondary cycle before the required amount of steam is generated, thus rendering further heat transfer impossible.

The power required to evaporate the *saturated* liquid (secondary cycle in the steam generator) is:

$$P_{\sec,evap} = \dot{m}_{\sec}(h_{2out} - h_{liq,sat}(T_{2out})) \qquad \text{Equation 121}$$

The maximum power that can be transferred by the primary fluid to *evaporate* the secondary fluid (i.e. the power transferred before the primary fluid reaches the saturation temperature of the secondary cycle) is:

$$P_{pri,evap,\max} = \dot{m}_{pri}(h_1 - h(P_1, T_{2out})) \qquad \text{Equation 122}$$

The thermal design of the steam generator is therefore possible only if:

$$P_{pri,evap,\max} > P_{\sec,evap} \quad \text{Equation 123}$$

This criterion is checked by the model and if it is not verified, an error message is displayed.

4.1.4.2 Condenser heat exchange

If the cooling water reaches the saturation temperature of the condenser before all the heat has been transferred, further heat-exchange is impossible and the condenser cannot fulfill its role.
The thermal design of the condenser is therefore possible as long as:

$$\dot{m}_{cool}(h_6 - h(P_6, T_5)) > \dot{m}_{\sec}(h_5 - h_{5out}) \quad \text{Equation 124}$$

This criterion is also checked by the model and an error message is displayed if it is not satisfied.

4.1.5 Implementation of the model with an excel macro

All the calculations have been entered in an excel spreadsheet: the user only needs to enter the desired operating conditions.
Unfortunately, it turns out that the iterative process which has to be implemented converges quite slowly towards the solution. Carrying out the iterations manually with the spreadsheet would be a very time-consuming and tedious work: an excel macro in which an important number of iterations were recorded has therefore been added. This feature enables the user to obtain an answer instantly.

4.2 Simulation and result interpretation on a hypothetical plant

The following simulations have been carried out in order to work out general trends and to understand the underlying thermodynamics. Therefore, the operational parameters need not be that of an existing plant. However, the simulations were run with operating conditions adapted from the real Neckarwestheim 1 power plant.

4.2.1 Adaptation of the operating conditions of Neckarwestheim 1

In GKN I, three identical steam generators transfer the heat produced by the core (2610 MW) between primary and secondary cycle. 4815 kg/s of pressurized water (inlet temperature: 321,27°C, pressure: 155 bar) flow on the primary side of each one of these steam generators. On the secondary side, the saturation pressure is 60,45 bar [21], [22].
The plant is equipped with two condensers, one for the “normal” power plant and one for the plant powering the railway line. They are supplied with 32028 kg/s and 7222 kg/s of 12,5°C cooling-water respectively. The feedwater flowing from these two condensers is

pre-heated in a train of LP pre-heaters (one for each feedwater line) and is finally mixed before the HP pre-heater.
There are in fact two twin HP pre-heaters operating *in parallel* which means that the previous stream of feedwater is divided into two identical streams which feed into the twin HP pre-heaters. The twin pre-heaters finally feed into the secondary side of the steam generators.

In our simplified model, this complicated layout cannot be modeled directly: it is only possible to model one steam generator powering one turbine with one line of feedwater feeding into one pre-heater.
Since the real operating conditions are only valid for two pre-heaters operating in parallel, all the extensive values characterizing the cycle where divided by two. We therefore consider two identical and independent cycles with the following extensive operating conditions:

- Power generation in core: 2610/2=1305 MW
- Primary mass flow rate: 4815*3/2=7222 kg/s
- Mass flow rate of cooling water: (32028+7222)/2=19625 kg/s

In the model, the condensation zone and the Kühlkasten were considered separately (possibility to enter independent heat transfer coefficients and heat exchange areas). The influence of these two components will therefore be analyzed separately.

4.2.2 Impact of the condensation zone

In the first set of simulations, the heat-exchange surface in the condensation zone was modified. This heat-exchange surface controls the amount of steam that is bled from the turbine. The greater the heat exchange surface, the greater the amount of heat transferred and the greater the amount of HP steam required.
The operating conditions used in this simulation are the following:

operating conditions		unit
Thermal power generation in core	1305	MW
Inlet temperature of the pressurized water in primary cycle	321	°C
pressure of primary cycle	155	bar
mass flow rate in primary cycle	7225	kg/s
Inlet temperature of cooling water	12,5	°C
Pressure of cooling water	1	bar
mass flow rate of cooling water	19625	kg/s
steam generator pressure	60,45	bar
pressure of bled steam	21,85	bar
condenser pressure	0,0765	bar
Temperature of the dead state	12,5	°C
U (Kühlkasten)	5000	$W.m^{-2}.K^{-1}$
A (Kühlkasten)	425	m^2
U (in condensation zone)	4000	$W.m^{-2}.K^{-1}$

Table 6: operating conditions for the first set of simulations

4.2.2.1 Impact of the heat exchange surface in the condensation zone on the mass flow rate of bled steam

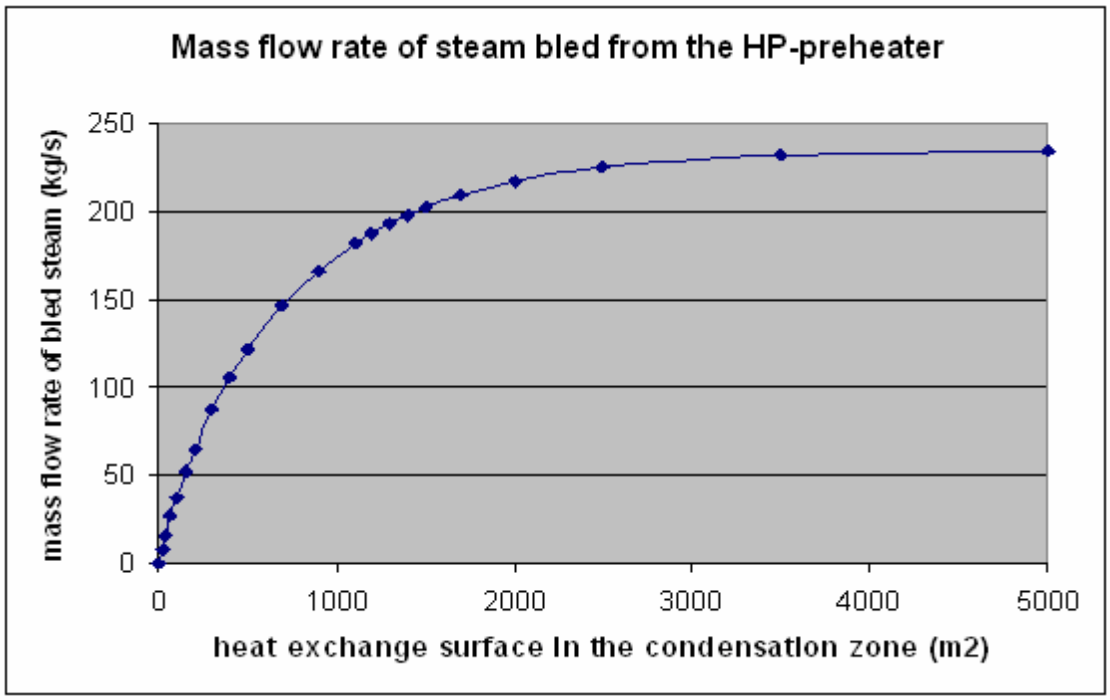

Figure 27: Mass flow rate of steam bled from the HP-preheater

The first result of the simulation is that the amount of steam that is drawn from the turbine does indeed depend on the heat exchange surface, but that this amount cannot exceed a given limit.
If we greatly increase the heat exchange area, the mass flow rate of bled steam levels off in an exponential way and converges towards a finite value (see Figure 27). This can easily be explained. Heat can only be exchanged if the two fluids are not in thermal equilibrium. If the heat-exchange area in the condensation zone is increased, more steam is drawn from the turbine and more energy is transferred to the feedwater, the temperature of which draws closer to the saturation temperature of the bled steam. The maximal amount of heat exchangeable (and therefore the maximal amount of steam that can be bled) is obtained when the feedwater's temperature equals that of the bled steam (infinite heat exchange surface).

$$\left(\dot{m}_{bled}\right)_{\max} = \dot{m}_{\sec}\frac{h(T_8, p_7) - h_9}{h_8 - h_{liq,sat}(T_8)} \qquad \text{Equation 125}$$

4.2.2.2 Impact of the heat exchange area in the condensation zone on the performance of the various components of the plant

It is interesting to plot the overall entropy generation rate and that of each component against the heat-exchange surface in the condensation zone (see Figure 28 and Figure 29). This enables us to understand why feed-heating is interesting from a thermodynamic point of view.

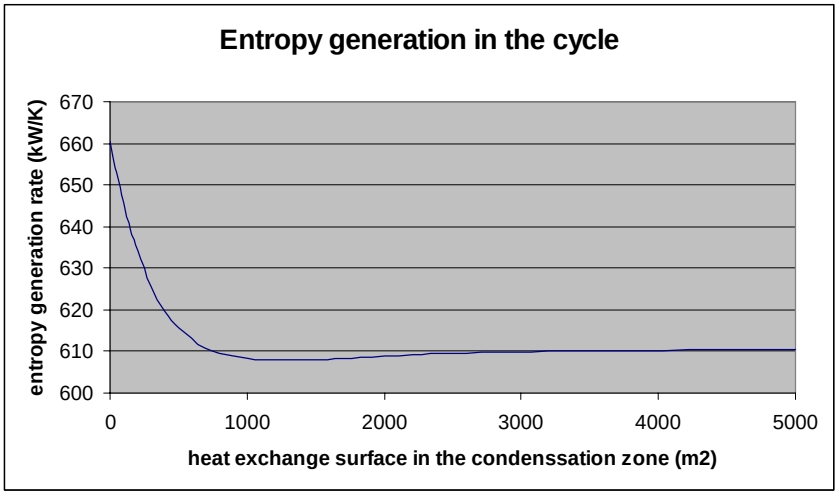

Figure 28: Overall entropy generation in the cycle plotted against the heat exchange surface in the condensation zone

We can first note that there is an optimal heat-exchange surface in the condensation zone which leads to an (overall) minimal entropy generation. This means that a peak in the turbine output should be expected. Consequently, bleeding as much steam as possible from the turbine is not the optimal solution.

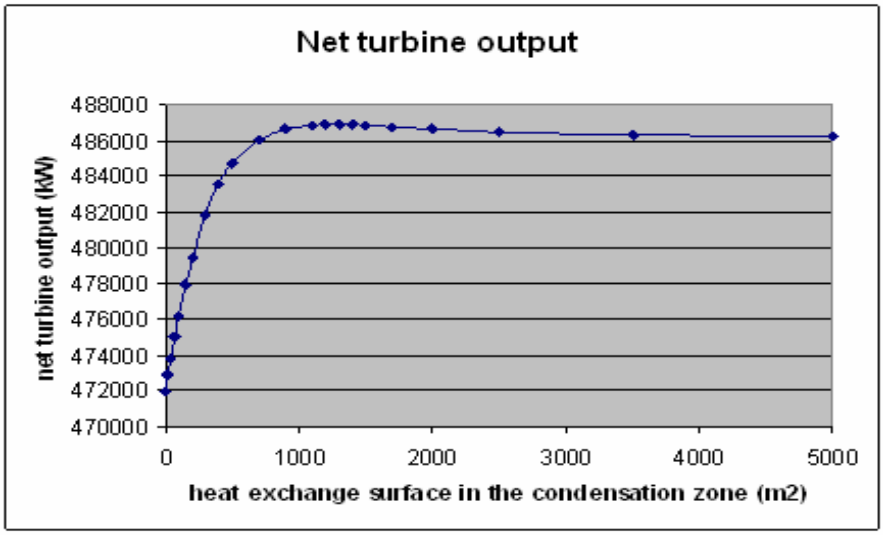

Figure 29: Net turbine output plotted against the heat-exchange surface in the condensation zone

To understand the existence of this optimum we can either use an intuitive or a thermodynamic approach.
Intuitively, we know that since the inlet, bled and outlet properties of the steam in the turbine are fixed (points 2out, 8 and 3 respectively of Figure 25) the power output of the turbine only depends on the two following parameters: the amount of steam generated in the steam-generator and the amount of steam bled from the turbine. Increasing the amount of bled steam (by increasing the heat-exchange area in the condensation zone) will simultaneously tend to:
-lower the amount of steam flowing through the turbine (because more is bled): output power drop
-increase the amount of steam generated in the steam-generator (since warmer water is fed into the steam-generator and the power transferred between primary and secondary cycles is fixed): more steam will flow in the turbine, which leads to a power output increase

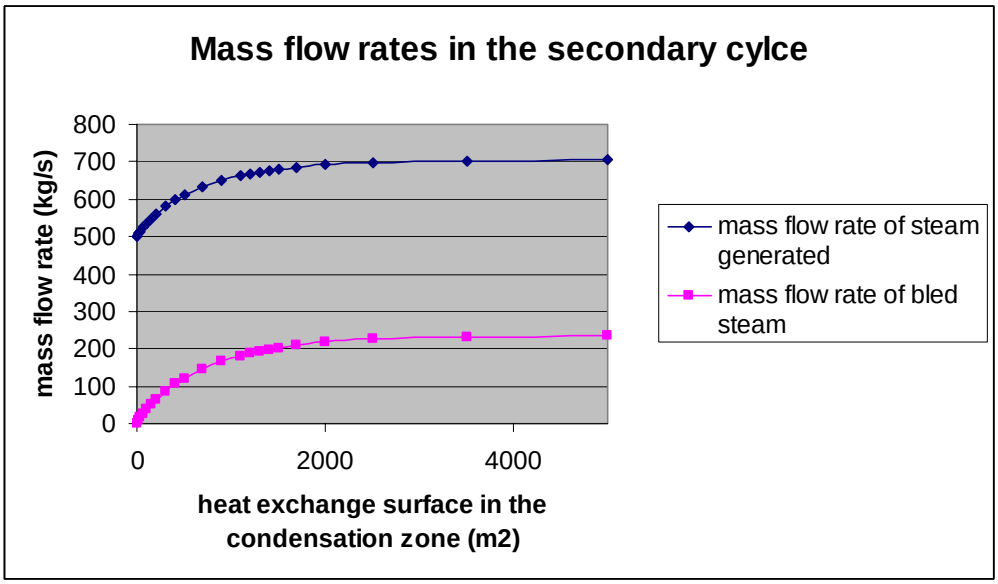

Figure 30: Mass flow rate of generated and bled steam

There is an optimal trade-off between these two competing effects, trade-off which leads to maximal power output.

From a thermodynamic point of view, this problem can be seen as the competition between two entropy-generating processes.
Increasing the amount of bled steam decreases the irreversibility of the steam generator: warmer water is fed into the steam-generator, which leads to a smaller average temperature difference between primary and secondary fluids (and thus less entropy generation).
On the other hand, increasing the amount of bled steam increases the entropy generation (i.e. the irreversibility) of the pre-heater since more and more heat is transferred in the component.

The impact of the heat-exchange area in the condensation zone on the other components of the cycle (condenser, cooling water and throttle) is small and does not really influence the optimum.

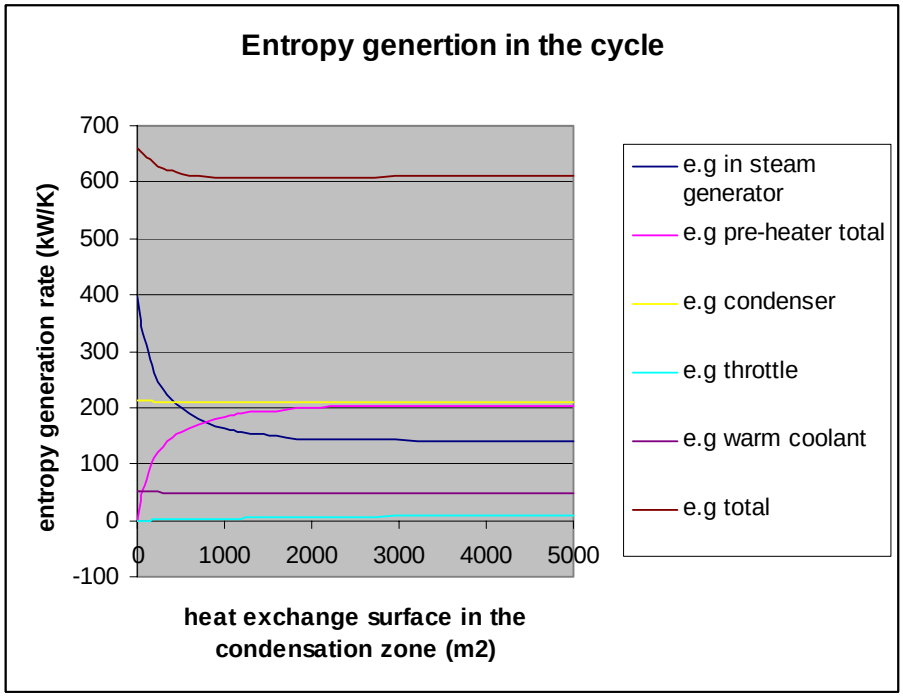

Figure 31: Entropy generation rate in the cycle

Figure 31 also shows that designing the HP pre-heater on the basis of minimal entropy creation *in the HP pre-heater* is misleading. Generally speaking, it is possible to compare the performance of two components and select the best one by comparing the entropy generation rate. This is an important design criterion in thermodynamic optimization.
In our case however, this principle does not hold: the cycle efficiency increases as the entropy generation rate in the pre-heater increases (for small heat-exchange surfaces). The minimal amount of entropy created by the HP pre-heater is 0, value which is obtained when the heat exchange surface is equal to 0 m^2, in other words when the heat-exchanger has disappeared! In fact the minimal entropy generation rule holds as long as a component is *thermodynamically isolated* [17] from other components (in which case the total entropy generation of the cycle is the sum of two independent terms: the entropy generated by the component in question and the entropy generated by the rest of the system).
In our case, an entropy generation rise in the HP pre-heater leads to a greater entropy generation decrease in the steam-generator (for heat-exchange surfaces smaller than the optimal condensation surface): the two systems are coupled. In other words, reducing the entropy generation of the pre-heater leads to a greater increase of the entropy generation rate elsewhere in the cycle (in the steam generator in this case).

4.2.2.3 Optimal amount of bled steam

As explained previously, there is an optimal heat exchange surface in the condensation zone for which the turbine output presents a maximum. In other words, there is an optimal $\frac{\dot{m}_{bled}}{\dot{m}_{\sec ondary}}$ ratio for which the turbine output peaks.

It is possible to define a mathematic criterion for which the peak efficiency is obtained.
Differentiating the net turbine output with respect to the amount of bled steam we obtain:

$$\frac{\partial W_{net}}{\partial \dot{m}_b} = \frac{\partial\left(\dot{m}_{\sec}(h_{2out} - h_8) + (\dot{m}_{\sec} - \dot{m}_{bled})(h_8 - h_3) - \dot{m}_{\sec}(h_7 - h_{5out})\right)}{\partial \dot{m}_{bled}} \quad \text{Equation 126}$$

$$\frac{\partial W_{net}}{\partial \dot{m}_b} = (h_3 - h_8) + (h_{2out} - h_3 + h_{5out} - h_7)\frac{\partial \dot{m}_{\sec}}{\partial \dot{m}_{bled}} \quad \text{Equation 127}$$

Unlike points like 8_{out} or 2 which are "floating" points (i.e. the state of which depends on the inputs of the user and the consequent $\dot{m}_{bled}$ and $\dot{m}_{\sec}$), points 2_{out}, 8, 3, 5_{out} and 7 are fixed points (always the same position on the T-s diagram). Therefore, they are independent of $\dot{m}_{bled}$, hence the differentiation result.

A *necessary* condition for the existence of a maximum is:

$$\frac{\partial W_{net}}{\partial \dot{m}_{bled}} = 0 \quad \Leftrightarrow \quad \frac{\partial \dot{m}_{\sec}}{\partial \dot{m}_{bled}} = \frac{h_8 - h_3}{h_{2out} - h_3 + h_{5out} - h_7} \quad \text{Equation 128}$$

In practice, the turbine output curve presents neither minimums nor inflexion points which means that the previous criteria is sufficient to define the maximum.

Unfortunately, this criterion is not directly useable since it does not give a relationship between $\dot{m}_{bled}$ and $\dot{m}_{\sec}$ but between the derivative of $\dot{m}_{\sec}$ with respect to $\dot{m}_{bled}$. In theory, we could use this criterion to determine the optimum by expressing $\frac{\partial \dot{m}_{\sec}}{\partial \dot{m}_{bled}}$ via an energy balance such as $\dot{m}_{\sec} = \dot{m}_{bled}\frac{h_8 - h_{8,out}}{h_2 - h_7}$ (energy balance on the pre-heater) but this leads to the differentiation of points 2 and 8_{out} with respect to $\dot{m}_{\sec}$, which is not possible analytically given the underlying NTU equations. It is therefore not possible to express the optimal $\frac{\dot{m}_{bled}}{\dot{m}_{\sec ondary}}$ ratio analytically. It can only be obtained through a trial and error process with the model.

4.2.3 Impact of the heat-exchange area in the subcooling zone enclosure (Kühlkasten)

In the second set of simulations, the heat-exchange surface in the Kühlkasten was modified. This heat-exchange surface controls the degree of subcooling of the condensate and, to a lesser extent, the amount of bled steam (by impacting on the tube-side temperature in the condensation zone and thus the heat transfer).
The operating conditions used in the model are the following:

operating conditions		unit
Thermal power generation in core	1305	MW
Inlet temperature of the pressurized water in the primary cycle	321	°C
pressure of primary cycle	155	bar
mass flow rate in the primary cycle	7225	kg/s
Inlet temperature of the cooling water	12,5	°C
Pressure of cooling water	1	bar
mass flow rate of cooling water	19625	kg/s
steam generator pressure	60,45	bar
pressure of bled steam	21,85	bar
condenser pressure	0,0765	bar
Temperature of the dead state	12,5	°C
U (Kühlkasten)	5000	$W.m^{-2}.K^{-1}$
U (in condensation zone)	4000	$W.m^{-2}.K^{-1}$
A (condensation zone)	1000	m^2

Table 7: Operating conditions in the second set of simulations

4.2.3.1 Impact of the heat exchange area in the Kühlkasten on the amount of bled steam

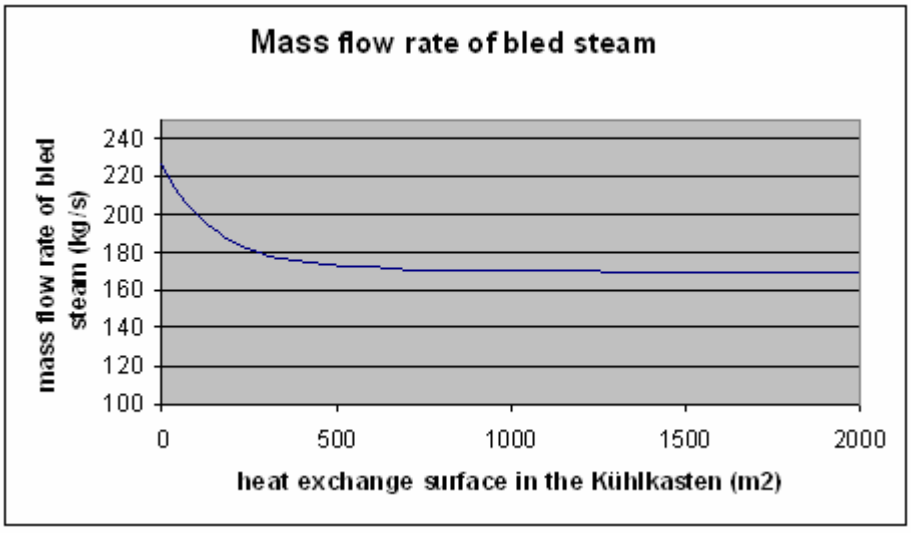

Figure 32: Mass flow rate of bled steam plotted against the heat exchange surface in the Kühlkasten

As the heat-exchange surface in the Kühlkasten increases, the feedwater outlet temperature from the Kühlkasten increases too and the amount of heat transferred in the condensation zone decreases (smaller temperature difference between feedwater and HP steam): the amount of bled steam required must therefore decrease. However, for very large heat-exchange areas, the amount of bled steam tends to asymptote since the outlet temperature from the Kühlkasten remains unchanged.

4.2.3.2 Impact of the heat-exchange area of the Kühlkasten on the performance of the various components of the plant

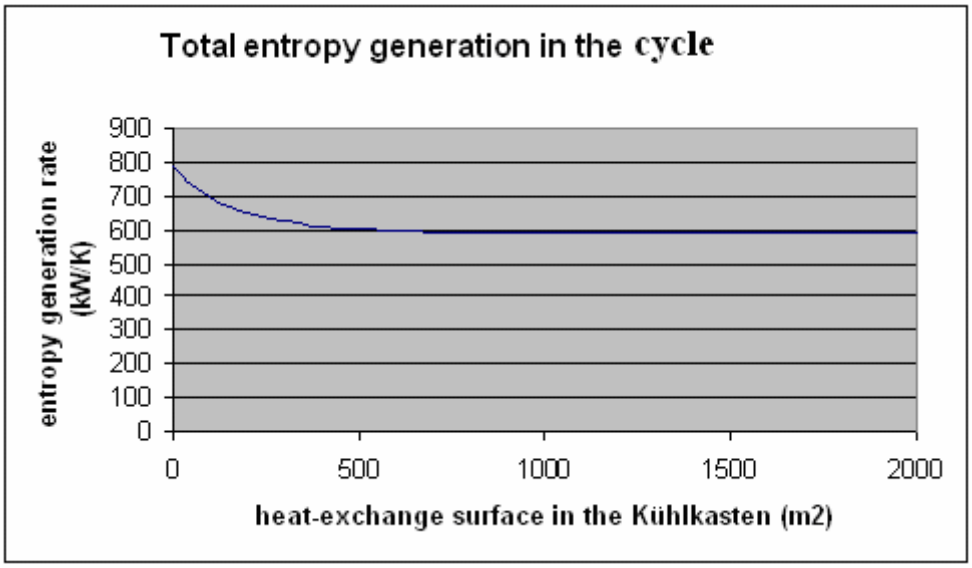

Figure 33: Total entropy generation rate in the cycle

Here again, we can plot the entropy generating rate of the various components against the heat-exchange area in the Kühlkasten. Unlike with the heat-exchange surface in the condensation zone, the overall entropy generating rate of the plant decreases monotonically with the heat-exchange surface in the Kühlkasten. This means that no turbine output peak should be expected: the turbine output will increase monotonically. In other words, the greater the heat-exchange surface in the Kühlkasten, the better. However, one must bear in mind that the efficiency improvement follows a law of diminishing returns: if the heat exchange area in the Kühlkasten is already very large, further increasing this area hardly decreases the entropy generation (i.e. hardly increases the turbine output).

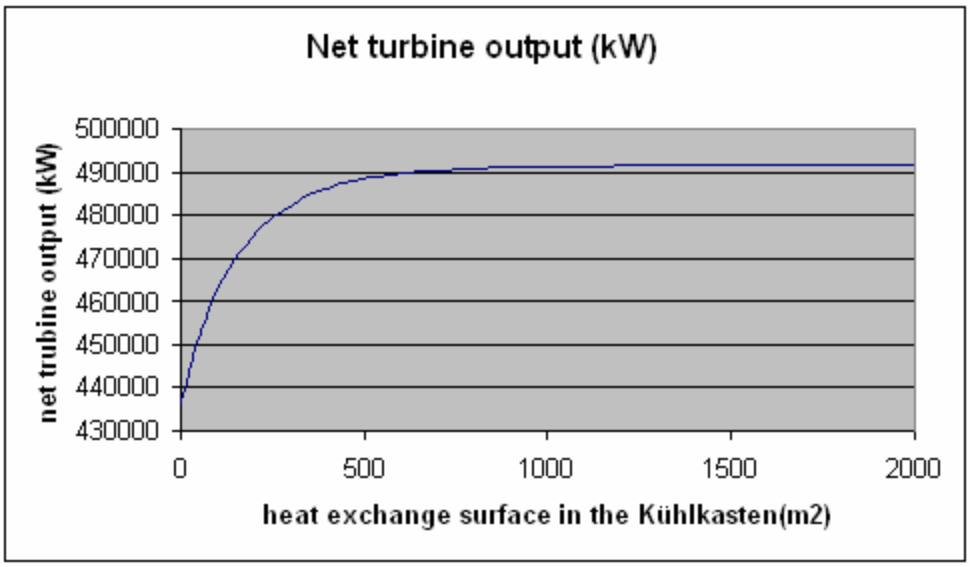

Figure 34: Net turbine output

Once again, we can either explain this with an intuitive reasoning or a more thermo dynamical one.
As explained previously, the power output of the cycle is determined by the amount of steam generated in the steam generator and the amount of steam bled in the turbine. In 4.2.3.1 we saw that increasing the heat exchange surface in the Kühlkasten reduces the amount of bled steam. Simultaneously, increasing the heat-exchange surface in the Kühlkasten leads to a greater overall heat-exchange rate which means that the temperature of the feedwater flowing out of the HP pre-heater will be greater, thus leading to more steam generation in the steam generator (warmer water input and fixed amount of heat transferred between primary and secondary cycles). Both trends (i.e. reduced amount of bled steam and increased amount of steam generated) lead to a power output increase since both trends tend to increase the amount of steam flowing in the turbine. In other words, there is no "competition" between these two phenomena (unlike in the condensation zone) which means that no optimum should be expected, both trends "pull in the same direction".

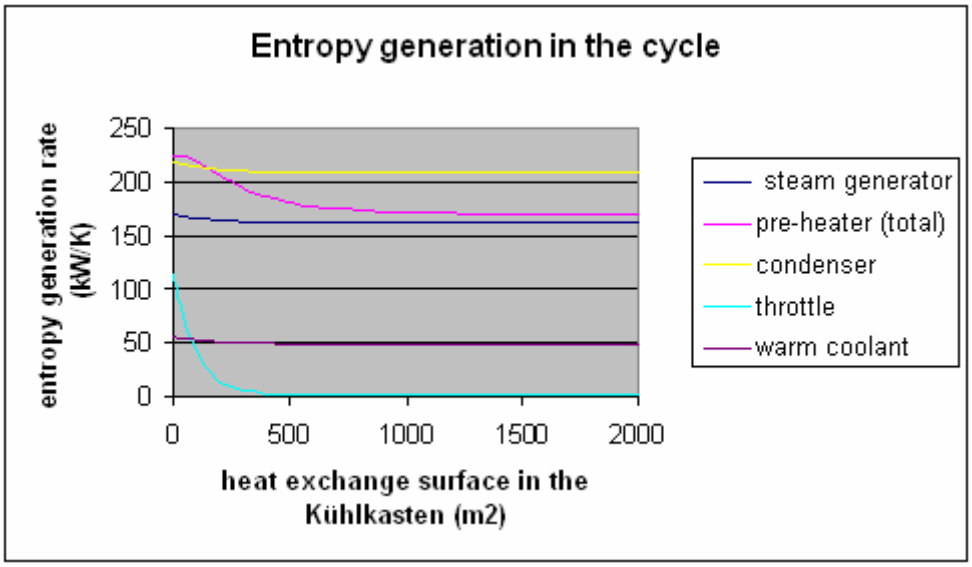

Figure 35: Entropy generation rate of the cycle's components

From a thermodynamic point of view, this overall entropy generation drop is mainly due to a sharp drop in entropy generation in the throttle and the HP pre-heater (the case of the HP pre-heater is in reality more complex than it appears and will be dealt with in section 4.2.3.3). The entropy generation rate decreases in all the other components but to a much lesser extent.

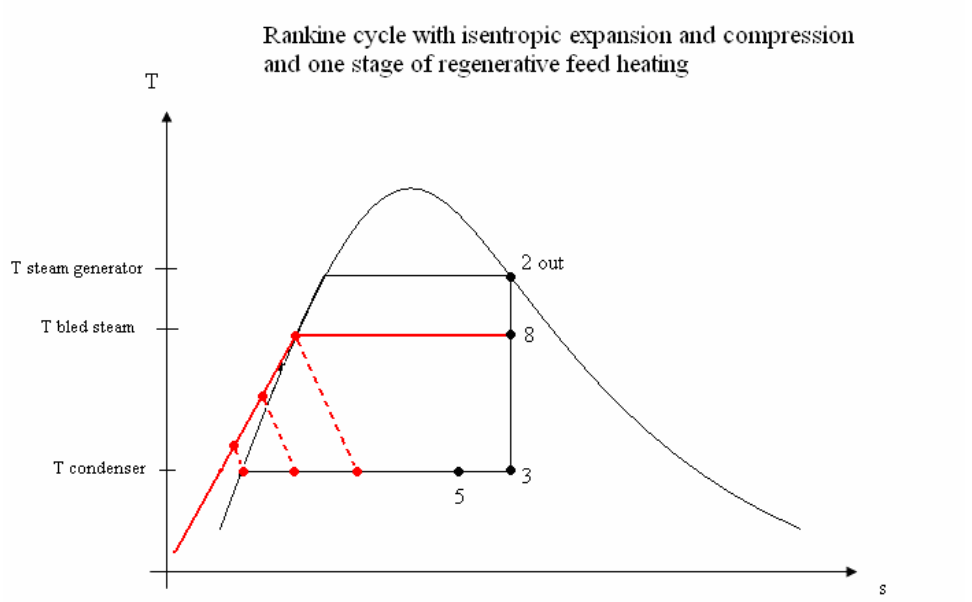

Figure 36: Entropy generation through throttling for various degrees of subcooling

The entropy generation drop in the throttle is easily understandable. The throttling process has been represented for various Kühlkasten configurations in Figure 36 and is an isenthalpic expansion between p_{bled} and $p_{condenser}$. The first throttling process would take place if there was no Kühlkasten at all (heat exchange surface = 0 m^2, throttling of

saturated liquid). As can be seen on the x-axis, this leads to an important entropy generation. The second throttling process was obtained with an intermediate heat exchange suface in the Kühlkasten. The throttling of subcooled liquid leads to less entropy generation. Finally, the last throttling process was obtained for a large heat-exchange surface (hardly any entropy creation since $T_{8out} \approx T_{sat}(p_{condenser})$).
In short, the greater the subcooling, the smaller the entropy generation in the throttle.

Note: physically speaking, the irreversibility of this isenthalpic throttling process can be understood by considering the temperature drop between inlet and outlet. The greater the temperature drop the fluid undergoes, the less "noble" its energy content becomes.

.

4.2.3.3 Entropy generation in the HP pre-heater for varying heat exchange surfaces in the Kühlkasten

If we take a closer look at the entropy generation in the HP pre-heater for various heat exchange surfaces inside the Kühlkasten, we notice a surprising behavior for small heat-exchange surfaces. The entropy generation rate increases and then decreases: there is a maximum entropy generation value for $A \approx 23 m^2$.

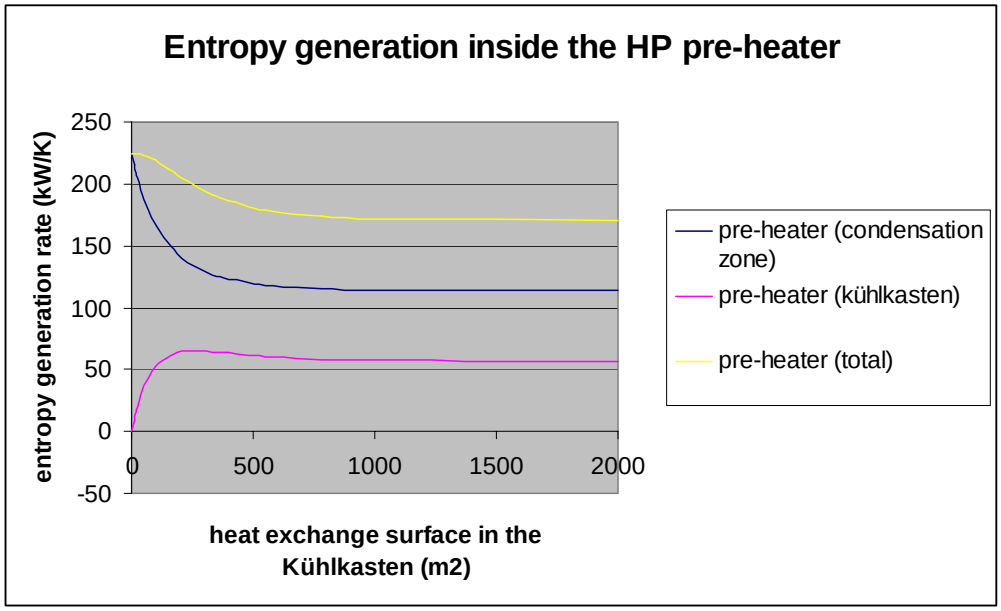

Figure 37: Entropy generation rate inside the pre-heater

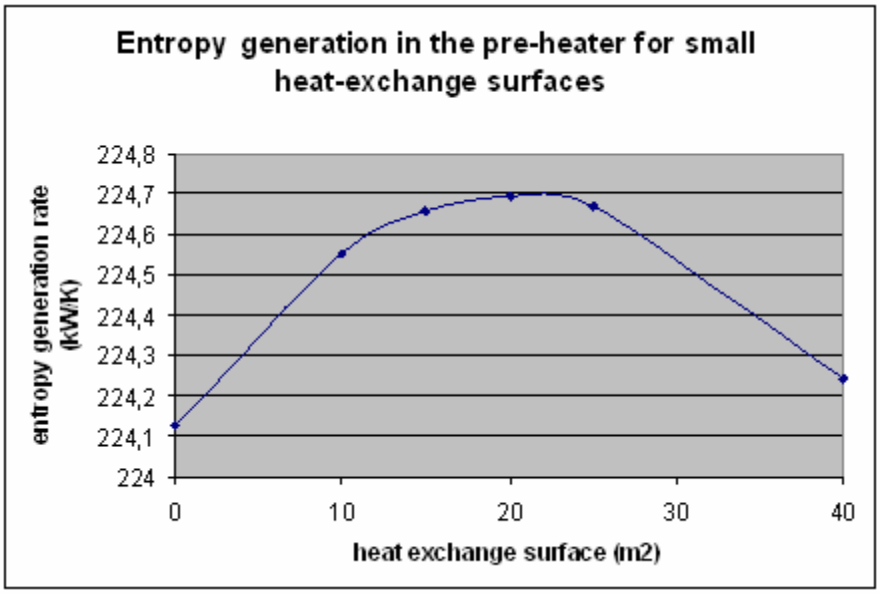

Figure 38: Close-up of the entropy generation rate in the pre-heater for small heat-exchange surfaces

On a more local scale, a peak entropy generation rate can also be observed in the Kühlkasten for A≈280m^2 (see figure 37).
This is the first time we come across a non-monotonous entropy generation rate in a *single* component. In 4.2.2.2 we had observed a non-monotonous overall entropy generation rate (which had led to a minimal entropy generation rate and the related peak turbine output), but this behavior was due to the superposition of monotonically varying entropy generation rates in the cycle components.

To understand this surprising result, we can consider the entropy generation rate associated to the heat transfer between two isothermal heat sources at T_{high} and T_{low}. The entropy lost by the hot source is: $\dot{S}_{high} = \frac{\dot{Q}}{T_{high}}$ and the entropy received by the cold source is $\dot{S}_{low} = \frac{\dot{Q}}{T_{low}}$ where $\dot{Q}$ is the rate of heat exchange between the two sources. The entropy generated during this process is therefore:

$$\dot{S}_g = \dot{S}_{low} - \dot{S}_{high} = \dot{Q}(\frac{1}{T_{low}} - \frac{1}{T_{high}}) = \dot{Q}\frac{(T_{high} - T_{low})}{T_{low}T_{high}} \qquad \text{Equation 129}$$

This simple example shows that the entropy generation rate is a function of two factors: the rate of heat exchange ($\dot{Q}$) and the temperature difference between cold and hot sources. This result will help us explain what is observed in the Kühlkasten.

- If the heat-exchange surface in the Kühlkasten is small (say $10m^2$) and if this surface is further decreased, we notice that the entropy generation rate rapidly decreases and draws nearer to 0. This is due to the fact that the heat transfer rate in the Kühlkasten is being dramatically reduced (from $10m^2$ to $1m^2$, there is an order of magnitude drop of the surface, which leads to a significant heat transfer rate drop since the temperatures gap between fluids is large) while the temperature difference between fluids only slightly increases.

- For large heat-exchange surfaces (say $700m^2$), if we further increase the heat exchange surface we notice that the entropy generation rate slowly decreases. Once again we have two competing effects with respect to entropy generation:
  -on the one hand the heat exchange rate increases (but only slightly given that the temperature difference between fluids is already low)
  -on the other hand, the average temperature difference between the fluids decreases
  This second effect has a greater impact, hence the overall entropy generation rate decline.

4.3 Conclusion of the analysis

Even though the previous analysis was carried out with a simplified power plant model, a number of important points valid for any real power plant can been deduced.

-Thermodynamically speaking, the role of the pre-heater is to reduce the entropy generation rate inside the steam generator (i.e. its irreversibility)

-Increasing the heat transfer surface in the condensation zone *increases* the amount of bled steam from the HP turbine, but only to a certain extent (for high heat exchange surfaces, the amount of bled steam levels off)

-Increasing the heat transfer surface in the Kühlkasten *decreases* the amount of steam bled from the HP turbine (also to a certain extent after which the amount of bled steam levels off).

-There is a fundamental difference between the addition of extra heat exchange surface in the condensation zone and in the Kühlkasten:

- Increasing the amount of heat transfer surface in the Kühlkasten will always improve the efficiency of the cycle since is increases the overall heat-exchange rate *without* bleeding more steam from the turbine. However, if the heat exchange surface in the Kühlkasten is already very large, the efficiency gain might be negligible and might not justify the additional costs: this fact can be estimated by calculating the effectiveness of the Kühlkasten.

$$\varepsilon_{Kühlkasten} = \frac{h_{liq,sat}(p_{bled}) - h_{8,out}}{h_{liq,sat}(p_{bled}) - h(p_{bled}, T_7)} \quad \text{Equation 130}$$

The closer the effectiveness to 1, the smaller the potential improvement.

- Increasing the amount of heat transfer surface in the condensation zone does not always improve the efficiency of the cycle because the heat-exchange rate in the HP pre-heater is increased *at the expenses of the steam flowing through the turbine*: there exists an optimal amount of bled steam. This optimal amount depends on the general cycle layout (e.g. number of steps of pre-heating, pressures at which the steam is bled and so forth), its calculation can therefore only be carried out by taking into account the characteristics of the entire cycle in the real plant (which is unfortunately far beyond the scope of this work!). The HP pre-heater designer should therefore bear in mind that this heat exchange surface must not be modified randomly or maximized.
  A criterion to assess the amount of steam actually bled over the amount of steam that could be bled with infinite surface is:

$$\tilde{\varepsilon} = \frac{\dot{m}_{bled}}{(\dot{m}_{bled})_{\max}} = \frac{\dot{m}_{bled}}{\dot{m}_{\sec}\dfrac{h(T_8, p_7) - h_9}{h_8 - h_{liq,sat}(T_8)}} = \frac{\dot{m}_{bled}(h_8 - h_{liq,sat}(T_8))}{\dot{m}_{\sec}(h(T_8, p_7) - h_9)} \quad \text{Equation 131}$$

The closer this ratio to 1 is, the nearer the actual amount of bled steam will be to the maximal amount of bled steam. Remember that this is not a criterion with which the component can be optimized.

5 Pressure drop and head loss calculations

Before starting the head loss and pressure drop calculations, it is important to highlight the difference between these two aspects of the energy equation: a head loss does not always lead to a pressure drop and a pressure drop does not always mean that the fluid has undergone a head loss. This introduction will clarify the upcoming calculations and avoid interpretation mistakes.

-A head loss is usually expressed in meters (but could also be expressed in Pa by multiplying by the earth's acceleration in $m.s^{-2}$ and the density of the fluid in $kg.m^{-3}$) and is always associated to a dissipative process: mechanical energy (i.e. freely convertible energy, for example $P + \frac{1}{2}\rho V^2 + \rho g z$) is degraded into thermal energy. Such a process is irreversible and is accompanied by entropy generation.

-A pressure drop can, under certain circumstances, be the direct consequence of a head loss. However, a pressure drop may also occur with no associated head loss, in which case the kinetic energy and/or the potential energy of the fluid will increase since the mechanical energy of the flow must remain constant (no head loss).

Most of the forthcoming calculations will be concerned with head loss calculations. However, in some cases it is also interesting to assess the static pressure drop and the corresponding calculations will be presented.

5.1 Shell-side pressure drop and head loss calculations

As seen previously, the shell-side flow consists of various stages:
-the steam flows into the pre-heater (sudden flow area expansion): the associated head loss must be calculated
-the steam flows through the bundle and condenses: we will show that the losses at this stage are negligible
-the condensate flows through the Kühlkasten: the fluid undergoes a significant head loss. In addition to this effect, we must take into account the *reversible* pressure drop due to the water column (upwards water flow) and the *reversible* static pressure variation due to fluid acceleration in the outlet tube.

5.1.1 Head loss at the HP-steam inlet

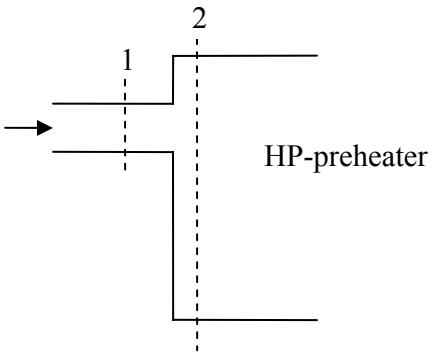

Figure 39: Isenthalpic expansion of steam

Since there is no work or heat transfer between sections 1 and 2, the energy equation reads:

$$\dot{m}(u_1 + p_1 v_1 + \frac{1}{2}V_1^{\,2} + gz_1) = \dot{m}(u_2 + p_2 v_2 + \frac{1}{2}V_2^{\,2} + gz_2) \qquad \text{Equation 132}$$

Since z_1=z_2 and $v = \frac{1}{\rho} \approx cte$, we obtain:

$$p_1 - p_2 = \rho(\frac{1}{2}(V_2^{\,2} - V_1^{\,2}) + (u_2 - u_1)) \qquad \text{Equation 133}$$

.The internal energy difference is what is quantified by the head loss: u_2-u_1>0 because mechanical energy has been degraded into thermal energy (hence the higher internal energy of state 2). $\rho(u_2 - u_1)$ is usually referred to as Δp even though it is not (always) the static pressure difference, and it is quantified as follows [9]:

$$\rho(u_2 - u_1) = \xi\rho\frac{V_1^{\,2}}{2} = (1 - \frac{A_1}{A_2})^2 \rho\frac{V_1^{\,2}}{2} \qquad \text{Equation 134}$$

Where A_1 and A_2 are the flow areas before and after the expansion.
Since A_2>>A_1, we obtain:

$$\rho(u_2 - u_1) = \rho\frac{V_1^{\,2}}{2} \qquad \text{Equation 135}$$

which entails: $p_1 - p_2 = \rho(\frac{1}{2}(V_2^{\,2} - V_1^{\,2}) + (u_2 - u_1)) = \rho\frac{V_2^{\,2}}{2}$ Equation 136

Since we consider $A_2 >> A_1$, then V_2 is very small and we obtain:

$$P_1 \approx P_2$$

Consequently, there is a non-negligible head loss, but hardly any static pressure drop. This is not contradictory: the mechanical energy that has been degraded is mainly the kinetic energy of the flow before 1.

5.1.2 Steam flow through the bundle

The head loss associated with the flow through the bundle cannot be calculated accurately because as the steam travels through the bundle, it condenses thus leading to a varying flow velocity. To remain on the safe side, the calculations can be carried out as if the steam did not condense (i.e. as if the amount of vapor flowing in the bundle remained constant).
The bundle inlet velocity was calculated in a section 3.3 and will be used in the following calculations.
The head loss can be calculated as follows:

$$\Delta P = \xi N_W \rho \frac{w_e^{\ 2}}{2} \quad \text{Equation 137}$$

Where ξ is the resistance coefficient associated to the flow through a tube-row, N_W is the number of major flow resistances and w_e is the velocity in the narrowest cross-section. For a staggered tube layout, the calculation of w_e depends on the orientation of the tube pattern with respect to the flow. This leads to another problem since the steam flows in from *all* sides, and there is therefore no preferential orientation.
In order to remain as conservative as possible, we are going to consider a hypothetical bundle configuration where the tubes on the outer periphery are all 21mm apart.

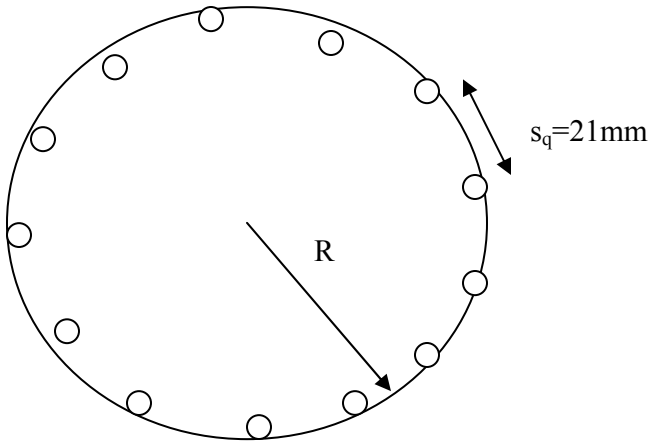

Figure 40: Bundle with tubes on its periphery

The velocity in the narrowest cross-section is then defined as the velocity between the tubes in this circular tube-row. The fraction of the circle available for flow is therefore:

$$\tilde{\alpha} = 1 - \frac{2\pi R}{s_q}\frac{2r}{2\pi R} = 1 - \frac{2r}{s_q} \quad \text{Equation 138}$$

Where r is the outer tube radius. The velocities calculated in section 3.3 were based on the "average" free flow surface α which does not correspond to our current worse-case scenario. The velocities obtained in section 3.3 will therefore have to be adapted by multiplying by an $\frac{\alpha}{\tilde{\alpha}}$ coefficient:

$$\tilde{v}_i(z) = \frac{\alpha}{\tilde{\alpha}} v_i(z) = \frac{\alpha}{\tilde{\alpha}} \frac{\dot{m}_i(z)}{\alpha \rho S*} = \frac{\dot{m}_i(z)}{\tilde{\alpha}\rho S*} \quad \text{Equation 139}$$

This velocity will be used instead of w_e.

The pressure drop calculations can then be carried out for a staggered pattern with $b \geq \frac{1}{2}\sqrt{2a+1}$ according to [7]:

$$\mathrm{Re} = \frac{\tilde{v}_i d \rho}{\eta} \quad \text{Equation 140} \qquad a = \frac{s_q}{d} \quad \text{Equation 141} \qquad b = \frac{s_1}{d} \quad \text{Equation 142}$$

$$\xi = \xi_l + \xi_t (1 - e^{-\frac{\mathrm{Re}+1000}{2000}}) \quad \text{Equation 143}$$

$$\xi_l = \frac{f_{a,l,v}}{\mathrm{Re}} \quad \text{Equation 144} \qquad f_{a,l,v} = \frac{280\pi((b^{0,5} - 0,6)^2 + 0,75)}{(4ab - \pi)a^{1,6}} \quad \text{Equation 145}$$

$$\xi_t = \frac{f_{a,t,v}}{\mathrm{Re}^{0,25}} \quad \text{Equation 146}$$

$$f_{a,t,v} = 2,5 + \frac{1,2}{(a - 0,85)^{1,08}} + 0,4\left(\frac{b}{a} - 1\right)^3 - 0,01(\frac{a}{b} - 1)^3 \quad \text{Equation 147}$$

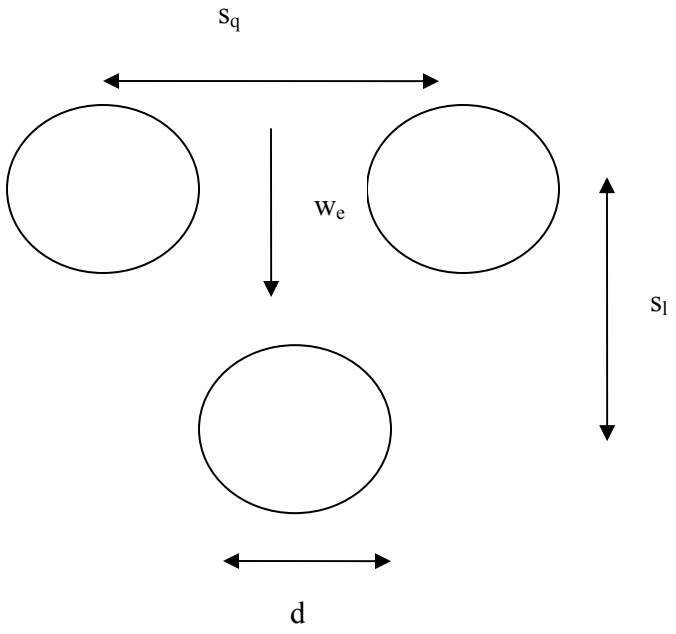

Figure 41: Tube layout

Since the flow is isothermal (condensation of saturated steam), no further coefficients (taking into account the temperature variation of the steam) need to be considered.
The number of tube rows across which the steam flows cannot be calculated exactly since the real flow pattern in the bundle does not correspond to the simple scenarios of [7]. An order of magnitude of the number of tube rows (i.e. number of tube rows along the bundle's radius) was therefore used in the calculations.

5.1.3 Condensate flow through the Kühlkasten

5.1.3.1 General analysis of the Kühlkasten

Static pressure drops and head losses have to be treated with particular care in the Kühlkasten since this component of the heat exchanger consists in a vertical upward flow around a series of baffles.
Figure 42 shows a schematic representation of the Kühlkasten which will be helpful when it comes to understanding the pressure and head variation inside the component.

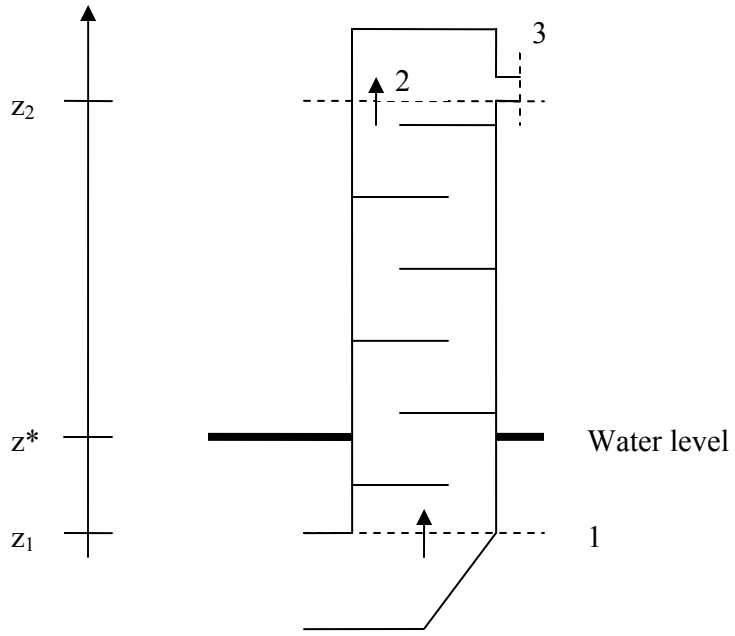

Figure 42: Simplified representation of the Kühlkasten

The energy equation between sections 1 and 2 of Figure 42 reads:

$$\rho u_1 + p_1 + \frac{1}{2}\rho V_1^{\,2} + \rho g z_1 = \rho u_2 + p_2 + \frac{1}{2}\rho V_2^{\,2} + \rho g z_2 \quad \text{Equation 148}$$

Since velocities 1 and 2 are identical (same cross-section and negligible density variation), the static pressure difference between 1 and 2 is:

$$p_1 - p_2 = \rho(u_2 - u_1) + (z_2 - z_1)\rho g \quad \text{Equation 149}$$

$\rho(u_2-u_1)$ is the head loss. The pressure drop between 1 and 2 is therefore due to:
-an irreversible head loss due to friction against tubes and eddy dissipation
-a reversible pressure drop due to the hydrostatic effect of the water column

The static pressure of the fluid will finally slightly decrease as it flows through the (narrow) outlet tube due to the velocity increase and the additional mechanical energy dissipation. According to the energy equation, the static pressure variation is:

$$p_2 - p_3 = \frac{1}{2}\rho(V_3^{\,2} - V_2^{\,2}) + \rho(u_3 - u_2) \qquad \text{Equation 150}$$

Finally, if we neglect the small head loss in the flooded zone and the small fluid acceleration as it enters the Kühlkasten, the pressure difference between section 1 and the water surface is entirely hydrostatic:

$$p_1 = p^* + \rho g(z^* - z_1) \qquad \text{Equation 151}$$

The total static pressure drop between the water surface and the outlet tube is therefore:

$$p^* - p_3 = \rho g(z_2 - z^*) + \rho(u_3 - u_1) + \frac{1}{2}\rho(V_3^{\,2} - V_2^{\,2}) \qquad \text{Equation 152}$$

Since there is hardly any static pressure drop through the HP steam inlet (see 5.1.1) and the pressure drop inside the bundle is small, p*- p_3 is also roughly equal to the shell-side static pressure drop between the inlet and the outlet of the HP pre-heater.
The head loss $\rho(u_3-u_1)$ is calculated in section 5.1.3.2

5.1.3.2 Calculation of the head loss inside the Kühlkasten

According to [8], the head loss in the Kühlkasten can be calculated as follows.

5.1.3.2.1 Cross flow pressure loss

This component of the head loss is obtained via:

$$(n_u - 1)\Delta p_Q \quad \text{Equation 153}$$

Where n_u is the number of baffles in the heat-exchanger and Δp_Q is equal to:

$$\Delta p_Q = \Delta p_{Q,0} f_L f_B = \xi n_W \rho \frac{w_e^{\,2}}{2} f_L f_B \quad \text{Equation 154}$$

Where n_W is the number of major resistances, ξ is the resistance coefficient and f_L and f_B are correction factors taking into account the leakage flow between the tubes and bores in the baffles and the by-pass flow between the outer tubes and the shell respectively.

For a staggered tube layout with $b \geq \frac{1}{2}\sqrt{2a+1}$, ξ is calculated as follows:

$$\xi = \xi_l f_{z,t} + \xi_t f_{z,t}(1 - e^{-\frac{\mathrm{Re}+1000}{2000}}) \qquad \text{Equation 155}$$

$$\xi_l = \frac{f_{a,l,v}}{\mathrm{Re}} \quad \text{Equation 156} \qquad f_{a,l,v} = \frac{280\pi((b^{0,5} - 0{,}6)^2 + 0{,}75)}{(4ab - \pi)a^{1,6}} \quad \text{Equation 157}$$

$$\xi_t = \frac{f_{a,t,v}}{\mathrm{Re}^{0,25}} \qquad \text{Equation 158}$$

$$f_{a,t,v} = 2{,}5 + \frac{1{,}2}{(a-0{,}85)^{1{,}08}} + 0{,}4\left(\frac{b}{a}-1\right)^3 - 0{,}01\left(\frac{a}{b}-1\right)^3 \qquad \text{Equation 159}$$

$$\mathrm{Re} = \frac{w_e d \rho}{\eta} \quad \text{Equation 160} \qquad w_e = \frac{\dot{V}}{A_E} \quad \text{Equation 161}$$

$A_E = SL_E$ where S is the distance between baffles, L_E is the smallest available flow length measured along the diameter of the bundle and $\dot{V}$ is the volume flow rate.
The correction factor f_L is obtained via:

$$f_L = e^{-1{,}33(1+R_M)R_L{}^r} \quad \text{Equation 162} \qquad r = -0{,}15(1+R_M)+0{,}8 \quad \text{Equation 163}$$

$$R_M = \frac{A_{SMU}}{A_{SG}} \quad \text{Equation 164} \qquad R_L = \frac{A_{SG}}{A_E} \quad \text{Equation 165}$$

$$A_{SG} = A_{SRU} + A_{SMU} \quad \text{Equation 166}$$

$$A_{SRU} = (n - \frac{n_F}{2})\frac{\pi(d_B{}^2 - d_a{}^2)}{4} \qquad \text{Equation 167}$$

$$A_{SMU} = \frac{\pi}{4}(D_i{}^2 - D_l{}^2)\frac{360-\gamma}{360} \qquad \text{Equation 168}$$

where γ is the angle defined by the two ends of the straight edge of the baffle and the centre of the baffle, n is the number of tubes in the bundle, $n_F/2$ is the number of tubes in a "window" (tubes free from a given baffle), d_B is the bore diameter and d_a is the outer tube diameter.
The correction factor f_B is obtained via:

$$f_B = e^{-3{,}7R_B} \quad \text{Equation 169} \qquad \text{where} \qquad R_B = \frac{A_B}{A_E} \quad \text{Equation 170}$$

$$\text{where } A_B = S(D_i - D_B - e) \qquad \text{Equation 171}$$

where D_i is the inner shell diameter, D_B is the diameter of the smallest circle encompassing the outer tubes of the bundle, D_l is the diameter of a baffle and e is the flow length between two adjacent tubes.

5.1.3.2.2 Pressure loss in the end zones

Most of the calculation of the pressure loss in an end zone is similar to that presented in 5.1.3.2.1:

$$\Delta p_{QE} = \Delta p_{QE,0} f_B = \xi n_{WE} \rho \frac{w_{e,E}^{\ 2}}{2} f_B \qquad \text{Equation 172}$$

where n_{WE} is the number of major resistances in an end zone and $w_{e,E}$ is calculated via:

$$w_{e,E} = w_e \frac{S}{S_E} \qquad \text{Equation 173}$$

where S_E is the distance between an end baffle and the corresponding axial extremity of the heat-exchanger. All correlations used in 5.1.3.2.1 are then valid, as long as $w_{e,E}$ is used instead of w_e if $S \neq S_E$ (which is the case for the top end zone).

5.1.3.2.3 Pressure losses in the window zones

The total pressure loss in the window zone is:

$$\Delta p = n_U \Delta p_F \qquad \text{Equation 174}$$

Where n_U is the number of baffles and

$$\Delta p_F = \sqrt{\Delta p_{F,l}^{\ 2} + \Delta p_{F,t}^{\ 2}} f_z f_l \qquad \text{Equation 175}$$

f_l is defined in 5.1.3.2.1 and f_z is not defined since, in our case, water (and not colder steam) flows along the wall. Therefore f_z=1 was assumed.

$$\Delta p_{F,l} = \left(\frac{56}{e w_z \rho / \eta} n_{WF} + \frac{52}{d_g w_z \rho / \eta} \frac{S}{d_g} + 2 \right) \frac{\rho w_z^{\ 2}}{2} \qquad \text{Equation 176}$$

$$\text{and } \Delta p_{F,t} = (0{,}6 n_{WF} + 2) \frac{\rho w_z^{\ 2}}{2} \qquad \text{Equation 177}$$

$$n_{WF} = \frac{0{,}8H}{s_l} \qquad \text{Equation 178} \qquad \text{and} \qquad d_g = \frac{4A_F}{U_F} \qquad \text{Equation 179}$$

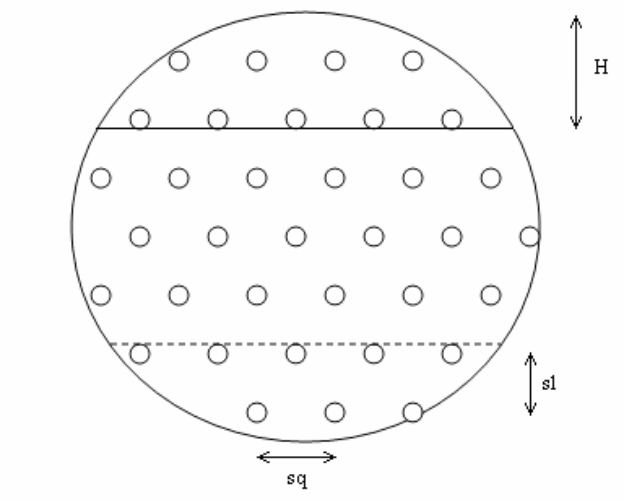

Figure 43: Tube pattern and baffles in the Kühlkasten

$$A_F = A_{FG} - A_{FR} \qquad \text{Equation 180}$$

$$A_{FG} = (\frac{\pi}{4} D_i^{\,2} - \frac{(D_i - 2H)D_1}{4} \sin(\frac{\gamma}{2})) \qquad \text{Equation 181}$$

$$A_{FR} = \frac{\pi}{4} d_a^{\,2} \frac{n_F}{2} U_F = \pi D_i \frac{\gamma}{360} + \pi d_a \frac{n_F}{2} \qquad \text{Equation 182}$$

$$w_z = \sqrt{w_e w_p} \qquad \text{Equation 183} \qquad w_p = \frac{\dot{V}}{A_F} \qquad \text{Equation 184}$$

$$w_e = \frac{\dot{V}}{A_E} \qquad \text{Equation 185} \qquad \text{(as previously defined)}$$

5.1.3.2.4 Head loss at the inlet and outlet of the Kühlkasten

The shock loss pressure drop due to the sudden flow contraction at the Kühlkasten's outlet can be calculated via:

$$\Delta p_{outlet} = \xi_s \frac{\rho w_s^{\,2}}{2} \qquad \text{Equation 186}$$

where

$$w_s = \frac{\dot{V}}{\pi d_s^{\,2}/4} \qquad \text{Equation 187}$$

where d_s is the diameter of the outlet tube and $\dot{V}$ is the volume flow rate.
Since the outlet configuration of the Kühlkasten is more complicated than a mere shock-loss due to contraction, a shock loss coefficient equal to 1 was chosen (to remain on the safe side).

The shock loss at the Kühlkasten's inlet is much smaller than at the outlet given the relatively low velocities involved. However, it can again be estimated via:

$$\Delta p_{inlet} = \xi_s \frac{\rho w_s^{\,2}}{2} \qquad \text{Equation 188}$$

Where w_s is the velocity at the inlet of the Kühlkasten. Once again, a shock loss coefficient equal to 1 was used.

5.1.3.2.5 Grid shock loss

At the bottom of the Kühlkasten, the tubes are held together by means of a grid. The associated shock loss can be calculated according to [12]:

$$\Delta p_G = \xi \rho \frac{w^2}{2} \qquad \text{Equation 189}$$

where w is the velocity before the obstacle and ξ is calculated as follows:

$$\xi = 1{,}3(1-f) + \left(\frac{1}{f} - 1\right)^2 \qquad \text{Equation 190}$$

Where f is the ratio of the clear area over the total flow area before the obstacle (reduced flow area of the obstacle).

5.1.3.2.6 Total head loss in the Kühlkasten

The total head loss in the Kühlkasten is the sum of the previous head losses, namely:

$$\Delta p = (n_u - 1)\Delta p_Q + \Delta p_{inlet} + \Delta p_{outlet} + \Delta p_{end\ zones} + n_u \Delta p_F + \Delta p_G \qquad \text{Equation 191}$$

5.2 Tube-side pressure drop and head loss calculations

The tube-side head loss is due to:
-flow from the inlet pipe to the inlet chamber (shock loss)
-flow from the inlet chamber to the tube bundle (shock loss)
-flow inside the bundle (frictional loss)
-flow from the tube bundle to the outlet chamber (shock loss)
-flow from the outlet chamber to the outlet pipe (shock loss)

Since the altitude and the diameter of the inlet and outlet feedwater tubes are the same (which implies equal velocities if we neglect the density variation), the head loss will be equal to the pressure drop.

5.2.1 Shock loss from the inlet tube to the inlet chamber (sudden expansion)

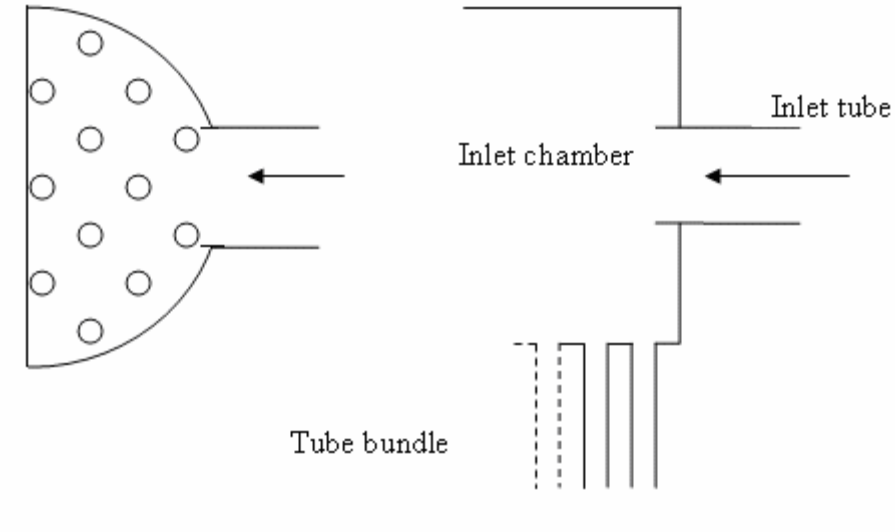

Figure 44: View from above and side view of the inlet chamber

According to [9] his component of the head loss can be calculated via the following equation:

$$\Delta p = (1 - \frac{f_1}{f_2})^2 \rho \frac{w_1^2}{2}$$ Equation 192

where f_1 and f_2 are the surfaces before and after the expansion respectively. In our case, it is difficult to define the flow surface after the expansion since the chamber is semi-cylindrical. Since $f_2 >> f_1$ and in order to remain conservative, we are going to take $(1-f_1/f_2)^2 \approx 1$

5.2.2 Shock loss from the inlet chamber to the tube bundle (sudden contraction)

The shock loss coefficient at a bundle inlet depends on the tube layout and whether the tubes protrude from the plate. Since this second point is not clear, the worst case scenario was envisaged (i.e. protruding tubes) and a shock loss coefficient of 0,3 was used (graphical result, see [10], obtained with the appropriate s/d_i ratio where s is the pitch between tubes and d_i is the inner tube diameter) .
The head loss is then obtained via:

$$\Delta p = \xi \rho \frac{w_1^{\,2}}{2} \qquad \text{Equation 193}$$

Where w_1 is the velocity inside the tube

5.2.3 Flow inside the bundle

Unlike the previous head loss calculations, the head loss inside the bundle is due to fluid friction against the walls. This effect can easily be taken into account [11]:

$$\Delta p = \xi \frac{l}{d_i} \frac{\rho w_i^{\,2}}{2} \qquad \text{Equation 194}$$

Where l is the tube length to be considered, d_i is the inner tube diameter and w_i is the velocity inside the tube. The friction factor ξ can be calculated with various correlations. The Colebrook and White correlation [23] is valid in a wide Re range:

$$\frac{1}{\sqrt{\xi}} = -2\lg\left(\frac{2{,}51}{\mathrm{Re}_i \sqrt{\xi}} + \frac{K/d_i}{3{,}71}\right) \qquad \text{Equation 195}$$

where K is the tube roughness and Re_i is the Reynolds number calculated with the inner tube diameter.
Note that this relation is implicit (ξ cannot be expressed directly as a function of Re_i, K and d_i) which means that ξ can only be determined iteratively.

5.2.4 Shock loss from the tube bundle to the outlet chamber (sudden expansion)

Once again, the usual expression: $\Delta p = (1 - \frac{f_1}{f_2})^2 \rho \frac{w_1^{\,2}}{2}$ Equation 196

was used with $(1-f_1/f_2)^2 \approx 1$

5.2.5 Shock loss from the outlet chamber to the outlet tube (sudden contraction)

Here again it is difficult to define the f1/f2 ration since the outlet chamber is cylindrical. To remain on the safe side, a resistance coefficient of 1 was used in the calculations:

$$\Delta p = \rho \frac{w_2^{\ 2}}{2} \qquad \text{Equation 197}$$

5.2.6 Total tube-side head loss

The overall tube-side head loss is obtained by adding all the previous head loss. As explained previously, since the velocity at the inlet and outlet is the same (if we neglect density variations) and the inlet and outlet tubes are at the same altitude, the head loss is equal to the static pressure drop between inlet and outlet.

5.3 Implementation of the excel calculations in the excel model

Carrying out all the previous calculations by hand is a time-consuming (and tedious) work. All the calculations have therefore been automated on an excel spreadsheet alongside the thermal calculations. The head loss calculations do indeed require results from the thermal analysis in order to be carried out (for example, the average fluid temperature in the heat-exchanger).
Note that in the spreadsheet, the user can manually adjust the value of the various shock loss coefficients if they do not appear to be satisfactory.
In addition to the head loss, the static pressure difference between various sections has been included.

5.4 Results

5.4.1 Order of magnitude of the head loss in the bundle

The maximal v_i obtained in the velocity profile calculation will be used here:

$$(v_i)_{max}=0{,}65 \text{m/s}$$

$$(\tilde{v}_i)_{\max} = \frac{\alpha}{\tilde{\alpha}}(v_i)_{\max} = \frac{0{,}473}{0{,}238} * 0{,}65 = 1{,}292 m/s$$

$$\mathrm{Re} = \frac{1{,}292 * 16E-3 * 10{,}891}{1{,}629E-5} = 1{,}382E4$$

$$\xi = \xi_l + \xi_t (1 - e^{-\frac{\mathrm{Re}+1000}{2000}}) = \frac{194{,}87}{1{,}382E4} + \frac{5{,}259}{(1{,}382E4)^{0{,}25}}(1 - e^{-\frac{1{,}382E4+200}{1000}}) = 0{,}4983$$

An order of magnitude of the number of tube rows the steam has to flow across is 50. The associated pressure drop is therefore:

$$\Delta p = \xi N_W \rho \frac{w_e^{\ 2}}{2} = 0{,}4983 * 50 * 10{,}891 * \frac{1{,}292^2}{2} = 226\ Pa$$

The pressure drop in the bundle is therefore very small and turns out to be negligible with respect to the head loss in the Kühlkasten.

5.4.2 Head loss and static pressure difference in the HP pre-heater

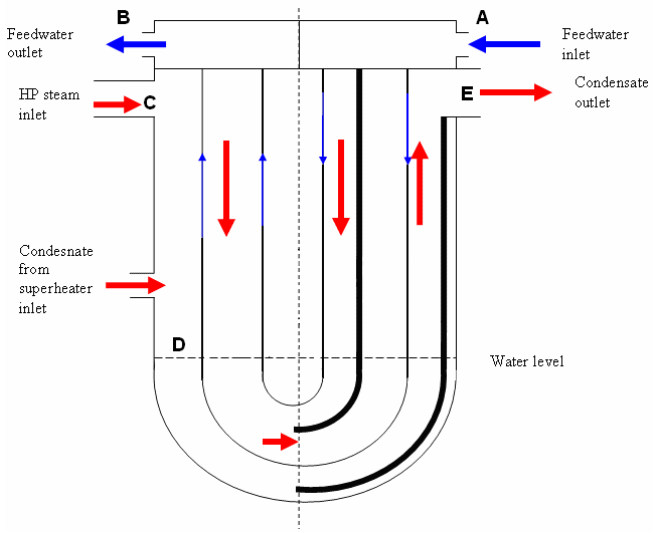

Figure 45: The HP pre-heater

	head loss (Pa)	static pressure difference (Pa)
A-B	5,32E+04	5,32E+04
C-D	8,58E+03	≈0
D-E	7,13E+04	1,15E+05
C-E	7,99E+04	1,15E+05

Table 8: Head losses and static pressure differences

One must bear in mind that pressure drop and head loss calculations are usually based on empirical correlations and are therefore approximate calculations. The previous values should therefore be considered as *orders of magnitude*.

6 Flow-induced vibrations

The HP pre-heater is subject to cross-flow both in the condensation zone since steam is drawn into the bundle and in the Kühlkasten when the condensate flows around the baffles. The HP pre-heater is therefore prone to flow-induced vibrations in both zones, each one of which will be treated separately.

Two different mechanisms are of concern for the tube bundle:
-vortex induced vibrations
-fluid-elastic instability
The physics underpinning both mechanisms are different and will be presented in distinct paragraphs.

6.1 Theory

6.1.1 Vortex induced vibration

When a tube is subject to cross-flow, it sheds vortices on both sides alternately. The entire phenomenon has a frequency f_w. This shedding disturbs the pressure distribution around the tube and it is therefore submitted to periodically-varying forces. In the lift direction (orthogonal to the flow), the period of this force is equal to f_w and in the drag direction (i.e in the flow direction), it is equal to $2f_w$.
If f_w or $2f_w$ happen to draw close to one of the natural frequencies of the tube, a phenomenon called lock-in may occur: the shedding frequency will shift to the natural frequency of the tube which will lead to the resonance of the structure. The associated high amplitude vibrations in the tubes may cause substantial damage [14].

The shedding frequency is calculated via the Strouhal number:

$$Sr_w = \frac{f_w d_a}{u_\tau} \qquad \text{Equation 198}$$

Where f_w is the shedding frequency, u_τ is the velocity inside the bundle and d_a is the outer tube diameter. S_r is independent of Re in large Re ranges, a typical value is 0,2. It is however strongly dependent on the tube pattern in the tube bundle (30°, 60°, 90° etc…) and on the pitch to diameter ratio of the pattern.

For a 30° tube pattern, the following correlations are proposed [15]:

$$Sr_{w1} = \frac{1}{3{,}62(\tau - 1)^{0{,}45}} \qquad \text{Equation 199}$$

$$Sr_{w2} = \frac{1}{2{,}41(\tau - 1)^{0{,}41}} \qquad \text{Equation 200}$$

Where τ is the ratio of the pitch between adjacent tube centers and the tube diameter. The fundamental vibration frequency of a tube (length l, mass m) loosely maintained on both tips is:

$$f^* = \frac{\pi}{2l^2}\sqrt{\frac{EI}{m}} \qquad \text{Equation 201}$$

where

$$I = \frac{\pi}{64}(d_a{}^4 - d_i{}^4) \qquad \text{Equation 202}$$

d_a is the outer tube diameter, d_i is the inner tube diameter and E is the modulus of elasticity of steel. The tube mass per unit length m must also take into account the fluid flowing inside the tube and the mass of outside fluid vibrating with the tube:

$$m = m_R + m_h \qquad \text{Equation 203}$$

$$m_R = \frac{\pi}{4}(\rho_R(d_a{}^2 - d_i{}^2) + \rho_i d_i{}^2) \qquad \text{Equation 204}$$

$$m_h = c_h \rho_f \frac{\pi}{4} d_a{}^2 \qquad \text{Equation 205}$$

Where ρ_R is the density of the metal the tube is made of, ρ_f is the density of the fluid flowing outside the tube, ρ_i is the density of the fluid flowing inside the tube and c_h is a mass coefficient depending on the pitch to diameter ratio in the bundle.

The fundamental frequency obtained is only valid for a tube with pinned ends and will vary if, for example, one end is firmly fixed or unsupported. The respective fundamental frequencies of any of these configurations can be worked out on the basis of the "pinned ends" case by using the correction factors provided by [16].

The tubes in the bundle are in reality held in position by a series of grids. This configuration leads to complex vibration patterns along the tube. However, a conservative way to carry out the calculations is to consider each tube section between two consecutive grids (or between a tube end and the first grid) as a separate tube in itself with the appropriate support conditions.

In order to determine if the tubes are prone to resonance, the flow velocity inside the bundle leading to synchronous tube vibration and vortex shedding must be calculated and compared with the actual velocity in the bundle.
If the actual velocity is 0,7 times smaller than the resonance velocity, lock-in is not likely to take place.

Note: the periodic forces triggered off by eddy shedding (if lock-in occurs) are high enough to lead to serious vibration problems only if the fluid density is high. Therefore, eddy shedding is ignored if the fluid is a gas or a vapor.

6.1.2 Fluid-elastic instability

If the velocity in the bundle exceeds a critical velocity, the tube vibration amplitude inside the bundle will start increasing very rapidly. This instability is due to the interaction of the flow with the entire tube row: unlike vortex-induced vibrations which can affect an isolated tube, fluid-elastic instability is only possible if an entire tube row is subject to cross flow. The tubes follow an elliptic motion which can lead within short periods to serious damage (either caused by tube-to-tube impacting, fatigue failure or severe fretting wear) [14].

The dimensionless critical velocity can be calculated by means of the following equation [20]:

$$u_k* = \frac{u_{sk}}{f_i d_a} = K(\tau)\left[\frac{m\Lambda}{\rho_f {d_a}^2}\right]^P \quad \text{Equation 206}$$

where m is the tube mass per unit length (calculated as before), ρ_f is the density of the fluid flowing around the tube, d_a is the outer tube diameter and Λ is the logarithmic decrement. This logarithmic decrement is a function of the damping inside the bundle. If the tube is not maintained by any grids, this logarithmic decrement can be calculated as follows.

- If a vapor or a gas is flowing through the bundle, the damping is due to the material and the fixed ends of the tube. Depending on the length of the tube, Λ_M varies between 0,005 and 0,02.
- If a liquid is flowing through the bundle, a viscous damping must be added:

$$\Lambda_V = \pi \frac{\rho_f {d_a}^2}{mST^{0,42}} \frac{1+(\frac{1}{\tau'})^3}{(1-(\frac{1}{\tau'})^2)^2} \quad \text{Equation 207}$$

where the Stokes number is $ST = \frac{\pi f_i {d_a}^2}{2\nu_f}$ (Equation 208) and $\tau'=1,7\ \tau$ for a triangular tube layout.

The total logarithmic decrement is then $\Lambda=\Lambda_V+\Lambda_M$. For a 60° tube pattern and a vapor or a gas flowing in the bundle, P=0,4 and $K(\tau)=3,1$. For a 30° tube layout and a liquid flowing in the bundle, P=0,15 and $K(\tau)=1,5(\tau+0,5)$

6.2 Results

6.2.1 Fluid-elastic instability and vortex-induced vibration in the Kühlkasten

6.2.1.1 Vortex-induced vibrations

The resonance velocity with the first vortex mode is 5,37 m/s; it is 3,74 m/s with the second mode (see 6.3 for detailed calculations). They are significantly higher than the typical cross-flow velocity in the Kühlkasten which does not exceed 1,5 m/s. Lock-in is therefore unlikely.

6.2.1.2 Fluid-elastic instability

As explained previously, the calculations were carried out with a tube pinned at both ends, the length of which is equal to the distance between two adjacent support grids. This is a very conservative way of estimating the critical velocity since the damping corresponding to this configurations is much lower than the real damping (which is mostly due to the presence of the grids).
Despite these conservative assumptions, the critical velocity (4,35 m/s, see 6.3) is still significantly higher than the velocities encountered in the bundle (<1,5 m/s).

6.2.2 Fluid-elastic instability in the condensation zone

6.2.2.1 Conservative calculations

Once again, the calculations were carried out with a tube pinned at both ends, the length of which was taken equal to the distance between two adjacent support grids (see 6.3). A critical velocity of 3,67 m/s was obtained. Even though this velocity is much higher than those calculated in section 3 (which means that the inside of the bundle is not endangered), this critical velocity is problematic since it was estimated that cross-flow velocities as high as 7,59 m/s could be expected at the edge of the protection plate, near the impact point of the inlet stream of HP steam. More accurate calculations need to be carried out (with more realistic damping coefficients).

6.2.2.2 The software package PIPO

This program [19] relies on the same equations and correlations as presented in 6.1 but has the advantage of being able to consider much more complicated tube configurations (with support grids, various velocity levels and a number of tube vibration modes). The real support conditions of the straight part of a U-tube were therefore entered, that is to say:

- Tube sheet at z = 0 (clamped tube)

- Support grids at z = 0,67 / 1,34 / 2,07 / 2,8 / 3,53 / 4,26 / 4,99 / 5,72 (pinned tube)

A conservative velocity distribution was selected with the highest velocity possible (7,59 m/s) along all the protection plate edges and then linearly decreasing velocity steps up to both edges of the tube.

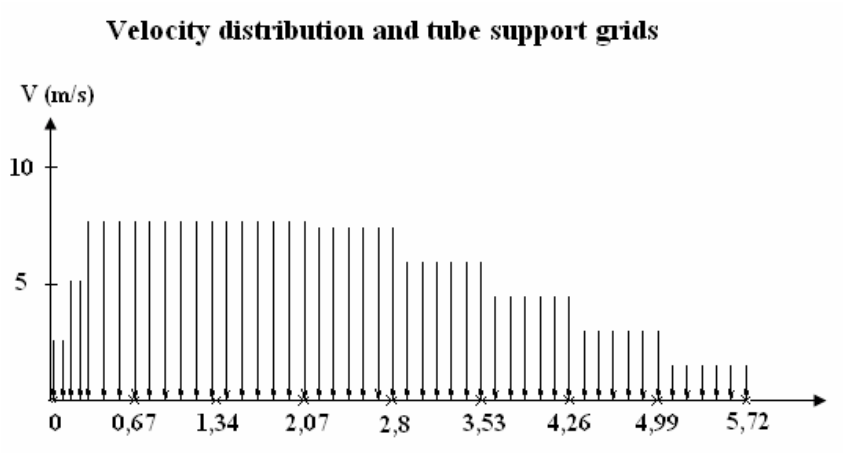

Figure 46: Velocity distributions and tube support grids

Since there is a series of grids contributing to the damping, the damping ratio has to be recalculated (it is indeed an input required by PIPO). According to [18], the logarithmic decrement is:

$$\Lambda_{Sg} = \frac{\pi}{10}\frac{N-1}{N}\sqrt{\frac{b}{0,8}} \quad \text{Equation 209}$$

where b is the width of a support grid and N is the number of grids (0,2m and 8 respectively).
The damping ratio required by PIPO can then simply be obtained by dividing by 2π:

$$\zeta = \frac{\Lambda}{2\pi} \quad \text{Equation 210}$$

The results of the simulation are presented in Figure 47.

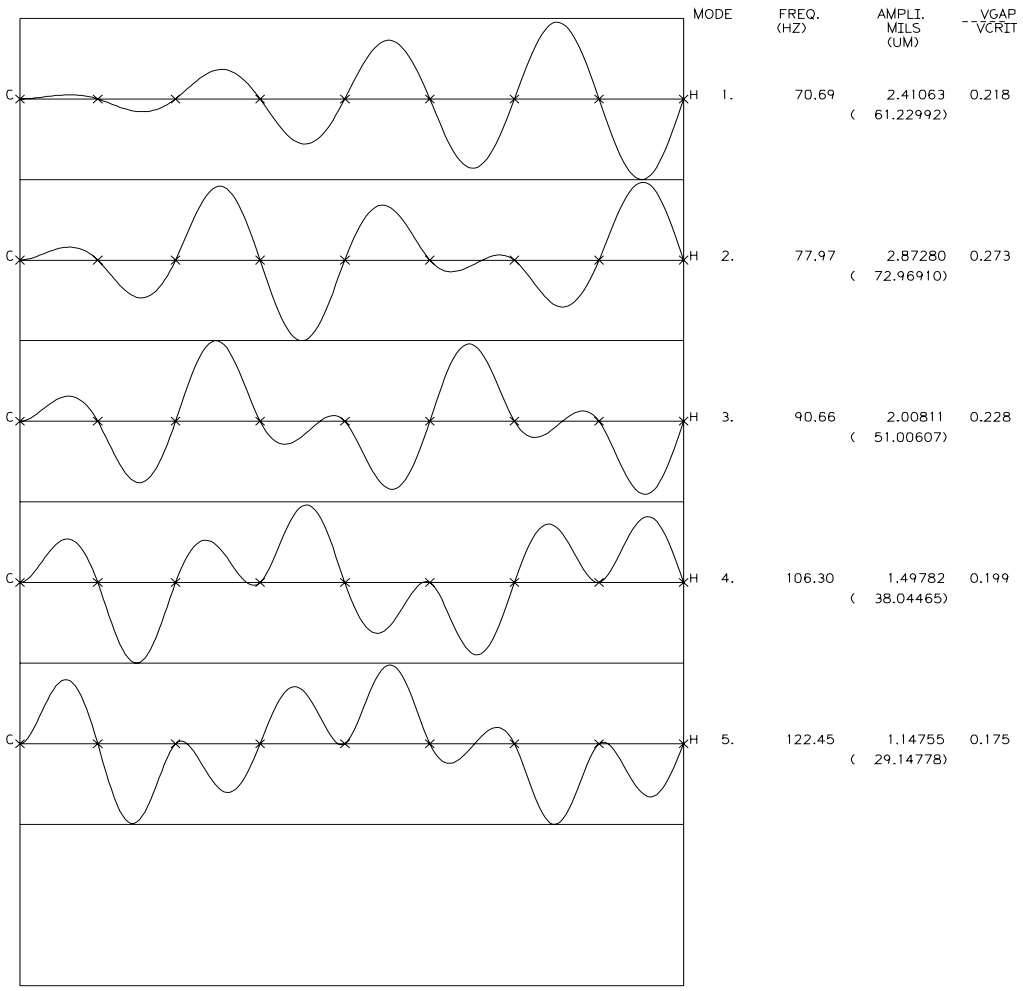

Figure 47: PIPO simulation results

The critical velocities associated with the 5 first modes are not attained since the $v_{gap}/v_{critical}$ ratio does not exceed 0,3. Even with the unfavorable velocity distribution selected, there is no flow-induced vibration risk.

6.3 Detailed calculations

shell-side conditions		unit
shell-side water pressure	21.73	bar
shell-side water temperature	195	°C
Shell-side water density	871.0	kg/m^3
tube-side conditions		
tube-side water temperature	185	°C
tube-side water pressure	80	bar
density of water	886.3	kg/m^3
Properties of steel		
density of steel	7800	kg/m^3
Elasticity module of steel	2.00E+11	$N.m^{-2}$
Tube geometry		
outer diameter	1.60E-02	m
inner diameter	1.30E-02	m
distance between tube centres	0.021	m
Vibration conditions		
distance between tube sheet and grid	0.42	m
dimensionless first eigenfrequency	1	-
Results		
τ	1.31E+00	-
Sr_{w1}	4.66E-01	-
Sr_{w2}	6.68E-01	-
m_R	6.506E-01	kg/m
c_h	3	-
m_h	5.254E-01	kg/m
m	1.176E+00	kg/m
I	1.82E-09	m^4
eigenfrequency of a tube in reference conditions	1.565E+02	Hz
eigenfrequency of tube	1.56E+02	Hz
resonnance velocity for the first vortex-mode	**5.37E+00**	**m/s**
resonnance velocity for the second vortex-mode	**3.74E+00**	**m/s**

Table 9: Vortex-shedding induced vibrations in the Kühlkasten

shell-side conditions		unit
shell-side water pressure	21.73	bar
shell-side water temperature	195	°C
Shell-side water density	871.0	kg/m^3
tube-side conditions		
tube-side water temperature	185	°C
tube-side water pressure	80	bar
density of water	886.3	kg/m^3
Properties of steel		
density of steel	7800	kg/m^3
Elasticity module of steel	2.00E+11	$N.m^{-2}$
Tube geometry		
outer diameter	1.60E-02	m
inner diameter	1.30E-02	m
distance between tube centres	0.021	m
Vibration conditions		
distance between tube sheet and grid	0.42	m
dimensionless first eigenfrequency	1	-
Results		
τ	1.31E+00	-
C_h	3	-
m_R	6.51E-01	$kg.m^{-1}$
m_h	5.254E-01	$kg.m^{-1}$
m	1.1760E+00	$kg.m^{-1}$
eigenfrequency of a tube in reference conditions	1.56E+02	Hz
I	1.82E-09	m^4
eigenfrequency of the tube	1.565E+02	Hz
logarithmic decrement (material contribution)	0.005	-
Stokes number	396664	-
τ'	2.23E+00	-
logarithmic decrement (fluid contribution)	4.528E-03	-
logarithmic decrement (total)	9.528E-03	-
Δ	5.02E-02	-
P	0.15	-
K	2.72E+00	-
u_k*	1.74E+00	-
u_{sk}	**4.35E+00**	**m/s**

Table 10: Fluid-elastic instability in the Kühlkasten

Shell-side conditions		unit
saturated steam pressure	21.73	bar
Saturated steam density	10.89	kg/m^3
Tube-side condtions		
water temperature	206	°C
water pressure	80	bar
density of water	862.44	kg/m^3
Properties of steel		
density of steel	7800	kg/m^3
Elasticity module of steel	2.00E+11	$N.m^{-2}$
Tube geometry		
outer tube diameter	1.60E-02	m
inner diameter	1.30E-02	m
distance between tube centres	0.021	m
Vibration conditions		
distance between adjacent support	0.73	m
dimensionless first eigenfrequency	1	-
Results		
τ	1.31E+00	-
C_h	3	-
m_R	6.47E-01	$kg.m^{-1}$
m_h	6.57E-03	$kg.m^{-1}$
m	6.54E-01	$kg.m^{-1}$
I	1.82E-09	m^4
eigenfrequency of a tube in reference conditions	6.94E+01	Hz
eigenfrequency of the tube	6.94E+01	Hz
logarithmic decrement	0.005	-
Δ	1.17E+00	-
P	0.4	-
K	3.1	-
u_k*	3.30E+00	-
u_{sk}	**3.67E+00**	**m/s**

Table 11: Fluid-elastic instability in the condensation zone

7 Appendix A: Thermodynamic performance of a steam generator

7.1 Introduction

This section is not directly linked to the pre-heater, however this work was given to me as a follow-up to the second-law analysis of pre-heating in the HP pre-heater.
Various steam generators have been designed by AREVA, some of which include an economizer. This piece of equipment is designed to pre-heat the subcooled feedwater by means of heat exchange with the outlet primary-cycle fluid (instead of a direct mixture of the subcooled feedwater and saturated liquid).
Using such a design leads to a higher saturation pressure (and temperature) inside the steam generator which in turn leads to a higher cycle efficiency (warmer hot source in the cycle).

The questions which arise from these considerations are the following:
-is there a limit to the pressure / temperature rise that can be achieved in the steam generator by improving the layout? If there is a theoretical limit, what is it?
-how much does a pressure / temperature rise in the steam generator increase the efficiency of the cycle (i.e. the output of the turbine)?

7.2 Boundary conditions and parameters of the analysis

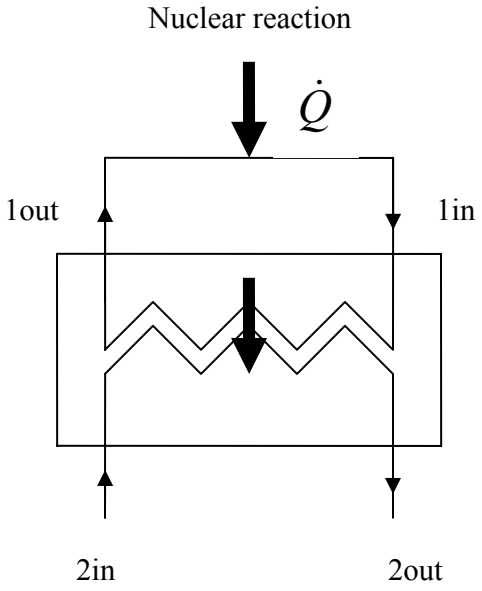

Figure 48: A simple representation of the steam generator

In order to model the performance of the steam generator, a number of boundary conditions must be provided:

Primary-side data:

- Inlet temperature of the primary fluid: T_{1in}
- Pressure in the primary loop: p_1
- Mass flow rate in the primary loop: $\dot{m}_1$
- Power generation in the core: $\dot{Q}$

Secondary-side data:

- Inlet temperature of the feedwater: T_{2in}

As will become obvious later on, these parameters are not sufficient to solve the problem. The last degree of freedom will be fixed by the second law efficiency (see 1.4.1) of the steam generator:

$$\eta_{II} = \frac{\dot{m}_2 \Delta ex_2}{\dot{m}_1 \Delta ex_1} \qquad \text{Equation 211}$$

Where Δex_1 is the exergy difference between the inlet and outlet of the primary-side fluid and Δex_2 is the exergy difference between the outlet steam and the inlet feedwater on the secondary side. In order to define the exergy of a given fluid, the temperature of the dead state must also be provided.

There are four unknowns which have to be determined:

- Primary outlet temperature
- Secondary mass flow rate
- Secondary-side pressure in the steam generator
- Secondary outlet temperature

The two last unknowns are directly linked since the steam is saturated.

7.3 Problem solving

The outlet enthalpy on the primary side can easily be determined by setting up an energy balance:

$$\dot{m}_1 (h_{1in} - h_{1out}) = \dot{Q} \qquad \text{Equation 212}$$

$$h_{1out} = h_{1in} - \frac{\dot{Q}}{\dot{m}_1} \qquad \text{Equation 213}$$

Since h_{1out} and p_1 are known, point 1out is entirely determined.
An energy balance on the secondary side of the heat-exchanger yields:

$$\dot{m}_2(h_{2out} - h_{2in}) = \dot{Q} \qquad \text{Equation 214}$$

The previous equation cannot be used directly since $\dot{m}_2$, h_{2out} and h_{2in} are unknown. Even though the previous equation contains 3 unknowns, there are only two degrees of freedom: if T_{2out} and $\dot{m}_2$ are known then all three unknowns are determined (since T_{2out} controls p_2). Therefore only one additional independent equation is required to solve the problem: the second-law efficiency of the component.

$$\eta_{II} = \frac{\dot{m}_2((h_{2out} - h_{2in}) - T_0(s_{2out} - s_{2in}))}{\dot{m}_1((h_{1in} - h_{1out}) - T_0(s_{2in} - s_{2out}))} \qquad \text{Equation 215}$$

Where T_0 is the temperature of the dead state.
A possible solving path goes as follows:
-assume T_{2out}
-deduce p_2 (saturation pressure at T_{2out})
-deduce h_{2out} and h_{2in} (this is possible since p_2, T_{2in} and T_{2out} are known)
-calculate $\dot{m}_2$ via the energy balance
-check that $\frac{\dot{m}_2((h_{2out} - h_{2in}) - T_0(s_{2out} - s_{2in}))}{\dot{m}_1((h_{1in} - h_{1out}) - T_0(s_{2in} - s_{2out}))}$ is equal to the second-law efficiency specified. If not, re-iterate for a different T_{2out}.

Note: if the user wants to assess the performance of a real steam generator, the problem must be solved the other way round i.e. T_{2out} is known and we must assume a second law efficiency and iterate the model until it has converged

7.4 Second-law efficiency, worst and best-case scenarios

The previous paragraph showed that the first law was not sufficient to solve the problem. In other words, for a given amount of heat transferred between primary and secondary loops, there are an infinite number of $\{\dot{m}_2; T_{2out}\}$ solutions on the secondary side of the steam generator: each one of these $\{\dot{m}_2; T_{2out}\}$ couples is associated with a second law efficiency of the component.
This second-law efficiency indicates the degree of perfection of the heat-exchange: it quantifies the exergy destruction (or the entropy creation) inside the steam-generator.

In most simple cases, this second law efficiency can vary between 0 and 1. If we consider for example a balanced (i.e. same $\dot{m}c_p$ on both sides) counter-flow heat-exchanger with infinite heat-exchange surface and negligible head loss, the outlet temperature of the cold side will be equal to the inlet temperature of the hot side (and conversely). No entropy

has been generated, the heat-exchanger is reversible and its second-law efficiency is equal to 1.
On the other hand, if heat is exchanged from a hot source to a cold source nearly at the dead state's temperature and with a much higher $\dot{m}c_p$, the second-law efficiency of the heat exchanger will be close to 0: thermal energy is being degraded from a high temperature to a temperature near that of the dead state.

In our case however, the extremities of the scale are not attainable. There is a minimal and a maximal second law efficiency (different from 0 and 1 respectively) that the component cannot exceed regardless of its perfection. These boundaries (especially the upper one!) are interesting for the steam-generator designer since they define the best and worse performances expectable.

7.4.1 Worst case scenario

From a thermodynamic point of view, the worst case scenario is obtained when the steam generated is as cold as possible (this leads to the lowest pressure possible on the secondary side of the steam generator). Indeed, the greater the temperature difference between the two loops, the greater the entropy generation (i.e. the greater the exergy destruction) when heat is transferred.
The worst case scenario is therefore obtained when the saturation temperature in the steam-generator is equal to the inlet temperature of the feedwater (which is an input entered by the user). Note that this is a theoretical lower limit since there is no way the feedwater could be exactly at the steam generator's saturation temperature (the feedwater is indeed pre-heated by means of steam bled from the turbine, the temperature of which is below that of the steam generator).
An energy balance on the secondary-side of the steam-generator yields:

$$\dot{m}_2 \Delta h_{l-v}(T_{2in}) = \dot{Q} \quad \Leftrightarrow \quad \dot{m}_2 = \frac{\dot{Q}}{\Delta h_{l-v}(T_{2in})} \qquad \text{Equation 216}$$

Where $\Delta h_{l\text{-}v}(T_{2in})$ is the enthalpy of evaporation at T_{2in}. Bearing in mind that

$$s_{2out} - s_{2in} = \Delta s_{l-v} = \frac{\Delta h_{l-v}}{T_{2in}} \qquad \text{Equation 217}$$

we obtain a simple expression of the lower limit of the second law efficency:

$$(\eta_{II})_{\min} = \frac{\dot{m}_2((h_{2out} - h_{2in}) - T_0(s_{2out} - s_{2in}))}{\dot{m}_1((h_{1in} - h_{1out}) - T_0(s_{2in} - s_{2out}))} = \frac{\dot{Q}(1 - \frac{T_0}{T_{2in}})}{\dot{m}_1((h_{1in} - h_{1out}) - T_0(s_{2in} - s_{2out}))}$$

Equation 218

Note that the denominator of the previous ratio is independent of the efficiency of the steam generator and will always be the same provided that T_{1in} , p_1, $\dot{m}_1$ and $\dot{Q}$ are maintained constant: the primary loop is independent of the second-law efficiency of the steam generator.

7.4.2 Heat-exchange surface increase for a given energy transfer rate

Let us compare two steam generators transferring the same amount of heat between the primary and secondary loops but with different heat-exchange surfaces (steam generator 1 has a low heat-exchange surface and steam generator 2 has a much larger heat-exchange surface). This can be done by considering a simple counter-flow heat exchanger.

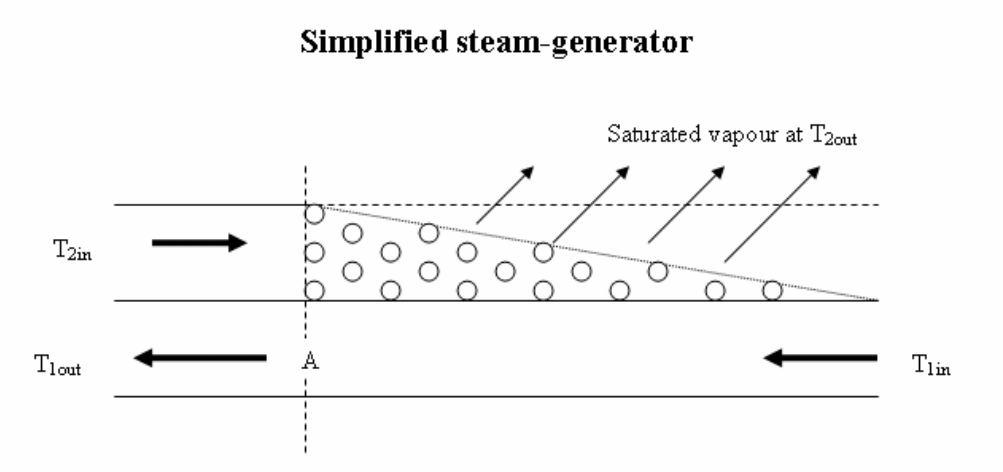

Figure 49: Simplified counter-flow steam generator

If we have a closer look at what is taking place inside this simple steam-generator, we can distinguish two separate zones:
-near the secondary-side inlet, the heat exchange takes place between two subcooled fluids because the feedwater has not yet reached its boiling temperature. The temperature of the primary fluid decreases and the temperature of the secondary fluid increases
-Once the secondary fluid starts boiling (after point A) the temperature in the secondary loop remains constant and saturated steam is generated. On the primary side of the steam-generator, the temperature drops steadily.

Since steam-generator 1 has a small heat-exchange surface but transfers *the same amount of heat* as steam-generator 2, the average temperature difference between the primary and secondary fluids must be greater in steam-generator 1 (since the heat-exchange rate increases with temperature difference and surface) . This can only be the case if the boiling temperature in steam-generator 1 is lower than in steam-generator 2. In other

words, the saturation pressure in steam-generator 1 must be smaller than the saturation temperature in steam-generator 2.
Therefore, for a given heat-transfer rate, the smaller the heat-exchange surface, the lower the saturation pressure (and temperature) in the steam generator.

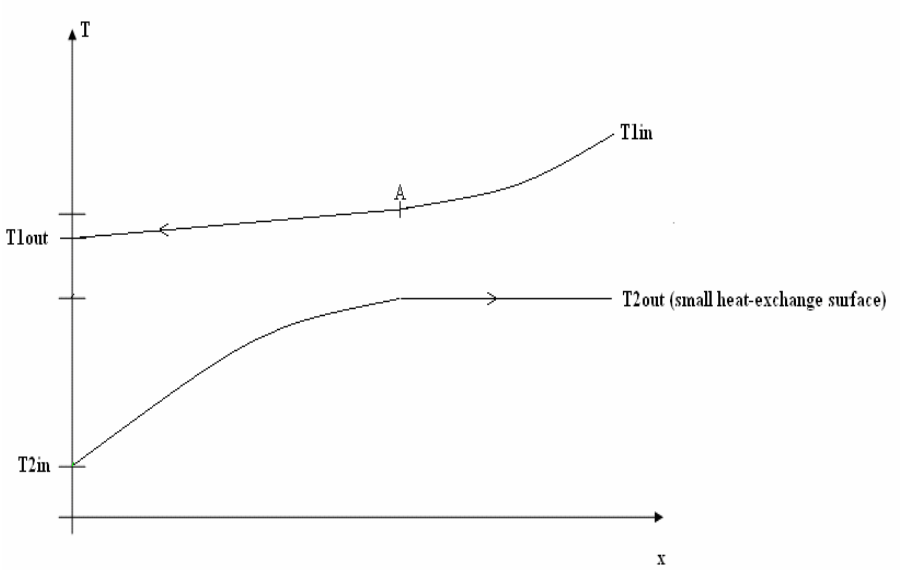

Figure 50: Temperature profile in a steam-generator with a small heat-exchange surface

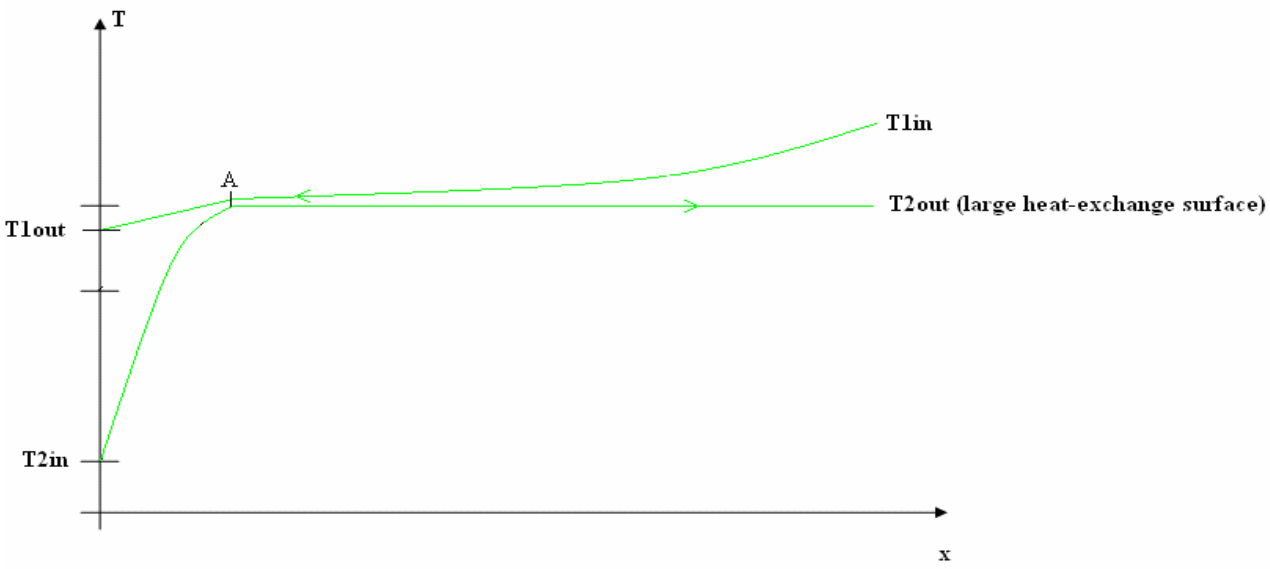

Figure 51 : Temperature profile in a steam-generator with a large heat-exchange surface

7.4.3 Best case scenario

The previous analysis brings us to the best possible layout for the heat-exchanger: an infinite heat-exchange surface. This layout is indeed associated to the smallest average temperature difference between primary and secondary fluids and will lead to the highest outlet temperatures and pressures possible (for the same given heat transfer rate).
The highest possible saturation temperature on the secondary side is equal to the temperature of point A (see Figure 51) since the temperature of the primary side must remain greater than the temperature of the secondary side. Such a performance (T_{2out}= T_{1A}) is only possible if the heat-exchange surface in the evaporation zone is infinite. This criterion is sufficient to determine the upper performance limit of the steam-generator.
An energy balance between the primary inlet and point A yields:

$$\dot{m}_1(h_{1in} - h_{1A}) = \dot{m}_2(\Delta h_{l-v}(T_{2out}))$$ Equation 219

For infinite heat-exchange surface T_{2out}= T_{1A} which entails:

$$\dot{m}_1(h_{1in} - h(p_1, T_{2out})) = \dot{m}_2(\Delta h_{l-v}(T_{2out}))$$ Equation 220

The previous equation contains two unknowns T_{2out} and $\dot{m}_2$. We need to add the overall energy balance to solve the system:

$$\dot{m}_1(h_{1in} - h(p_1, T_{2out})) = \dot{m}_2(\Delta h_{l-v}(T_{2out}))$$ Equation 221

$$\dot{Q} = \dot{m}_2(h_{2out} - h_{2in})$$ Equation 222

A possible solving path goes as follows:
-assume T_{2out}
-deduce p_2 (saturation temperature at T_{2out})
-deduce h_{2out} and h_{2in} (this is possible since T_{2in}, T_{2out} and p_2 are known)
-deduce h_{1A} (this is possible since p_1 and T_{1A}=T_{2out} are known)
-deduce $\dot{m}_2$ via the overall energy balance
-calculate h_{1A}= $h(p_1,T_{2out})$ via equation 221 and compare with h_{1A} obtained previously. If necessary re-iterate for a different T_{2out}

Once T_{2out} and $\dot{m}_2$ have been determined it is once again possible to calculate the second-law efficiency of the "ideal" steam-generator with the usual definition:

$$\eta_{II} = \frac{\dot{m}_2((h_{2out} - h_{2in}) - T_0(s_{2out} - s_{2in}))}{\dot{m}_1((h_{1in} - h_{1out}) - T_0(s_{2in} - s_{2out}))}$$ Equation 215

The second law efficiency of the "ideal" steam-generator is smaller than 1 which means that even with infinite heat-exchange surface, the heat-transfer process is irreversible (unlike that of a balanced counterflow heat-exchanger). The temperature difference between fluids is indeed never vanishingly small (except near point A), despite the infinite heat-exchange surface. This unavoidable irreversibility is sometimes referred to as "remanent" in the literature [13].

7.5 Estimation of the additional power output from the turbine

Up to now, we have answered the first question of the introduction, i.e. "how well does the steam-generator perform and what are the best and worst performances expectable?" We can now focus on the second question, i.e. how much does a pressure / temperature rise on the secondary side of the steam generator improve the performance of the cycle?

First of all, it must be pointed out that this question cannot be answered accurately by considering the steam-generator alone since the performance of the cycle is also determined by the performance and the response of all the other components. An accurate result can only be obtained by simulating the entire cycle. However, an order of magnitude of the turbine output increase/drop can be obtained by considering that the steam-generator is connected to a series of reversible components with a condenser operating at the temperature of the dead state. In this idealized reversible case, all the exergy that enters the secondary loop exits as shaft power in the turbine.

In this case, the turbine power output (which is the maximal turbine output expectable with the associated steam generator efficiency) can be calculated as follows:

$$W_{turbine} = \dot{m}_2 \Delta ex_2 = \dot{m}_1 \Delta ex_1 \eta_{II} \qquad \text{Equation 223}$$

Therefore, if we want to replace steam-generator a (operating at p_a on the secondary side) with a better steam-generator b (operating at p_b on the secondary side) with $p_b > p_a$, an order of magnitude of the expected turbine output increase can be determined as follows:

-estimate $(\eta_{II})_a$ and $(\eta_{II})_b$ with the model (by entering $(T_{2out})_a = T_{saturation}(p_a)$ and $(T_{2out})_b = T_{saturation}(p_b)$ as inputs, see the note in 7.3)

-calculate the turbine output variation: $\Delta W_{turbine} = \dot{m}_1 \Delta ex_1 \left((\eta_{II})_a - (\eta_{II})_b \right)$

7.6 Example: performance of Neckarwestheim's steam generator

7.6.1 Operating conditions

The operating conditions of one of Neckarwestheim's three steam generator [21],[22] are recapped in Table 12.

thermal power generation in the core	870	MW
primary mass low rate	4815	kg/s
primary inlet temperature	321,27	°C
pressure in primary loop	155	kg/s
secondary inlet temperature	216,6	°C

Table 12: Operating conditions of one of Neckarwestheim's three steam generators

The temperature of the dead state was taken equal to that of the cooling water (12,5°C).

7.6.2 Second-law efficiency of the steam generator and associated maximal turbine output

The actual pressure level on the secondary-side of the steam generator is 60,45 bar which corresponds to a saturation temperature of 276,1°C.
After running the model, we obtain a second-law efficiency of:

$$\eta_{II} = 0{,}9392$$

The maximal turbine output associated to this steam generator is:

$$W_{turbine} = 413{,}8\ MW$$

7.6.3 Maximal and minimal second-law efficiencies

- The minimal efficiency of the steam generator is:

$$(\eta_{II})_{\min} = \frac{\dot{Q}(1-\frac{T_0}{T_{2in}})}{\dot{m}_1((h_{1in}-h_{1out})-T_0(s_{2in}-s_{2out}))} = \frac{870*10^6(1-\frac{273+12{,}5}{273+216{,}6})}{4815*91492} = 0{,}8233$$

This minimal efficiency is associated to a saturation temperature of 216,6°C and a saturation pressure of 21,7 bar.
The associated maximal turbine output for this configuration is 362,7 MW

- The maximal efficiency calculated by the model is:

$$(\eta_{II})_{\max} = 0{,}9692$$

This maximal efficiency is associated to a saturation temperature of 296,6°C and a saturation pressure of 81,8 bar.
The associated maximal turbine output is 427,0 MW

7.6.4 Impact of the implementation of a new steam generator

If the actual steam generator was replaced by the "minimal efficiency steam generator", a rough estimation of the turbine output drop (per steam generator) is:

$$\Delta W = 413{,}8 - 362{,}7 = 51{,}1\,MW$$

Since there are 3 steam generator in the plant, the overall turbine drop would be around 155,4 MW.

If the actual steam generator was replaced by an ideal steam generator, the turbine output increase would be equal to:

$$\Delta W = 427 - 413{,}8 = 13{,}2\,MW$$

Since there are 3 steam generator in the plant, the maximal turbine output increase that could be obtained by improving the steam generator is 39,6 MW.

The performance of Neckarwestheim's steam-generator can be situated on the following graphs at $\eta_{II} = 0{,}9392$

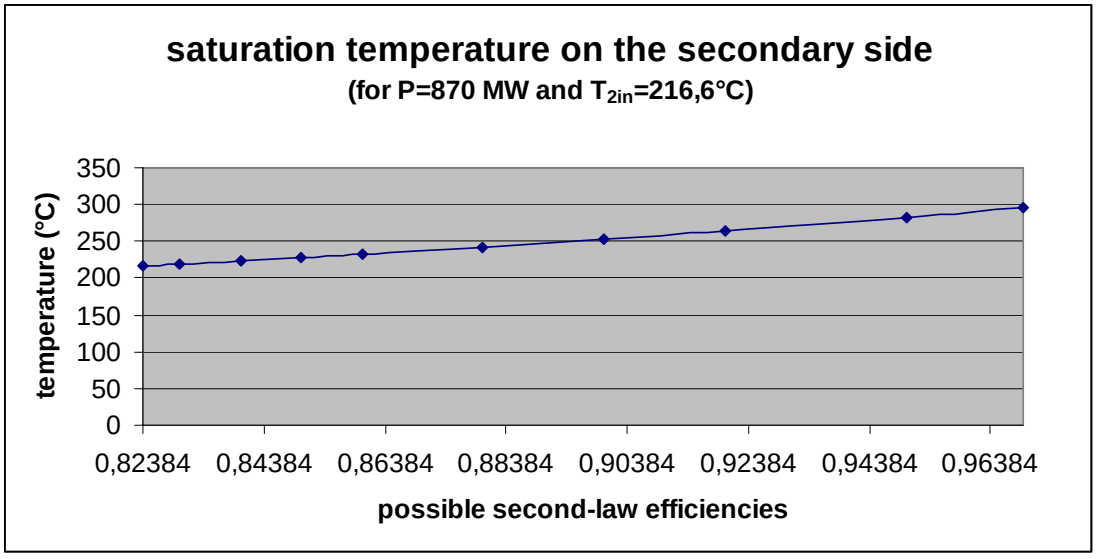

Figure 52: Possible saturation temperatures in the boiler

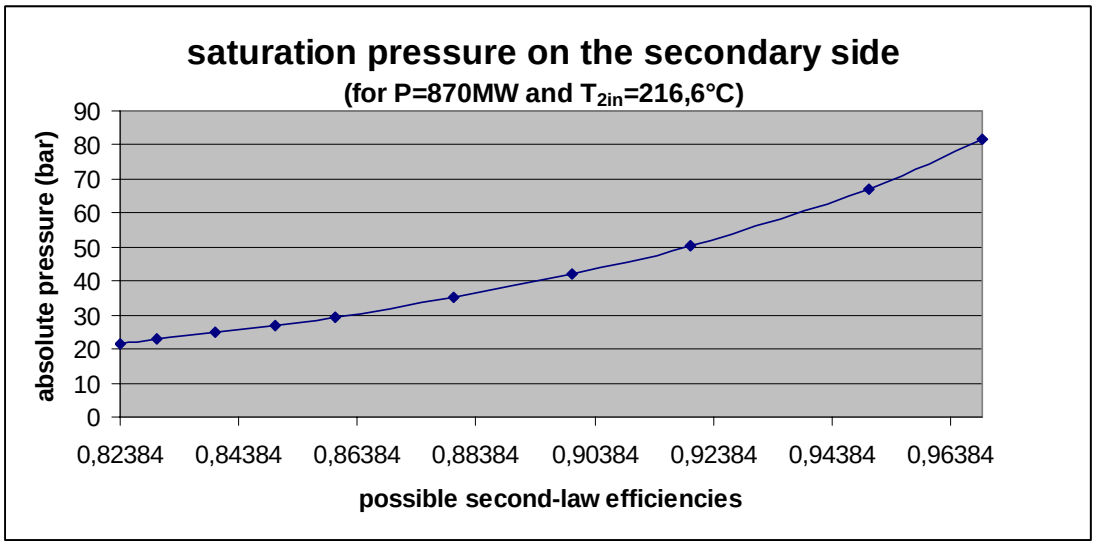

Figure 53: Possible saturation temperatures in the boiler

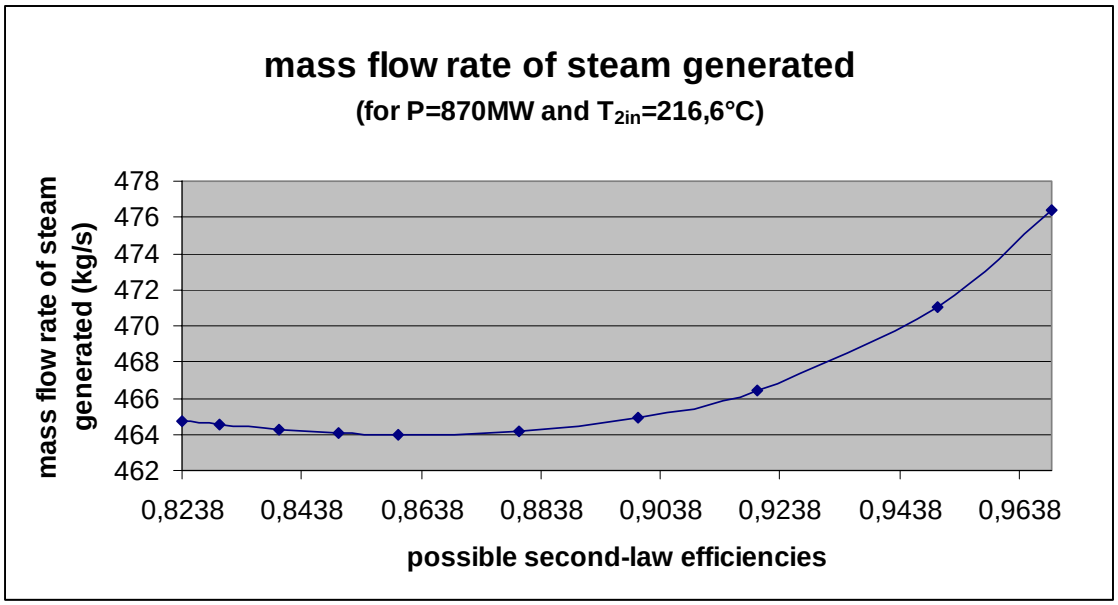

Figure 54: Possible mass flow rates of steam generated

For the boiler designer it is also interesting to assess an order of magnitude of the extra turbine output that could be expected if the boiler was modified (i.e. new saturation temperature and new saturation pressure). In Figure 55, Figure 56 and Figure 57, the additional turbine output (with respect to the currently-operating boiler) is plotted against the saturation temperature in the new boiler, the saturation pressure in the new boiler and the second law efficiency of the new boiler respectively. Remember that this power output increase/decrease is what would be obtained if the new boiler and the reference

boiler where both coupled to a reversible cycle with a condenser operating at the temperature of the dead state (i.e as if the rest of the cycle was endo- and exoreversible).

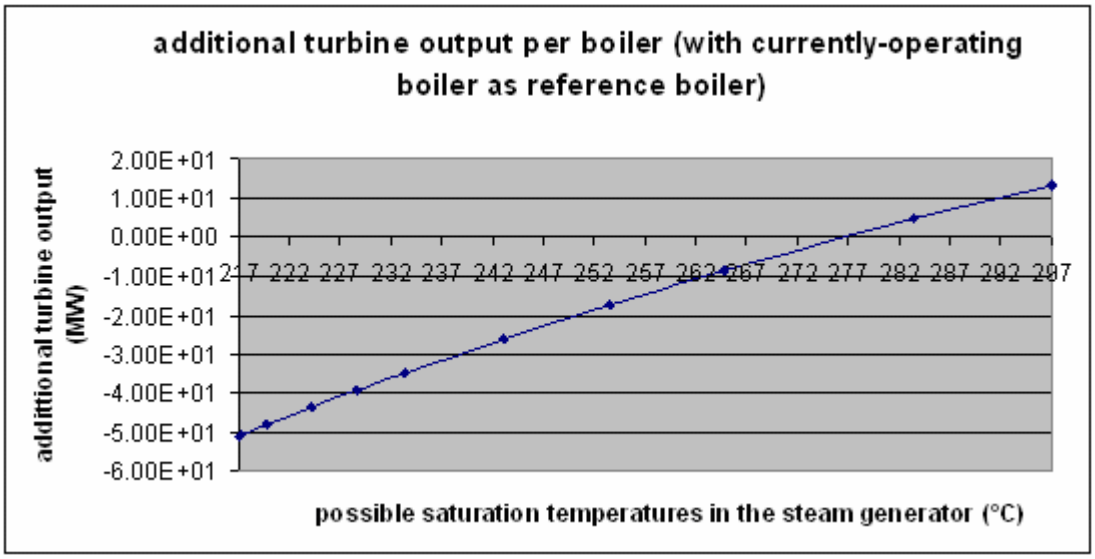

Figure 55:Additional turbine output plotted against possible saturation temperatures

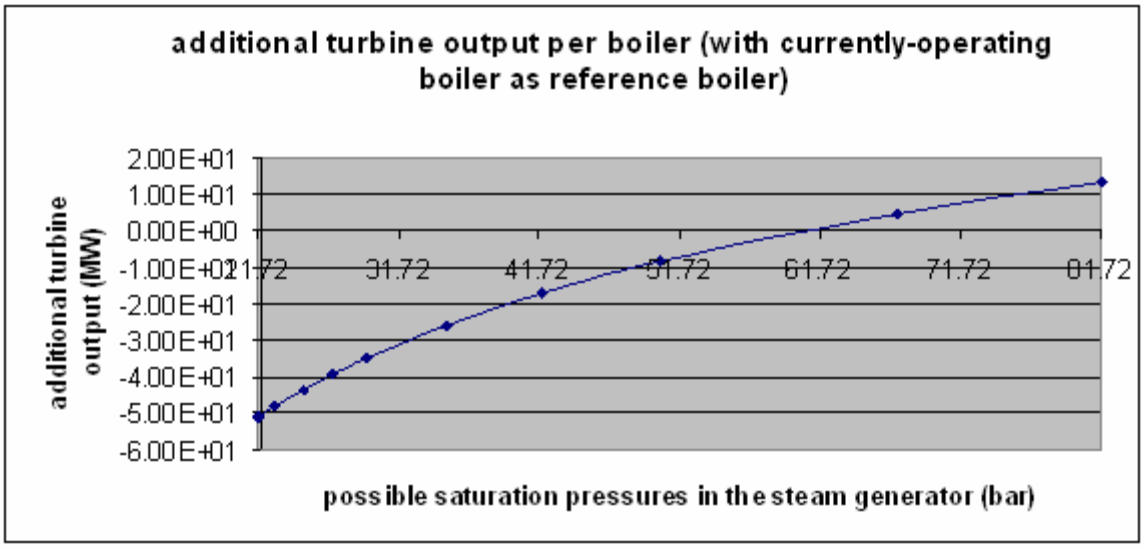

Figure 56: Additional turbine output plotted against possible saturation pressures

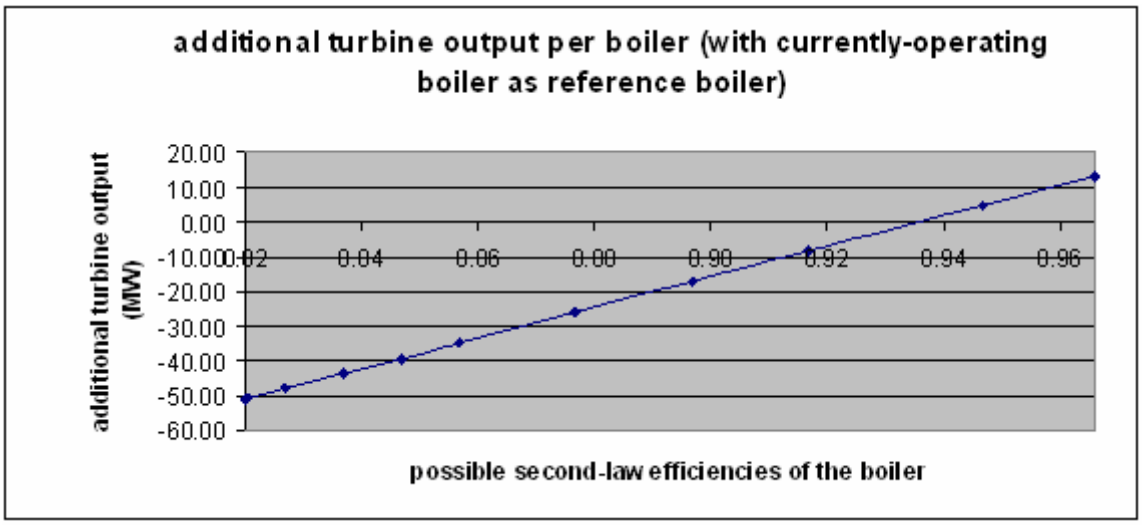

Figure 57: Additional turbine output plotted against possible second-law efficiencies

8 Appendix B: Development of a model calculating the influence of temperature and velocity distributions on the heat-exchange rate inside a helium heat exchanger

This aspect of my work is not linked to the analysis of the HP pre-heater and is therefore only included as an appendix in the report. However, it was given to me because of the similarities existing between the analyses of heat-exchangers. The tools and concepts used in this work are indeed the same as those that were used in the thermal model of the pre-heater.

8.1 Background

The design of this helium/helium heat-exchanger fits in the R&D work carried out on the future generation of nuclear reactors, the VHTR (Very-high-Temperature Reactor). The basic concept of these reactors is also based on a primary loop exchanging heat with a secondary loop. However, unlike usual power plants, the working fluid is not water but helium (on the primary-side) and a He-N_2 mix on the secondary side. Therefore, the component linking both loops is not a steam-generator but a plain single-phase heat-exchanger.
This heat-exchanger is composed of a helicoidal tube bundle (in which the secondary fluid flows) which exchanges heat with the primary fluid on the shell-side.

The heat-exchange rate of this exchanger has already been estimated via appropriate programs under the assumption of uniform temperature and velocity profiles on the shell-side.
In practice however, the temperature of the primary-fluid is higher near the extremities of the bundle, as is also its velocity. The heat-exchanger tends to act as a great number of separate heat-exchangers in parallel, as if there was no thermal contact between the different streams of primary-fluid. This leads to the following question: for a given average shell-side velocity and temperature, how does the heat-exchange rate vary if the temperatures and velocities are not uniform but higher towards the edge of the bundle?

The goal of the following calculations is to provide an answer to this question. Note that no attempt will be made to predict the outlet temperature of the real heat-exchanger with all its geometrical details. The goal of the calculations is solely to assess qualitatively the consequence of non-uniform velocity and temperature profiles.

Note: I was not asked to run simulations with the model, no interpretations or analysis of the results will therefore be presented here. This section will only be concerned with the creation of the mathematical model.

8.2 Mathematical model

The user of the model will be able to specify the following parameters:

Primary side:

- Average primary inlet temperature $\overline{T}_{1in}$
- The temperature difference between the average inlet temperature and the temperature at the outer edge of the bundle: ΔT
- Total primary mass flow rate $\dot{m}_1$
- The velocity ratio: $V_{extremity}/V_{average}$

Secondary side:

- Secondary inlet temperature T_{2in}
- Secondary mass flow rate $\dot{m}_2$

General parameters:

- Overall heat-transfer coefficient U
- Heat-exchange surface A

The heat-exchanger can be visualized as a great number of independent parallel channels in which the primary and secondary fluids exchange heat.

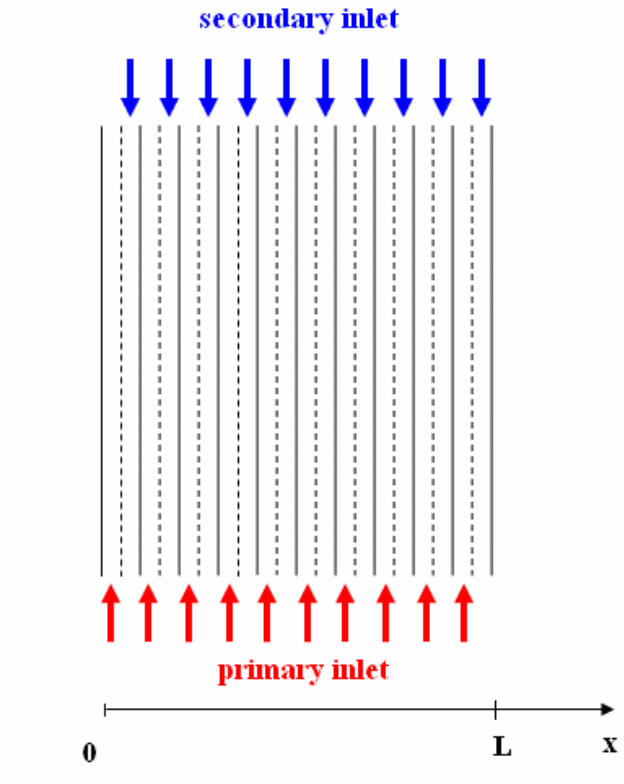

Figure 58: A simplified representation of the heat-exchanger

In the following calculations, it will appear that the numerical value assigned to L has no importance. It will be set to 1 (in order to simplify the calculations) in the excel spreadsheet (see 8.2.3).

8.2.1 Determination of the inlet velocity and temperature profiles

The first step of the calculations is to determine the inlet velocity and temperature profiles on the basis of the input parameters. These profiles must satisfy the mass conservation equation (energy conservation equation respectively) and the boundary conditions (velocity and temperature at the extremity of the bundle respectively). The energy conservation equation can only be expressed once the velocity profile is known: therefore, the velocity profile must be determined first.

8.2.1.1 Determination of the velocity profile

The designers of the helium heat exchanger specified that the shell-side velocity (primary fluid) at both edges of the bundle is higher than in the center of the bundle. A simple way to model these specifications it to use a second degree polynomial for the velocity profile.

$$\dot{m}'_1(x) = a'x^2 + b'x + c' \qquad \text{Equation 224}$$

where $\dot{m}'_1(x)$ is the mass flow rate per unit length and a', b' and c' are constants that have to be determined. The three independent equations that will be used to determine these unknowns are:

$$\dot{m}_1 = \int_0^L \dot{m}_1'(x)dx = a'\frac{L^3}{3} + b'\frac{L^2}{2} + c'L \qquad \text{Equation 225}$$

$$\dot{m}_1'(0) = \dot{m}_1'(l) \quad \Leftrightarrow \quad c' = a'L^2 + b'L + c' \qquad \text{Equation 226}$$

$$\dot{m}_1'(0) = \frac{V_{extremity}}{V_{average}}\dot{\bar{m}}'_1 \quad \Leftrightarrow \quad c' = \frac{V_{extremity}}{V_{average}}\dot{\bar{m}}'_1 \qquad \text{Equation 227}$$

where $\dot{\bar{m}}_1'$ is the average mass flow rate per unit length: $\dot{\bar{m}}_1' = \frac{\dot{m}_1}{L}$

Equation 225 is the mass continuity equation, equation 226 is a consequence of the symmetrical flow in the bundle and equation 227 ensures that the mass flow rate at the bundle's edges corresponds to the velocity ratio entered by the user.
Solving for a', b' and c' we obtain:

$$a' = \frac{6\Delta m}{L^2} \qquad \text{Equation 228} \qquad b' = -\frac{6\Delta m}{L^2} \qquad \text{Equation 229}$$

$$c' = \frac{V_{extremity}}{V_{average}} \dot{\overline{m}} \quad \text{Equation 230}$$

where $\Delta m = \dot{m}'_1(0) - \overline{\dot{m}}'_1$

8.2.1.2 Determination of the temperature profile

Here again, it was specified that the temperature of the primary fluid is higher near the extremities of the bundle. Once again this will be taken into account by using a second-degree polynomial for the temperature profile.

$$T_{in,1}(x) = ax^2 + bx + c \quad \text{Equation 231}$$

where a, b and c are constants that have to be determined. The three independent equations that are required are:

$$\dot{m}_1 c_p \overline{T}_{1,in} = \int_0^L \dot{m}_1'(x) c_p T_{1,in}(x) dx \quad \text{Equation 232}$$

$$T_{1,in}(0) = T_{1,in}(L) \quad \text{Equation 233}$$

$$T_{1,in}(0) = \overline{T}_{1,in} + \Delta T \quad \text{Equation 234}$$

Equation 232 is the energy conservation equation, equation 233 is a consequence of the symmetrical flow inside the bundle and equation 234 ensures that the temperature at the bundle's extremities is consistent with the user's input.

c_p was assumed to be constant over the inlet temperature distribution. Integrating Equation 232, we obtain:

$$\overline{T}_{in} = \frac{1}{\dot{m}_1}(\alpha a + \beta b + \gamma c) \quad \text{Equation 235}$$

where

$$\begin{cases} \alpha = \dfrac{a' L^5}{5} + \dfrac{b' L^4}{4} + \dfrac{c' L^3}{3} \\ \beta = \dfrac{a' L^4}{4} + \dfrac{b' L^3}{3} + \dfrac{c' L^2}{2} \\ \gamma = \dfrac{a' L^3}{3} + \dfrac{b' L^2}{2} + c' L \end{cases} \quad \text{Equation 236}$$

Solving equations 232, 233 and 234 we obtain:

$$a = \frac{\dot{m}\overline{T}_{1,in} - \gamma(\overline{T}_{1,in} + \Delta T)}{\alpha - \beta L} \qquad \text{Equation 237}$$

$$b = -L\left(\frac{\dot{m}_1\overline{T}_{1,in} - \gamma(\overline{T}_{1,in} + \Delta T)}{\alpha - \beta L}\right) \qquad \text{Equation 238}$$

$$c = \overline{T}_{1,in} + \Delta T \qquad \text{Equation 239}$$

8.2.2 Determination of the outlet temperature profile

Now that the inlet velocity and temperature profiles have been determined, the outlet temperature for any abscissa x can be calculated via the ε-NTU method. Note that this implies assuming a constant c_p on both sides which might be questionable given the magnitude of the temperature variation. However, there is no other way the problem can be solved analytically. More accurate calculations must rely on numeric simulation.
For any abscissa x, f(x) must be calculated, where f(x) is defined as:

$$f(x) = \frac{C'_{pri}(x)}{C'_{\text{sec}}} = \frac{\dot{m}'_{pri}(x)(c_p)_{pri}}{\dot{m}'_{\text{sec}}(c_p)_{\text{sec}}} \qquad \text{Equation 240}$$

This ratio will determine which fluid has the smallest C' The $\dot{m}'c_p$ of both fluids are indeed very close and the fluid with the smallest C'may vary with the abscissa. Typically, $C'_{pri}=C'_{min}$ in the middle of the heat-exchanger (since the mass flow rate of primary fluid is smaller there) and $C'_{sec}=C'_{min}$ towards the edges of the heat-exchanger (higher mass flow rate of primary fluid on the edge of the bundle). If f > 1, $C'_{sec}=C'_{min}$ and if f < 1, $C'_{pri}=C'_{min}$

The ε-NTU method can then be applied as usual (with a correlation for counter-flow):

$$NTU = \frac{UA'}{C'_{\min}} \qquad \text{Equation 241} \qquad C_R = \frac{C'_{\min}}{C'_{\max}} \qquad \text{Equation 242}$$

$$\varepsilon = \frac{1 - e^{-NTU(1-C_R)}}{1 - C_R e^{-NTU(1-C_R)}} \qquad \text{Equation 243}$$

Note that since $C' = \dot{m}'c_p$ is defined per unit length on the x-axis, the heat exchange surface A' is the heat exchange surface per unit length on the x-axis (hence the prime): A'=A/L.

$$\varepsilon = \frac{(T_{2out}(x) - T_{2in})C'_{\sec}}{(T_{1in}(x) - T_{2in})C'_{pri}} \quad if\ f < 1$$
$$\varepsilon = \frac{(T_{2out}(x) - T_{2in})C'_{\sec}}{(T_{1in}(x) - T_{2in})C'_{\sec}} = \frac{(T_{2out}(x) - T_{2in})}{(T_{1in}(x) - T_{2in})} \quad if\ f > 1$$

Equation 244

In equation 244, the only unknown is $T_{2out}(x)$. $T_{2out}(x)$ can therefore be obtained directly via equation 244.
In the calculations leading to $T_{2out}(x)$, no assumption has been made on the number of channels of the heat-exchanger. $T_{2out}(x)$ is indeed the temperature distribution which would be obtained with an infinite number of vanishingly small channels, i.e. as if the distribution was not discrete but continuous.

Now if we want to determine the heat-flux between fluids in the heat-exchanger, we need to integrate the $\dot{m}'(x)c_pT(x)$ outlet profile over the entire x-axis (from 0 to L). In theory, this could be done analytically but we would have to determine the abscissas where f changes sign (since ε is f-dependant) and break down the integration. We can however calculate an approximate numerical result (which is much easier if the calculations are automated in an excel spreadsheet, see 8.2.3 and Figure 59). Since c_p is assumed to be constant, the average outlet temperature is:

$$\overline{T}_{2out} = \frac{\int_0^L T_{2out}(x)\dot{m}'_{\sec}\,dx}{\dot{m}_{\sec}} \approx \frac{\sum_{i=1}^{n} T(x_i)\frac{\dot{m}_{\sec}}{L}\frac{L}{n}}{\dot{m}_{\sec}} = \frac{\sum_{i=1}^{n} T(x_i)}{n}$$

Equation 245

$$\overline{T}_{1out} = \frac{\int_0^L T_{1out}(x)\dot{m}'_{pri}(x)dx}{\dot{m}_{pri}} \approx \frac{\sum_{i=1}^{n} T(x_i)\dot{m}'_{pri}(x_i)\frac{L}{n}}{\dot{m}_{pri}} = \frac{\sum_{i=1}^{n} T(x_i)\dot{m}'_{pri}(x_i)L}{n\,\dot{m}_{pri}}$$

Equation 246

Note that the average outlet temperature on the primary side is more complicated to calculate because the mass flow rate is non constant over the x-axis.
Since the average outlet temperature is known, the heat-flux in the heat-exchanger can easily be obtained by either of the following energy balances:

$$\dot{Q} = \dot{m}_{pri}(\overline{h}_{1in} - \overline{h}_{1out}) = \dot{m}_{pri}(c_p)_{pri}(\overline{T}_{1in} - \overline{T}_{1out})$$

Equation 247

$$\dot{Q} = \dot{m}_{\sec}(\overline{h}_{2out} - \overline{h}_{2in}) = \dot{m}_{\sec}(c_p)_{\sec}(\overline{T}_{2out} - \overline{T}_{2in})$$

Equation 248

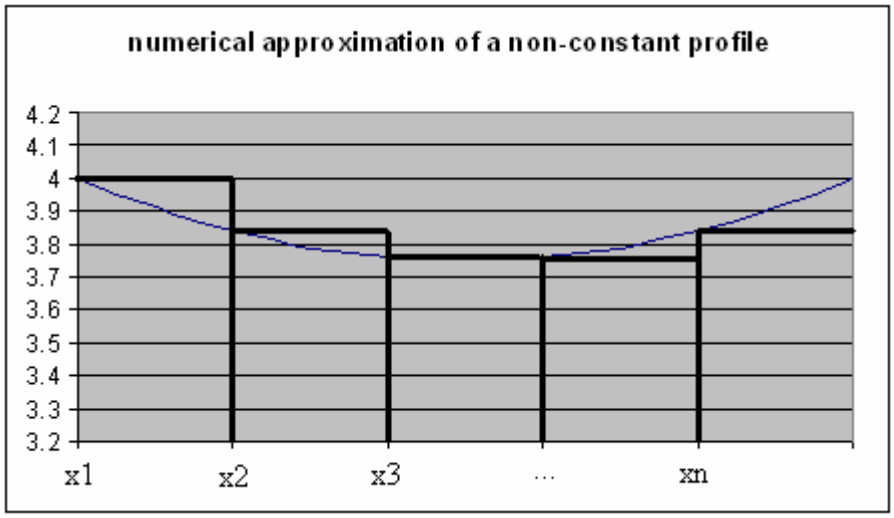

Figure 59: Approximation of a non-constant profile

8.2.3 Implementation of the model on an excel sheet

Carrying out all the previous calculations by hand is extremely tedious and time-consuming. The model was therefore entered into an excel spreadsheet: the user just needs to specify the desired parameters and the spreadsheet automatically updates the outlet temperature profiles and the resulting heat transfer rate (with n=50, which is enough to give accurate results).
By modifying the temperature and velocity distributions at the primary-side inlet, the user can therefore instantly assess the impact of these modifications on the performance of the heat-exchanger.

9 Appendix C: 3D view of the HP pre-heater

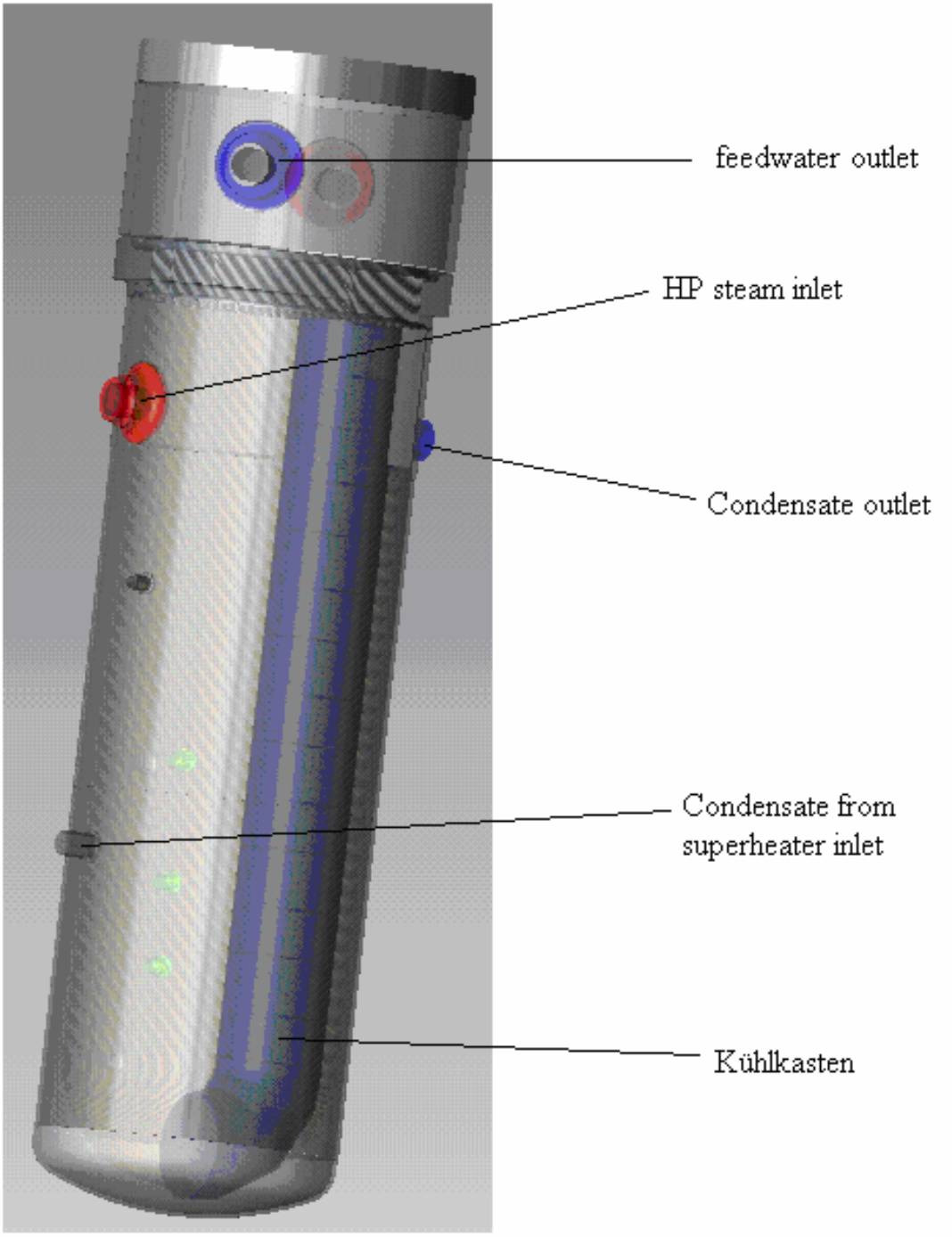

Figure 60: 3D view of the Kühlkasten

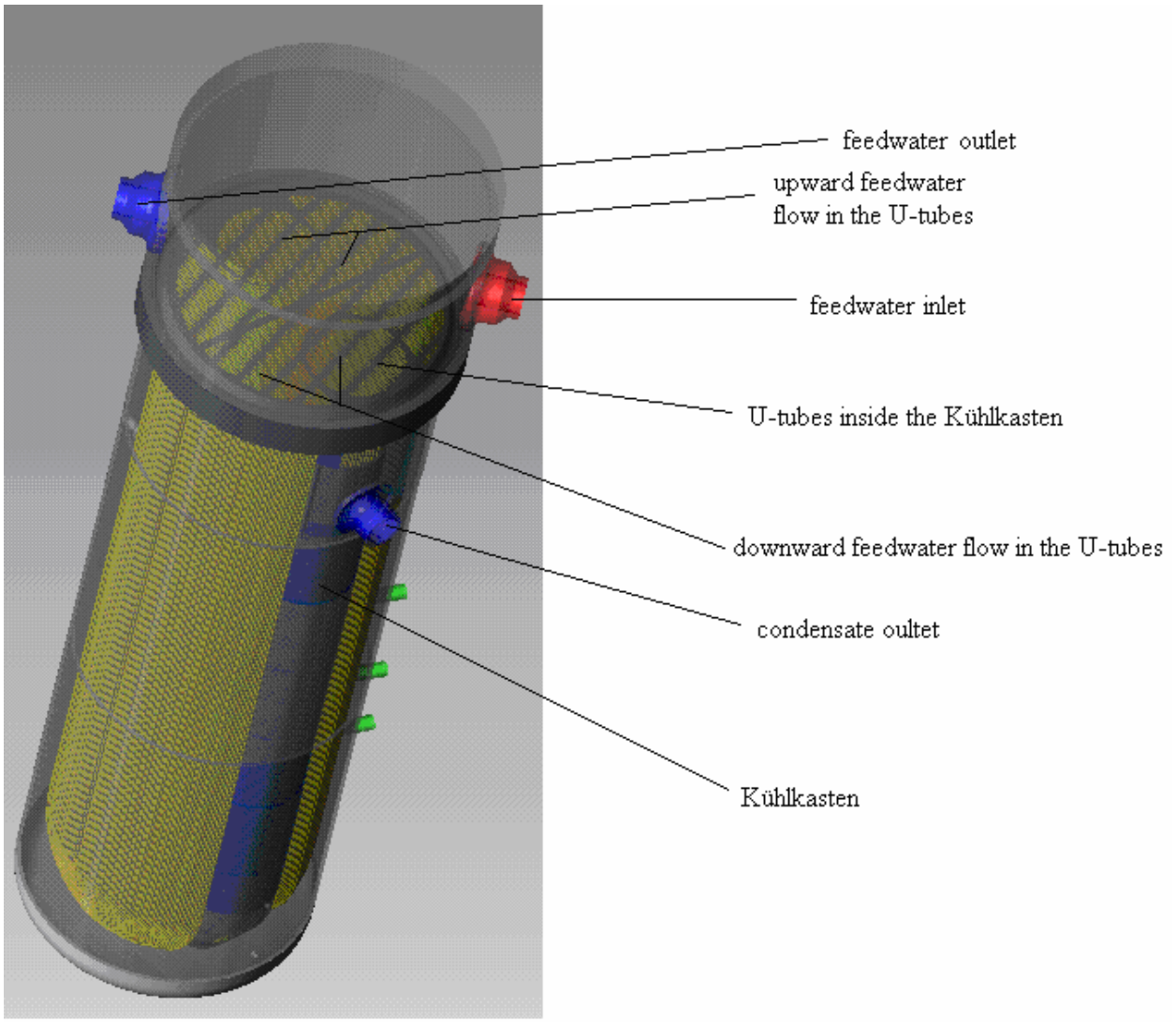

Figure 61: 3D view of the tube bundle and tube-side flow pattern

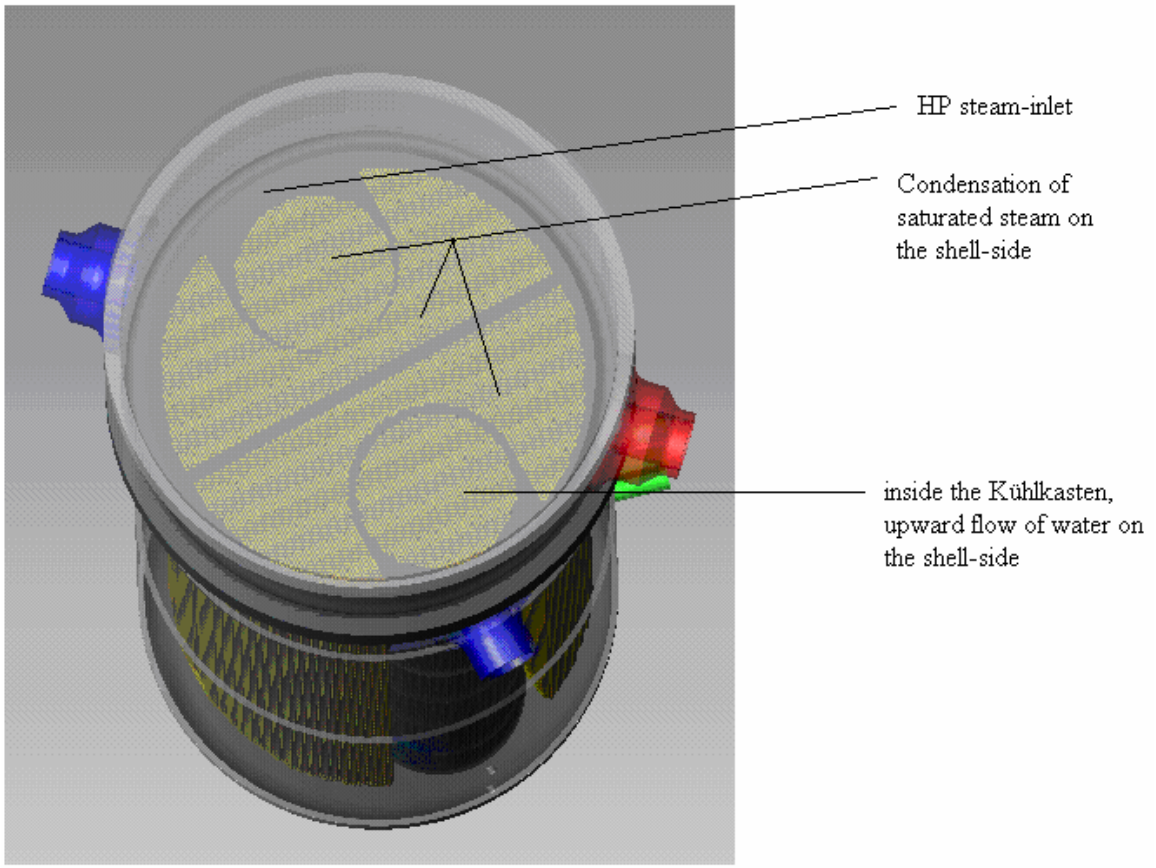

Figure 62: flow pattern on the shell-side

References and background reading

- References

[1] VDI-Wärmeatlas Berechnungsblätter für den Wäremübertrager. 7th ed. Düsseldorf: VDI-Verlag Gmbh; 1994. Chapter Gb. Paragraph 4.1.

[2] VDI-Wärmeatlas Berechnungsblätter für den Wäremübertrager. 7th ed. Düsseldorf: VDI-Verlag Gmbh; 1994. Chapter Ja. Paragraph 3.

[3] VDI-Wärmeatlas Berechnungsblätter für den Wäremübertrager. 7th ed. Düsseldorf: VDI-Verlag Gmbh; 1994. Chapter Gg.

[4]Auslegungsdatenblatt (Design sheet data) RF51/52 B001, designation: HD-Vorwärmer, Plant: GKN 1

[5] Griebel R. HD-Vorwärmer RF 51/52 B001 Wärme- und strömungsteschniche Auslegung Arbeitsbericht NDM1/2001/de/0062. Erlangen: F-ANP/BDE; 2001. p. 11

[6] geometrical parameters read from the following F-ANP/BDE technical drawings (Archive box 2088069 BRD016 20RB10/20 B001 GKN1 HD-Vorw RF51B001 9)

- Behältermantel-Schuss 1, 5 374 407
- Einbauter und Gitter, 5 374 412
- Prallblech, 5 374 414
- Masszeichnung, 5 372 789
- Kondensatkühlkasten, 5 374 413

[7] VDI-Wärmeatlas Berechnungsblätter für den Wäremübertrager. 7th ed. Düsseldorf: VDI-Verlag Gmbh; 1994. Chapter Ld. Paragraph 1.

[8] VDI-Wärmeatlas Berechnungsblätter für den Wäremübertrager. 7th ed. Düsseldorf: VDI-Verlag Gmbh; 1994. Chapter Lm.

[9] VDI-Wärmeatlas Berechnungsblätter für den Wäremübertrager. 7th ed. Düsseldorf: VDI-Verlag Gmbh; 1994. Chapter Lc. Paragraph 3.

[10] VDI-Wärmeatlas Berechnungsblätter für den Wäremübertrager. 7th ed. Düsseldorf: VDI-Verlag Gmbh; 1994. Chapter Lc. Paragraph 1.2.

[11] VDI-Wärmeatlas Berechnungsblätter für den Wäremübertrager. 7th ed. Düsseldorf: VDI-Verlag Gmbh; 1994. Chapter Lb. Paragraph 1.

[12] Idelchik IE. Handbook of hydraulic resistance. 2nd ed. New-York: Hemisphere publishing corporation; 1986. p. 407.

[13] Bejan A. Advanced engineering thermodynamics. Durham: John Wiley & sons; 1988. p.630.

[14] Au-Yang MK. Flow-induced vibrations of power and process plant components. Bury St. Edmunds: Professional engineering publishing; 2001.

[15] VDI-Wärmeatlas Berechnungsblätter für den Wäremübertrager. 10th ed. Düsseldorf: Springer; 2006. Chapter Oc. Paragraph 4.3.

[16] VDI-Wärmeatlas Berechnungsblätter für den Wäremübertrager. 10th ed. Düsseldorf: Springer; 2006. Chapter Oc. Paragraph 2.3.

[17] Bejan A. Advanced engineering thermodynamics. Durham: John Wiley & sons; 1988. p.624-629.

[18] VDI-Wärmeatlas Berechnungsblätter für den Wäremübertrager. 10th ed. Düsseldorf: Springer; 2006. Chapter Oc. Paragraph 2.5.

[19] Heat transfer and Fluid Flow service, Chalk River Laboratories. PIPO 1 Heat-exchanger tube vibrations, program technical manual. Canada: CRNL 3030; 1988. Part 1.

[20] VDI-Wärmeatlas Berechnungsblätter für den Wäremübertrager. 10th ed. Düsseldorf: Springer; 2006. Chapter Oc. Paragraph 3.2.

[21] Wärmeschaltplan Nr. 000000-S121-00002 GKN Neckarwestheim I, Siemens AG S121

[22] Schubert S. Auswertung des wärmetechnischen Verhaltens der Dampferzeuger von 1996 bis 2002, NGPM1/2003/de/0040. Erlangen: FRAMATOME ANP; 2003. p.10

[23] VDI-Wärmeatlas Berechnungsblätter für den Wäremübertrager. 7th ed. Düsseldorf: VDI-Verlag Gmbh; 1994. Chapter Ld. Paragraph 1.3

- Background reading

Schreiner J, Schreiner W. Anschauliche Thermodynamik. 1st ed. Wien: Moritz Diesterweg Gmbh & Co / Otto Salle Verlag Gmbh & Co; 1983.

The Thermodfluid Mechanics and Energy Course Team. Fluid mechanics: energy and momentum. Buckinghamshire: Open University Press; 1982.

The Thermodfluid Mechanics and Energy Course Team. The first and second laws of thermodynamics for flow processes. Buckinghamshire: Open University press; 1982.

The Thermodfluid Mechanics and Energy Course Team. Heat transfer analysis. Buckinghamshire: Open university Press; 1982.

The Course Team. Vapour power cycles, gas turbine cycles. Buckinghamshire : Open university press; 1982.

Haywood RW. Analysis of engineering cycles. 1st ed. Pergamon press; 1967.

Blevins, Robert D. Flow-induced vibration. 2nd ed. Krieger Pub Co; 1994.

Young DF, Munson BR, Okiishi TH. A brief introduction to fluid mechanics. 2nd ed. New York: Wiley; 2001.

Vargas JVC, Ordonez JC, Bejan A. Power extraction from a hot source in the presence of phase change. Int J Heat Mass Transfer. 1998 Sep 17; 43:191-201.

Bejan A. Thermodynamic optimization of geometry in engineering systems. Exergy Int J. 2000 Dec 31; 1(4): 269-277.